COURSE ON
RANDOM SETS AND FUNCTIONS

Jean Serra
Centre de Morphologie Mathématique
École Nationale Supérieure des Mines de Paris
35, rue Saint-Honoré
77305 Fontainebleau Cedex
FRANCE

Ecole des Mines de Paris, Mars 2002

Contents

Foreword

The text that follows is the second facet of a course holding on morphological operators and on random models. It is given yearly in November (morphological operators) and March (random models) at the Ecole des Mines de Paris during European sessions. Indeed, the chapters below correspond to half of the lectures on random sets and functions, the other part being taught by Dominique Jeulin. The Matheron axiomatics for random sets, which is introduced here as a counterpoint to the Boolean model, is more developed in Jeulin's part, as well as the dead leaves model, which is extended to numerical functions and to sequential structures. In addition, the relationships that link the physical properties of the materials with their geometrical structures are thoroughly treated in Jeulin second part.

The present part deals with three major themes. Firstly, the measurements. The functionals which are introduced and studied admit always both deteministic and random versions. Emphasis is put on their stereological aspects, but not exclusively. The second theme is that of the measurements associated with two basic erosions, namely with a segment, and with the extremities of a segment. Finally, two chapters are devoted to Boolean sets and functions, that turn out to be basic archetypes for random structures, and also the fathers of all usual models.

Pedagogically speaking, the course comprises the text that follows, plus two other elements. There is on the one hand the series of transparencies for the talks, in english and in french versions. Their classification follows that of the chapters but the theoretical aspects are more developed here. On the other hand a comprehensive collection of simulations show how to handle the morphological models. They run in real time by means of the "Micromorph" software.

Jean SERRA

March 2202

.

Chapter 1

Measurements

1.1 Set Functionals

There exists a rather important literature on digital surface description, and calculus, for 3-D sets [66][106][105]. However if one has in mind to bridge the gap between digital and continuous spaces, i.e. to provide a Euclidean meaning with digital measurements, the techniques based on digital boundary measurement (i.e. volume difference between dilate and object, or object and eroded set) are not sufficient, and one must deal with *stereology* [10][31][48] [93]. Below we follow this approach. Moreover we are not exclusively interested in surface area, but more generally in digital estimators of "good" Euclidean measurements, or *functionals*. A set functional is a finite number W measured on a set $X \in \mathcal{P}(\mathbb{R}^n)$, for purposes of describing it. In physics, it is also called measurement or parameter. For both physical and logical reasons, it often fulfills the following requirements :

- to lend itself to sampling, which allows the condition of c-additivity:

  $W(X \cup Y) + W(X \cap Y) = W(X) + W(Y) \quad X, Y \in \mathcal{P}(\mathbb{R}^n)$;

- to be homogenous, i.e. to commute under magnification :

  $W(kX) = k^p.W(X)$ where k is a positive integer with $0 \leq p \leq n$;

- to be invariant under translation :

  $W(X_b) = W(X)$
  or, more severely, to be invarariant under translation *and* rotation ;

- to satisfy a certain robustness, e.g. to be continuous, or be increasing, on the class of the compact convex sets.

For obtaining functionals that satisfy such properties, the first task consists in delineating a convenient class of sets. The whole class $\mathcal{P}(\mathbb{R}^n)$ is too general and cannot serve even to introduce the Lebesgue measure (e.g. in $\mathbb{R}^2$ the area). The class $\mathcal{K}'(\mathbb{R}^n)$ of the non empty compact sets is already better: the Lebesgue measure exists on it, and it is even upper semi-continuous, but such a class is still too comprehensive. For exemple, a compact fractal set in the plane $\mathbb{R}^2$ usually has no perimeter. Following H.Hadwiger [40] and L.A. Santalo [120], we shall base our approach on the *Convex Ring*, i.e. on the class $\mathcal{R}(\mathbb{R}^n)$ of the finite unions of compact convex sets in $\mathbb{R}^n$. This class is not only closed under displacement, magnification, intersection and finite union, but it allows one to derive all basic functionals from a unique one, namely the connectivity number, in a way which has a deep stereological meaning.

The main symbols used below for displacements are the following:

$\{x\}$	*represents the point* $x \in E$ *considered as an element of* $P(E)$*;*
α	*stands for the angles in the plane;*
$\Delta(x, \alpha)$	*straight line of* R^2 *of direction* α *and passing through point* x ;
ω	*stands for the solid angles in the space;*
$\Pi(x, \omega)$	*plane of* R^3 *going through* x*, with normal* ω;
$\Delta(x, \omega)$	*straight line of* R^3 *of direction* ω *and passing through point* x.

1.2 Euler-Poincaré Characteristic

Euler-Poincaré characteristic ν^n (also called connectivity number or again EPC) is defined by means of an induction on the dimension n of the Euclidean space $\mathbb{R}^n$.

For $n = 0$, the space is conventionally reduced to a unique point, and $\nu^0(X) = 1$ or 0 according to whether set X is this point or the empty set.

For $n = 1$, put

$$h^1(x) = \nu^0(X\{x\}) - \nu^0(X\{x + 0\}) \tag{1.1}$$

where $x + 0$ designates the right limit at point x. The term $h^1(x)$ is non-zero only at the right ends x_i of the segments that form X, where it is

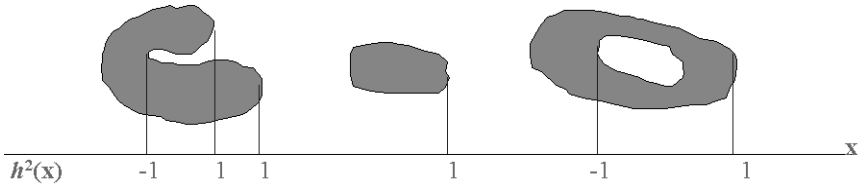

Figure 1.1: An example of the Euler Poncaré constant in $\mathbb{R}^2$.

equal to 1. Then the EPC in $\mathbb{R}^1$ is defined by the sum

$$\nu^1(X) = \sum h^1(x_i). \tag{1.2}$$

For $n = 2$, in $\mathbb{R}^2$, introduce similarly

$$h^2(x) = \nu^1(X \cap \Delta(x)) - \nu^1(X \cap \Delta(x + 0)) \tag{1.3}$$

Again, $h^2(x)$ differs from zero uniquely at the convex outputs x_g of the grains, where it is equal to $+1$, and at the convex inputs x_p of the pores, where it is equal to -1. In the convex ring, such locations are always in a finite number, so that the quantity

$$\nu^2(X) = \sum h^2(x_g) - \sum h^2(x_p) \tag{1.4}$$

is also finite, and defines the EPC in $\mathbb{R}^2$. Geometrically speaking, the constant $\nu^2(X)$ is nothing but the number of the grains of set X minus that of its pores, as we can verify on fig (1.1)

In $\mathbb{R}^3$, the principle is the same, and relation

$$h^3(x) = \nu^2[X \cap \Pi(x)] - \nu^2[X \cap \Pi(x + 0)] \tag{1.5}$$

induces, by summing in x, the Euler-Poincaré constant $\nu^3(X) = \sum h^3(x_i)$. In algebraic topology, the genus of a connected boundary ∂Y is defined as the maximum number of the loops one can trace on ∂Y without disconnecting it. It is equal to 0 for a sphere, to 1 for a torus, to 2 for a tore provided with an handle, etc... It can be proved that the E.P. C. $\nu^3(X)$ is equal to

$$\nu^3(X) = \sum [1 - G(\partial X i)] \tag{1.6}$$

where the ∂X_i are the connected components of the boundary ∂X.

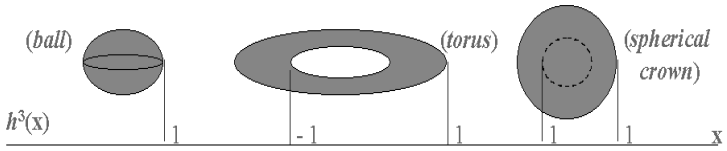

Figure 1.2: An example of the Euler-Poincaré constant in $\mathbb{R}^3$.

1.2.1 Geometrical Interpretation

The theory of Euclidean surfaces is classical, and dates back to the beginning of the 20th century (R. Poincaré). The comment below derives from [53], more information can be found in general documents such as Encyclopedia Britannica.

In $\mathbb{R}^n$, a *closed orientable surface* is topologically equivalent to a sphere with an even number $2p$ of holes (made by removing discs) which have been connected in pairs by p *handles* (shaped like the surface of half of a doughnut). A *closed non orientable surface* is topologically equivalent to a sphere which has had a certain number q of discs replaced by *cross-caps*. The numbers p and q are said to be the genus of the surface not being closed means that some discs have been removed and the hole left open. A torus is a sphere with one handle ; a Möbius strip is a sphere with one cross-cap and one "hole" ; a Klein bottle is a sphere with two cross-caps ; a cylinder is a sphere with two "holes". In general, the Euler-Poincaré number of a surface is equal to $2-2p-q-r$, where p is the number of handles, q is the number of cross-caps (zero for an orientable surface), and r is the number of holes (or boundary curves).

More simply, remember that the EPC of a simply connected object (i.e. homeomorphic to a cube) equals 1, that of a torus (typically, a donut) equals 0, and that of spherical crown (such as a football) equals 2. Moreover, the constant v is C-additive, which means that

$$v(A) + v\left(A'\right) = v\left(A \cup A'\right) + v\left(A \cap A'\right), \tag{1.7}$$

an equation that allows one to reduce complex figures to the most simple ones. Thus, the ECPC of lampshade pierced by 1000 pin holes equals -1000. The Euler Poincaré number of the union of disjoint surfaces is the sum of each of them.

The topological number ν allows to bridge the gap between Euclidean and digital spaces, since it can be equivalently defined in both modes when we interpret it in terms of graphs. Here, a convenient set model is the class of all finite unions of compact convex sets. This class, called "the convex ring of $\mathbb{R}^n$" allows to elaborate a theory about measurements (Hadwiger theorem below), and on the other hand lends itself to digitization. In this framework, a deep property of Euler-Poincaré number is stated by the following theorem [40].

Theorem 1.1 *(Hadwiger): the only functional defined on the convex ring in $\mathbb{R}^n$, of degree zero, invariant under displacements, C-additive and constant for the compact convex sets, is the Euler-Poincaré number ν.*

Moreover, this translation invariant EPC does not depend on the direction by which it has been constructed, hence it is isotropic and rotation invariant. In addition, it has dimension 0, therefore it is invariant under magnification. Finally note that unlike the number of particles, number ν is a *local measurement*: one needs only small neighborhoods around best points to estimate it statistically.

1.2.2 Digitization of the Euler-Poincaré Number

Historically, the Euler-Poincaré constant (in brief:EPC) appeared in two slightly different domains of mathematics. Firstly, there was Euler's reasoning about the relations between the polyhedrons vertices, edges and faces, which was formalized in terms of planar graphs by Cauchy. This way of thinking leads to counting algorithms, which are based on the elementary edges, squares and triangles (in the hexagonal grid). It extends to various cubic, cube-octahedron and rhombo-dodecahedron of $\mathbb{R}^3$, without any particular theoretical difficulty, but with a growing heaviness of the elementary operations to be carried out.

The second way, Poincaré's, and Hadwiger's later on, links the successive definitions of EPC thanks to an induction holding on the dimensions of the space [40]. When transposed to a digital grid, this approach is limited to cubic (or to parallelepipedic) grids, but, in return, leads to a much simpler and faster expression than the graphs one. Thus, for a bounded digital set A, we have :

In $\mathbb{Z}^1$, $v_1(A) = N(\text{vertices}) - N(\text{edges}) = N(\bullet) - N(-)$

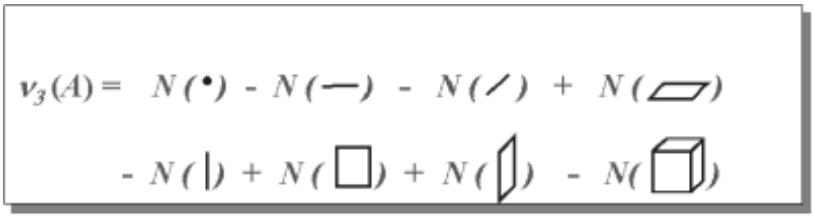

Figure 1.3: Decomposition of the 3-D Euler-Poincaré Constant into a series of elementary erosions.

In $\mathbb{Z}^2$, for the square grid :

$$\begin{aligned} v_2(A) &= N(\text{vertices}) - N(\text{edges}) + N(\text{faces}) \\ &= N(\bullet) - N(-) - N(|) + N(\square) \end{aligned}$$

Still in $\mathbb{Z}^2$, if we agree on calling $N_1(A)$ the sum of the constants $\overline{v_1}$ of the horizontal sections of A, we can see that

$$v_2(A) = \overline{\nu_1}(A) - \overline{\nu_1}(A \ominus |), \tag{1.8}$$

where $A \ominus |$ stands for the Minkowski substraction of A by the unit vertical segment.

In $\mathbb{Z}^3$, this is the same, and Euler's number $v_3(A)$ defined as

$$v_3(A) = N(\text{vertices}) - N(\text{edges}) + N(\text{faces}) - N(\text{blocks}) \tag{1.9}$$

is expressed by the same increment as before, for

$$v_3(A) = \overline{v_2}(A) - \overline{v_2}(A \ominus |) \tag{1.10}$$

when $\overline{v_2}(A)$ is the sum of Euler bidimensional numbers of the horizontal sections of A, and where $\ominus$ stands for he Minkowski substraction of A by the unit vertical segment (equation (1.10) can easily be extended to $\mathbb{R}^n$ by recurrence). Constant v_3 is independent of the choice of the "vertical" direction.

From an experimental point of view, the equation (1.10) is very convenient, for in image processing systems, Euler bidimensional constants are generally rapid to get and the unit linear erosion between two consecutive planes is a simple operation too. It is this equation (1.10) that has been implemented in the shinbone example in chapter 13.

1.3 Minkowski Functionals

When set X is an element of the convex ring $\mathcal{R}(\mathbb{R}^n)$, one can wonder about the ECP of the sections $X \cap \Pi_k$ of X by hyper-planes of dimension k ($0 \leq k \leq n$), and also about their averages under displacements as Π_k varies. These sums result in $n+1$ functionals which are, by construction, invariant under displacement, homogenous of degree n - k, c-additives, increasing and continuous for the compact convex sets. These so-called Minkowski functionals go back to H. Minhowski [101], and their importance derives from the following result, due to H. Hadwiger ([40]) :

Theorem 1.2 ***Theorem 1.3*** *: Every functional defined on the convex ring, and which is invariant under displacement, c-additive and continuous (or equivalently increasing) on the compact convex sets is a linear combination of the Minkowski functionals.*

In particular in $\mathbb{R}^n$, up to a multiplying constant:

- the first functional (of degree n) is the *Lebesgue measure* of X, it is increasing and upper-semi continuous ;
- the second one (of degree $n-1$) is the superficial measure of the boundary ∂X ;
- the last but one (of degree 1) is the so called *norm or mean width* it commutes under Minkowski addition, i.e. satisfies the *characteristic* relationship
$$M(\lambda X \oplus \mu Y) = \lambda M(X) + \mu M(Y) \tag{1.11}$$

For the three usesful cases in practice of $n = (1, 2, 3)$, the Minkowski functionals admit geometrical interpretations that make them the basic measurements in image processing. More precisely,

- In $\mathbb{R}^1$, the first functional reduces to the length $L(X)$ of set X, and the second and last one to the number $\nu^0(X)$ of segments which compose X,
- In $\mathbb{R}^2$, The three functionals are the area A, the perimeter U and the EPC ν^2 with
$$U(X) = \int_\pi d\alpha \int_R \nu^1[X \cap \Delta(x, a)]dx, \tag{1.12}$$

a relation that interprets the perimeter as the sum of the intercepts taken in all directions. Moreover, when set X is compact convex, the perimeter is related to the projections of X on the straight lines Δ_α by the relation

$$U(X) = \int_\pi L[X \mid \Delta_\alpha] d\alpha. \tag{1.13}$$

- In $\mathbb{R}^3$, the four functionals are the volume V, the area S, the mean width or *norm* M, and the EPC ν^3. We have the three expressions

$$\textit{volume} \qquad v(X) = \int_{\mathbb{R}^3} \nu_0 \left(X \cap \{x\}\right) \, dx \tag{1.14}$$

$$\textit{surface area} \quad \frac{1}{4} s(X) = \frac{1}{4\pi} \int_{4\pi} d\omega \int_{\pi\omega} \nu_1 \left[X \cap \Delta\left(x, \omega\right)\right] \, dx \tag{1.15}$$

$$\textit{mean caliper} \quad d(X) = \frac{1}{4\pi} \int_{4\pi} d\omega \int_{-\infty}^{+\infty} \nu_2 \left[X \cap \Pi\left(x, \omega\right)\right] \, dx \tag{1.16}$$

The three relations Eq.(1.14) to Eq.(1.16) attribute a *Euclidean* meaning to *digital* data. In $\mathbb{R}^3$, for example, Eq.(1.14) becomes by discretization

$$v^*(X) = (\text{Number of voxels of } X) \times v_0 \tag{1.17}$$

where $v_0 = a^3$ (cubic grid) or $a^{3/4}$ (fcc grid) or $a^{3/2}$ (cc grid). Similarly, Eq.(1.15) is written, in the cubic grid

$$s^*\left(X\right) = (\text{average number of intercepts}) \times 2a^2\sqrt{2}, \tag{1.18}$$

where the averaging is taken over the six directions going from the centre to the middles of the sides. Since estimate $s^*\left(X\right)$ concerns the Euclidean surface $s(X)$, it differs from the facets areas of the digital set X. For example, here, a facet of a zero thickness counts twice.

- When the 3-D boundary ∂X admits two curvatures C_1 and C_2 everywhere, the norm expresses the intergal of the mean curvature, i.e.

$$2M(X) = \int_{\partial X} (C_1 + C_2) ds. \tag{1.19}$$

In particular, when set X is convex, its area and its norm can be interpreted in terms of projections $X \mid \Pi_\omega$ and $X \mid \Delta_\omega$ on the planes Π_ω and lines Δ_ω

$$\pi S(X) = 4\pi \int A(X \mid \Pi_\omega) d\omega \tag{1.20}$$

$$2M(X) = 4\pi \int L(X \mid \Delta_\omega) d\omega = (2/\pi) \int_{4\pi} U(X \mid \Pi_\omega) d\omega \tag{1.21}$$

1.3.1 Stereology

Definition 1.4 *A measurement on a set family in $\mathbb{R}^n$ is said to be stereological when it can be written as a function of measurements performed on sets of $\mathbb{R}^k$, $k < n$ [153][159].*

By construction, all Minkowski functionals are stereological except the last one (the EPC). In $\mathbb{R}^3$ for example, for computing a volume (resp. an area, a width) the above relations show that it suffices to sample the space by points (resp.by lines, by planes).

More often, stereology intervenes between specific measures, hence in a stationary framework. Denote by $V_V(X)$ the volume of X by unit volume of the space, by $S_V(X)$ the specific surface, by N_A and N_L the specific EPC in $\mathbb{R}^2$ and $\mathbb{R}^1$ (or, if so, their rotation averages). Then the above relationships become

$$\begin{array}{lll} V_V & = A_A & = L_L \\ S_V & = 4N_L & = (4/\pi)U_A \\ M_V & = 2\pi N_A & \end{array}$$

1.3.2 Steiner Formulae for Convex Sets

When sets X and B are non empty compact convex, the functionals of the Minkowski dilate $X \oplus B$ derive from those of X and of B. The relation has already been given for the norm; as for the volume, we have

- in $\mathbb{R}^2$,

$$\overline{A}(X \oplus B) = A(X) + [U(X).U(B)]/2\pi + A(B) \tag{1.22}$$

- in $\mathbb{R}^3$,

$$\overline{V}(X \oplus B) = V(X) + [M(X).S(B) + S(X).M(B)]/4\pi + V(B) \quad (1.23)$$

where $\overline{A}$ and $\overline{V}$ stand for the rotation averages as B takes all possible orientations with respect to set X .

These formulae, established by Steiner in 1839 when B is a ball, are extensively used for calculating Boolean random sets and functions (see chapters 15 and 16). In such cases, set B is classically the unit segment, the unit disc or the unit ball and the general expressions become

for B the unit segment

in $\mathbb{R}^2$	$\overline{A}(X \oplus rB) = A(X) + rU(X)/\pi$
in $\mathbb{R}^3$	$\overline{V}(X \oplus rB) = V(X) + rS(X)/\pi$

for B the unit disc

in $\mathbb{R}^2$	$\overline{A}(X \oplus rB) = A(X) + rU(X) + \pi r^2$
in $\mathbb{R}^3$	$\overline{V}(X \oplus rB) = V(X) + \pi r S(X)/4 + r^2 M(X)/2$

and finally, for B is the unit ball in $\mathbb{R}^3$

$$V(X \oplus rB) = V(X) + rS(X) + r^2 M(X) + 4/3\pi r^3. \quad (1.24)$$

In all cases, the measure of the dilate is a polynomial function of the size of the structuring element, and has for degree the dimension of the latter. One easily proves that, for r small, the first order terms extend to the convex ring.

1.3.3 Global Measurements or individual analysis?

So far, set X was always considered as a whole. What additional results can be found when set X is generated by a union of disjoint convex grains Y? How the sizes of the sectioned grains are related to those of the space ones, for example? Denote by $E[*]$ the mean of $*$ over all objets, and by $\overline{*}$ the mean of $*$ for all sections of all objets in all directions. In $\mathbb{R}^3$, the major stereological relationship is the following

$$E[V(Y)] = \overline{A}(Y \cap \Pi).\overline{L}(Y \mid \Delta) = \overline{A}(Y \mid \Pi).\overline{L}(Y \cap \Delta) \quad (1.25)$$

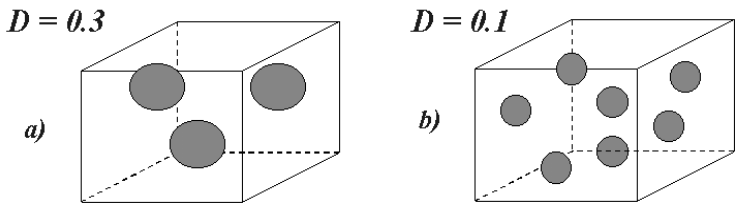

Figure 1.4: The average number of grains in sections equals 9 in case *a)*, and 7 in case *b)*.

A somewhat disappointing result, since none of the projection terms $\overline{L}(Y \mid \Delta)$ and $\overline{A}(Y \mid \Pi)$ can be accessed from plane sections. In other words, the mean volume $E[V(Y)]$ of the grains turns out to be inaccessible.

We will now examine the relationships between the numbers of objects in $\mathbb{R}^3$ and in its 2-D sections? Let I be the number of the 3-D particles Y, a quantity equal to the EPC of X since grains Y are convex. It can be shown easily that

$$\overline{I}(X \cap \Pi) = I(X).\overline{L}(X \mid \Delta) \tag{1.26}$$

which means in terms of dimensions

$$\text{"}number\ in\ \mathbb{R}^2\text{"} = \text{"}(number\ in\ \mathbb{R}^3)\text{"}.\text{"}(mean\ diameter)\text{"}. \tag{1.27}$$

An example is depicted in fig (1.4) which shows two groups of spheres in a unit cube. In case *a)* the average value $\overline{I}(X \cap \Pi)$ is 9 whereas in case *b)*, where there are more spheres, but smaller, one finds $\overline{I}(X \cap \Pi) = 7$.

1.3.4 Extension to Numerical Functions

In order to generalize the above results to numerical functions, we can model gray tone images by the class $\mathcal{F}_{\mathcal{R}}$ of those functions f from $\mathbb{R}^2$(or $\mathbb{R}^n$) into $[-\infty, +\infty]$ whose all sections $X_t(f) = \{x : x \in R^2, f(x) \geq t\}$ are elements of the convex ring. The W functionals under study become mappings from $\mathcal{F}_{\mathcal{R}}$ into $[-\infty, +\infty]$, and the prerequisites introduced in the previous set approach extend easily. Invariance under displacement holds now on horizontal translations only, and on rotations around the "vertical" axis of the gray tones. C - additivity becomes

$$W(f \vee g) + W(f \wedge g) = W(f) + W(g) \qquad f, g \in \mathcal{F}_{\mathcal{R}}; \tag{1.28}$$

However the generalization of the set oriented homogeneity requires more precautions: does it involve magnifications or affinities? In gray tone images, where the vertical axis T of the gray intensity represents quantities such as color, heat, electrical intensity, etc.. that are *physically heterogeneous* to the space coordinates. In such conditions, a global compatibility under magnification turns out to be cumbersome, and we must separate the space magnifications from the intensity ones. The convenient notion here is that of *dimensionality [131].* A functional W is said to be dimensional when

$$W[\lambda.f(\mu.x)] = \lambda^k.\mu^p.W[f(x)] \qquad x \in \mathbb{R}^n, f \in \mathcal{F}_{\mathcal{R}} \tag{1.29}$$

where k and p, integers $\neq 0$, are the dimensions of measurement W. Dimensionality preservation orients us towards products of planar operations by vertical ones (i.e. typically affinities). Each numerical Minkowski functional is then obtained by summing up the set corresponding one over the gray tone axis T. We will analyse in more detail the case of the numerical functions on $\mathbb{R}^2$ which allows to draw figures, but the results below are obviously valid in $\mathbb{R}^n$.

- **Integral and areas** : we draw from the areas of the sections the following (possibly infinite) volume $V(f)$ and cumulative histogram $G_f(t)$

$$V(f) = \int_{\mathbb{R}^2} f(x)dx = \int_T A[X_t(f)]dt \tag{1.30}$$

$$G_f(t) = \int_{-\infty}^{t} A[X_t(f)]dt/V(f) \tag{1.31}$$

- **Gradient and perimeter** : from Steiner formula (extended to the convex ring), the perimeter is equal to the derivative at the origin of the dilation by a disc

$$r \to\ 0 \Rightarrow [A(X_t \oplus rB) - A(X_t)] \to\ rU(X_t) \tag{1.32}$$

When X_t is a finite union of convex sets $Y_i(t)$, this limit is upper bounded by the finite sum $\sum[A(Y_i(t) \oplus rB) - A(Y_i(t)]$ so that we can write

$$\int_t U[X_t(f)]dt = lim_{r \to\ 0}[(V(f \oplus rB) - V(f))/r] \tag{1.33}$$

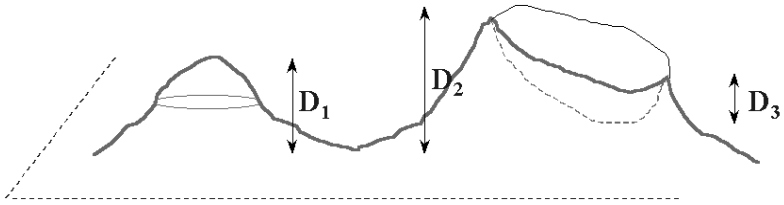

Figure 1.5: Euler Poincré Constant for numerical functions.

Now, the limit in the right member is nothing but the Beucher gradient by dilation g^+. Therefore the relationship proves the existence of the gradient g^+ on the convex ring of functions and provides it with the geometrical interpretation as the sum of the perimeters of the successive sections

$$\int_t U[X_t(f)]dt = \int_{\mathbb{R}^2} g^+(x)dx \tag{1.34}$$

- **Connectivity Number** : The sum of the ECP taken on the sections of function f measures the integral of the differences in height in f. For figure (1.5) for example, we obtain

$$\int_t \nu[X_t(f)]dt = D1 + D2 - D3 \tag{1.35}$$

- **A counter example : length l of a curve:** Although volume, cumulative histogram, gradient and connectivity number are dimensional functionals, it is not true that this property is satisfied for all usual measurements. It is not true for example for the length of a curve in $\mathbb{R}^1 \otimes T$, as given by the expression

$$l = \int [1 + [f\prime(x)]^2]dx \tag{1.36}$$

In an affinity of ratio two, the flat zones keep their lengths, and the other ones increase with the value of the slope: the length is no longer a convenient measurement !

1.4 Other measurements

Other measurements are introduced in the next chapters. They are sometimes stereological, such as the roughness, the range or the star in chapter 14, sometimes not.

We will conclude the current chapter by presenting three non hadwigerian measurements, the first two are defined in the convex ring (convexity number and 3-D contacts), and the third one in the more general class of the compact sets (fractal dimension).These three measurements are invariant under displacement, homogeneous, continuous on convex sets, but, unlike the Minkowski functionals, they do not fulfill the c-additivity condition

$$\mu\left(X \cup X\right) + \mu\left(X \cap X'\right) = \mu\left(X\right) + \mu\left(X'\right), \tag{1.37}$$

which is not essential here.

1.4.1 Convexity Number

Consider, in $\mathbb{R}^2$ the test line Δ_α of normal $\alpha \pm\ d\alpha/2$, and let $N^+(X,\alpha)$ be the number of its first contacts with set X when Δ_α sweeps the plane. When ∂X admits everywhere a radius of curvature R, we can split the contour ∂X into its convex portions for which we have

$$2\pi N^+(X) = \int_{2\pi} N^+(X,\alpha)d\alpha = \int_{R>0} du/R, \tag{1.38}$$

and its concave ones, yielding

$$2\pi N^-(X) = \int_{2\pi} N^-(X,\alpha)d\alpha = \int_{R<0} du/\mid R\mid, \tag{1.39}$$

The two functionals $N^+$and N^-, called *convexity numbers* [129] are not c-additive, but are linked with the EPC by the relationship

$$\nu(X) = N^+(X) - N^-(X) \tag{1.40}$$

1.4.2 3-D contacts

Consider a random packing of spheres of radius R, and a cross section through it. The spheres becomes discs, and the distribution of the shortest distances between discs follows a law

$$F(l) \simeq 1.438\ n_c(lR)^{1/2} \tag{1.41}$$

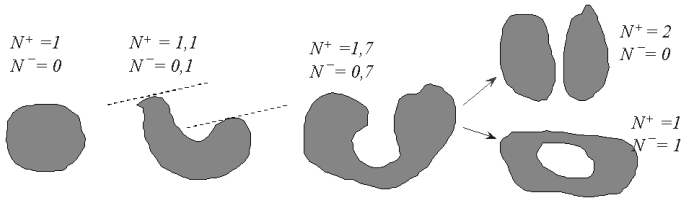

Figure 1.6: An example of convexity numbers.

where n_c is the number of contacts between spheres per unit volume [108]. This law, which governs some modes of thermic and electric permeabilities, has been experimentally verified [10].

1.4.3 Minkowski Dimension

Consider a compact set X in $\mathbb{R}^2$. When set X is dilated, or eroded, by a small disc rB, whose radius tends towards zero, it may happen that, under the development of finer and finer details, the area increment divided by r does not tend towards a finite perimeter, as in Steiner formula, but towards infinity. In such a case, there always exists a smaller value d, with $1 \leq d \leq 2$, such that the quantity

$$A(X \oplus rB) - A(X \ominus rB)/2r \tag{1.42}$$

tends towards the *finite* limit kr^{1-d}, where k is a constant.The value d then defines the *Minkowski Dimension* of set X. Indeed, the whole gamut of dimensions, from 1 to 2 is covered, since for all sets of the convex ring we have $d = 1$, but for a brownian trajectory, $d = 1,5$ and for a Peano curve, one finds $d = 2$. The fractal sets of B. Mandelbrot [70] admit also non-integer dimension d, i.e. a *local* notion, but they are richer, for they bring into play, in addition, the *global* notion of self-similarity.

Minkowski dimension extends to $\mathbb{R}^n$, but is not a stereological notion. In practice, in the isotropic case, ones passes from $\mathbb{R}^2$ to $\mathbb{R}^3$ by adding 1 to d. Experimentally, the object under study is accessed via a series of magnifications q, whose limit of resolution r decreases. For a given r, the perimeter of set X is

$$U_X(r) = A(X \oplus rB) - A(X \ominus rB)/2r = k/2r^{d-1}. \tag{1.43}$$

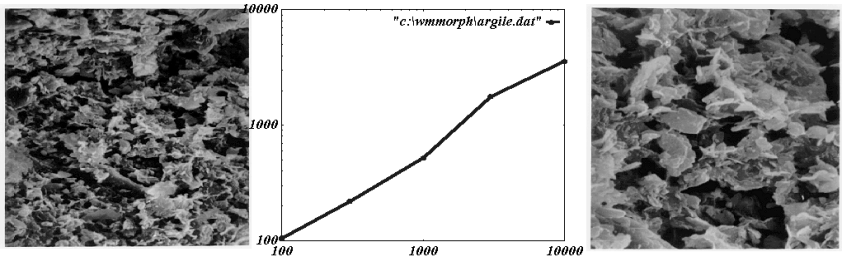

Figure 1.7: Two micrographs of clay material at magnifications $\times 300$ and $\times 1000$, and the plot of the contours increasingness. The slope of the line equals the fractal dimension minus one.

Therefore, we have to check whether $LogU_X(r)$, as a function of $Logr$ fits a straight line. If so, its slope provides an estimate of $d-1$. Finally, when the object under study is no longer a set but a numerical function, by applying the previous approach to the successive sections X_t, we obtain the following expression

$$Log\ grad_r(f) = (d-1)Logr + k\prime \tag{1.44}$$

We will apply the approach to a specimen of clay seen in scanning electron microscopy, at successive magnifications 10^2, 3.10^2, 10^3, 3.10^3 et 10^4, as depicted in Figure (1.7). The apparition of new details at each step suggests the fractal model. Indeed, the increments of the gradient yield the estimate $d^* = 1.8$

Chapter 2

Covariance and Linear Erosion

2.1 Introduction : two sister notions

The current chapter is devoted to the studies of the Lebesgue measure of two erosions. In the first one, the structuring element $B = B(r, \alpha)$ is made of two points separated by a distance r in direction α ; in the second one, it becomes the whole segment whose extremities are the two previous points. Both erosions are carried out in the Euclidean framework which allows nice geometrical interpretations (in stereology in particular). Indeed, since both erosion and Lebesgue measure are increasing and upper semi-continuous operations on the compact sets [82], the digital measurements are approximations of the Euclidean ones, and tend toward them as the spacing of the grid tends toward zero. The measurement associated with the doublet of points is named covariogram, or covariance, that corresponding to the segment is the linear moment. Both depend on the vector $h = (r, \alpha)$ introduced by the structuring element, therefore they yield curves.

The similarity of the two structuring patterns (a segment or its extremities) induces proximities in the measurements, but also differences. In case of a set X the two behaviors near the origin are identical as soon as the set under study is supposed not to be fractal, since then a very small segment hits the boundary ∂X at most once. For the sake of pedagogy, we share the presentation into Minkowski Functionals (covariance) and roughness (linear moment) but all results are valid for the two structuring elements.

Differences arise when one wishes to extend the set measurements to

gray tone images. If $h(x)$ stands for the indicator function of set X, then

- two point x and $x+h$ belong to X when $k(x) \cdot k(x+h) = 1$ or equivalently $\inf(k(x), k(x+h)) = 1$

- the segment $[x, x+h]$ belongs to set X when $\inf\{k(y), y \in [x, x+h]\} = 1$

This allows two different generalizations in the case of the covariance, but one only for the linear moment. The most useful representation of the former is $k(x) \cdot k(x+h) = 1$, because it corresponds to the very physical notion of a power spectrum. Unfortunately it does not admit an equivalent for the linear erosion.

Another, and deeper difference appears for sets and functions as soon as we leave the vicinity of the origin. As modulus r increases, the linear moment can only decrease (it is even a convex function) whereas the covariance may oscillate, which results in two complementary perceptions of the object under study. Linear moments inform us about size measurement (granulometries, average grain, star ...) and covariance about packing, fabric, periodicities, superimposition of scales, etc ...

In mathematical morphology the comparative study of covariance and linear erosion dates from the end of the sixties [39] ; it has been presented in full length and with number of examples in [129] where it occupies 90 pages. Here, more modestly, we have reduced this exhaustive study to 20 pages, and we have taken new examples.

2.2 The Covariance

2.2.1 Set Covariogram

Let h be a vector of origin 0, modulus r and direction α, in $\mathbb{R}^n$. Take for structuring element B the point doublet $\{0, h\}$ and consider the erosion

$$X \ominus B = X \cap X_{-h}. \tag{2.1}$$

made of all those points common to X and to its translate by vector -h.

Definition 2.1 *: The Lebesgue measure of $X \cap X_{-h}$ defines the* set covariogram *of X, it is denoted by*

$$K(h) = K_\alpha(r) = Mes[X \cap X_{-h}] = Mes[X \cap X_h] \tag{2.2}$$

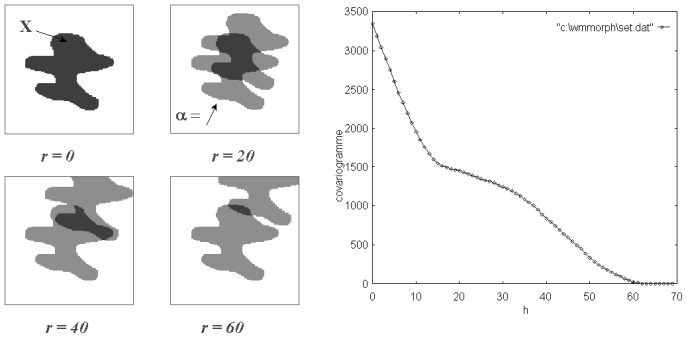

Figure 2.1: Covariogram of set X in direction α

We see that

$$K_\alpha(0) = MesX \qquad \text{and that} \qquad \int K(h)dh = [MesX]^2 \tag{2.3}$$

i.e. the integral of the covariogram equals the square of the area (volume) of X. The tangent at the origin $-K'\alpha(0) = -[\partial K\alpha(r)/\partial r]_{r=0}$ is nothing but the total variation of set X in direction α, (e.g. in the convex case its apparent contour), so that we can write, according to Crofton's formula

$$\begin{aligned} -\int K'\alpha(0)d\alpha &= 2U(X) \quad (in\ \mathbb{R}^2); \\ -\int K'\alpha(0)d\alpha &= \pi S(X) \quad (in\ \mathbb{R}^3) \end{aligned}$$

The set symbolism of rel. 2.2 may be rewritten more analytically by introducing the indicator function of set X. This gives

$$K_\alpha(r) = Mes[X \cap X_h] = \int f(x).f(x+h)dx \tag{2.4}$$

where the sum is extended to the whole space. If now f is no longer an indicator, but an arbitrary measurable numerical function, the the above integral (2.4) defines its covariogram.

It may happen that the object represented by f be reproduced as one likes (e.g. a crystal of quartz) or, even if it is unique, reproduces itself indefinitely through the space. Function f is then interpreted as a realization of

a Random Function. In the first case, for f^2 almost surely (a.s.) integrable, the covariogram becomes

$$\begin{aligned} K_\alpha(h) &= E\{Mes[X \cap X_{-h}]\} \quad (for\ sets) \\ K_\alpha(h) &= E[\int f(x).f(x+h)dx] \quad (for\ functions) \end{aligned}$$

In particular, when the object under study is large with respect to the working mask, a more convenient framework consists in interpreting X, or f in terms of stationary random closed sets, or functions. For the sake of clarity, we will treat the set case first, and then the function case.

2.2.2 Stationary Set Covariance

In a stationary random closed set X, the notion that corresponds directly to the above covariogram $K_\alpha(r)$ is the *non centered* covariance

$$C_{11}(r,\alpha) = C(r,\alpha) + p^2 = Prob\{x \in X \cap X_h\}. \tag{2.5}$$

By duality with respect to the complement, we can define the covariance $C_{11}(r,\alpha)$ of set X, that $C_{00}(r,\alpha) = Prob\{x \in X^c \cap X_h^c\}$ of "pores"set X^c, and also the cross covariance $C_{01}(r,\alpha) = Prob\{x \in X^c \cap X_h\}$, as well as $C_{10}(r,\alpha) = Prob\{x \in X \cap X_h^c\}$. Now these four moments correspond to a unique notion, up to a constant and to a multiplication by -1. Indeed, the probability that a point x belongs to set X can be decomposed into

$$Prob\{x \in X\} = Prob\{x \in X \text{ and } x+h \in X\} + Prob\{x \in X \text{ and } x+h \in X^c\} \tag{2.6}$$

which results in

$$C_{11}(r,\alpha) = p - C_{10}(r,\alpha) = p - C_{01}(r,\alpha) = p - (1-p) + C_{00}(r,\alpha) \tag{2.7}$$

Experimentally, the non centered set covariance is estimated in a zone Z as the ratio $C_{11}(h)^*$ of the favorable locations of the doublet B over all its possible locations inside the mask Z i.e.

$$C_{11}(h)^* = \frac{A[(X \cap Z) \ominus B]}{A[Z \ominus B]} \tag{2.8}$$

Behavior at the origin and infinity: We find again the properties of the covariogram $K(h)$, now enriched with stochastic interpretations. Near the origin 0, we have

$$C_{11}(0,\alpha) = A_A(X) = p; \tag{2.9}$$

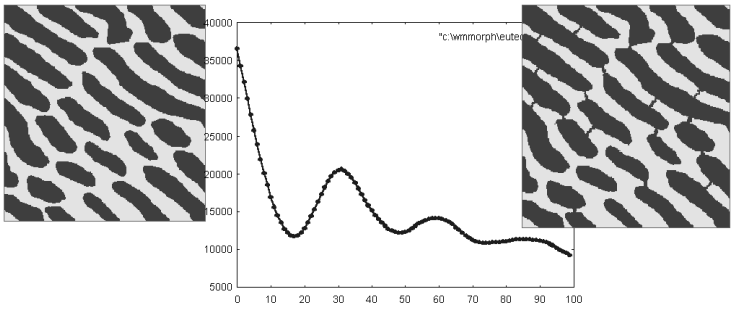

Figure 2.2: Pseudo-periodicities and covariance

The directional average of the tangent at the origin equals the specific perimeter (resp. surface) in $\mathbb{R}^2$ (resp.in $\mathbb{R}^3$)

$$\begin{aligned} -(1/2\pi)\int C_{11}(0,\alpha)d\alpha &= (2/\pi)U_A(X) \quad (in\ \mathbb{R}^2) \\ -(1/4\pi)\int C_{11}(0,\omega)d\omega &= S_V(X)/4 \quad (in\ \mathbb{R}^3) \end{aligned}$$

As h is very large, the two events $x \in X$ and $x \in X_h$ become independent, hence $lim\ C_{11}(r,\alpha) = p^2 = [A_A(X)]^2$.

Pseudo-periodicities: The maxima of the covariance, when their abcissae are multiple of each other, e.g. the three values 30, 60, 90 in fig.(2.2) , indicate pseudo-periodicities of the objet. However, the covariance is blind to connectivity : the covariances of the two sets depicted in fig.2.2 are graphically identical

Clusters and Noise: Features of different scales (in fig.2.3, the particles and their clusters) add their covariances and in particular the associated tangents at the origin. Moreover, we see in the present case an oscillation due to the equal inter particle distance in the clusters. As the limit when the lower scale tends towards 0, or in digital cases is equal to 1, we obtain a Poisson noise of variance $p_0(1-p_0)$, that appears as a jump down of the ordinate near the origin.

$\mathbb{R}$ectangle (or Cross) Covariance: The division of the space into a set and its complement is sometimes replaced by a partition of the space

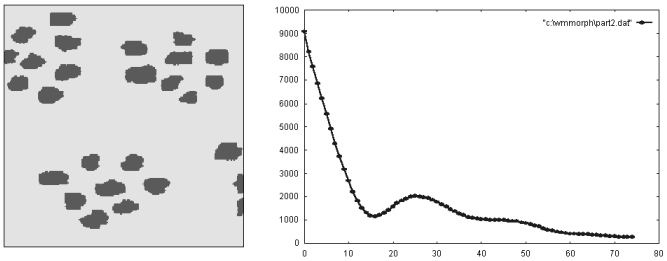

Figure 2.3: the two scales of the grains and of the clusters are added on the covariance.

into n phases $X_1, X_2...X_n$. The study of their space relations is then carried out by means of the rectangle covariances $C_{ij}(h) = C_{ij}(r, \alpha)$ for $i, j \in [1, n]$

Definition 2.2 *: The rectangle covariance of a stationary multiphased set is the joint probability that point x belongs to set X_i and point $x + h$ to set*

$$X_j : C_{ij}(r, \alpha) = Prob\{x \in X_i, x + h \in X_j\} \tag{2.10}$$

We have at the origin

$$A_A(X_i) = \sum C_{ij}(r, \alpha) and \quad i \neq j \ \Rightarrow C_{ij}(0, \alpha) = 0. \tag{2.11}$$

For h large, the two events $x \in X_i$ and $x + h \in X_j$ become independent, hence $\lim_{h \to \infty} C_{ij}(r, \alpha) = p_i p_j$.The directional average of the derivative at the origin is related to the specific perimeter (resp. surface) in $\mathbb{R}^2$ (resp.in $\mathbb{R}^3$) between phases i and j by the following equation

$$-\int C'_{ij}(0, \alpha) d\alpha = (2/\pi) U_L(X_i/X_j) = S_V(X_i/X_j)/4 \tag{2.12}$$

The metallographical example depicted in 2.4 concerns a specimen of iron ore sinter from Lorraine (France)[37]. The (grey) crystals of ferrite are due to a partial reduction of the (light grey) hematite during the sintering process. Their genesis appears on the cross-covariance *hematite-pore* that shows, by its hole effect, that the ferrite crystals surround the particles of hematite.

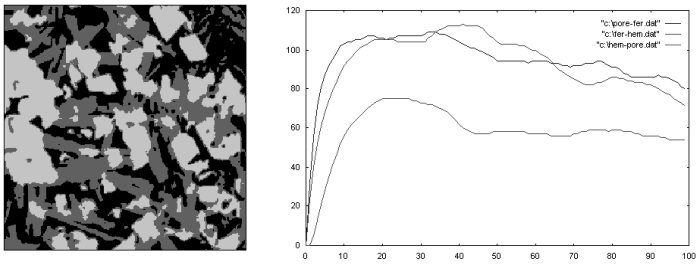

Figure 2.4: Specimen of iron ore sinter.Light gray: hematite ; dark gray : ferrite ; black: pores. The two cross covariances involving ferrite are quite identical. That between hematite and pores starts from more below (smaller contact surface) and exhibits a hole effect for h=50, which indicates a *halo* of ferrite around hematite

2.2.3 Stationary Function Covariance

We now approach the numerical functions when interpreted as realizations of stationary random functions. The former covariogram $K(h)$ of the deterministic case is replaced here by the centred covariance

$$C(h) = C(r, \alpha) = E[(f(x) - m).(f(x + h) - m)] = E[f(x).f(x + h)] - m^2. \tag{2.13}$$

where $m = E[f(x)]$ stands for the mathematical expectation of the process. The transition $sets \Rightarrow functions$ shows itself essentially in the behaviors near the origin and at the infinity. For $h = \infty$, the correlation between points x and $x + h$ vanishes, so that

$$C(h) = E[(f(x) - m)].E[(f(x + h) - m)] = 0 \tag{2.14}$$

Behavior near the origin For $h = 0$, we find

$$C(0, \alpha) = E[(f(x) - m)]^2 = \sigma^2. \tag{2.15}$$

The value at the origin of the covariance is thus equal to the *variance* of the process. In particular when function f is the indicator function of a closed random *set* X, with a volume proportion $m = p$, we find $C(0, \alpha) = p(1 - p)$, i.e. the variance of the binomial law of mean p.

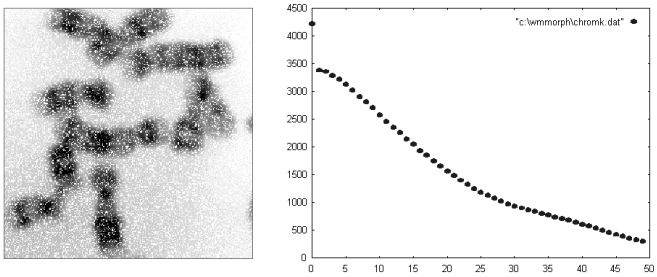

Figure 2.5: The function f of the chromosomes is derivable in quadratic mean (horizontal tangent of the covariance at the origin); the Poisson noise which is superimposed results in a "nugget effect" at the origin.

A random function f is q. m. continuous ("q. m." for "quadratic mean") when for any point x_0 we have

$$lim_{|x-x_0|\to 0} E[(f(x) - f(x_0)]^2 = 0 \tag{2.16}$$

The q.m. derivability of function f with respect to each of its variables is defined in a similar way, by taking the mathematical expectation of the square of the corresponding partial derivative. Numerical random functions may be q. m. derivable, random closed sets (via their indicator functions) are not. The various levels of regularity of functions f are transcribed on the behavior of their covariances near the origin:

- function f is derivable in quadratic mean if and only if its covariance is *derivable* at the origin, which implies by symmetry that the tangent at the origin is horizontal;

-the piecewise continuous functions (e.g. indicators) are m.q. *continous* only. Hence, their covariances are *not* derivable at the origin and exhibit oblique tangents;

-an additional Poisson noise is reflected on the covariance by a jump down at the origin (called nugget effect), whose value is equal to the variance of the noise. However, if the phenomenon and the noise are independent, the rest of the covariance is not further affected : a very useful robustness !

Sums of Stuctures The covariance sums up the structures that are non correlated. For proving it consider the sum $f = \sum f_i$, $1 \leq i \leq n$ of n independent random functions f_i of zero means (for the simplicity). To say

that they are non correlated is equivalent to saying that $E[f_i(x)f_j(x+h)] = 0$ for all x, h and i, j with $i \neq j$ Therefore the covariance $C(h)$of the sum f is equal to

$$C(h) = E[f(x)f(x+h)] = \sum E[f_i(x)f_i(x+h)] = \sum C_i(h) \qquad (2.17)$$

More deeply, one may wonder about the link between a basic shape (e.g. the lung nodule) and the stationary structure it generates by random duplication over the space. Can we build a stationary random function whose covariance be a given covariogram ? A very simple model to answer such a question consists in starting from Poisson points $\{x_i, i \in I\}$ in $\mathbb{R}^2$, of variance λ , putting at each point x_i an independent realization f_i of a primary set (or function) of covariogram $K_\alpha(r)$, and in taking the sum $f = \sum f_i$ of all these primary objects. One proves easily [129] that the resulting random function f is stationary and admits the covariance $C(r, \alpha) = \lambda K_\alpha(r)$.

Covariance and Power Spectrum A physical interpretation of the the behavior at the origin is provided by the famous theorem of Wiener-Khinchine

Theorem 2.3 *(Wiener-Khinchine) A given function $C(h)$ can model the covariance of a stationary random function f if and only if it is the Fourier transform of a non negative measure. Then the Fourier transform of $C(h)$ is the energy spectrum $\phi(\nu)$ of function f.*

Corollary 2.1 *1 This last condition amounts to saying that C(h) is definite positive, i.e. such that we have, for all positive weights λ_i and all points x_i we have*

$$\sum \lambda_i \lambda_j C(x_i - x_j) \geq 0. \qquad (2.18)$$

Corollary 2.2 *2 : Since Fourier transformation exchanges the behaviors at the origin and at infinity, we obtain, in particular*

$$\int \phi(\nu) d\nu = C(0) = E[(f(x) - m)]^2 = \sigma_0^2 \qquad (2.19)$$

The sum of the energies associated with all frequencies is thus equal to the point variance σ_0^2, i.e. to the value $C(0)$ of the covariance.

Behavior at infinity By duality, the theorem of Wiener-Khinchine, or more precisely the second corollary, also suggests that one takes into account

the beginning of the power spectrum. This allows one to introduce the *range* a of function f as follows

$$\phi(0) = \int C(h)dh = aC(0) = a\sigma^2 \tag{2.20}$$

Geometrically speaking, the range is the distance beyond which two data may be considered as independent. Moreover, when expressed in statistical terms, the notion gains an ergodic meaning. Let Z be a large working zone and denote by $f_Z(x)$ the integral $\int_Z f(x-y)dy$, then, as $Z \to \infty$, the variance σ_Z^2 of $f_Z(x)$ over the whole space admits the following limit

$$\sigma_Z^2 = E[(f_Z(x) - m)]^2 \to [a/MesZ]C(0). \tag{2.21}$$

With respect to the variance σ_Z^2 of a sample Z, the range turns out to be, asymptotically, the unit size of the phenomenon under study. More generally, whatever large Z is, if $\sigma_{0/Z}^2$ stands for the variance of the point function f inside Z, it can be shown that

$$\sigma_{0/Z}^2 = \sigma^2 - \sigma_Z^2. \tag{2.22}$$

This remarkable identity, known as Kriges formula, constitutes the starting point for Geostatistics[75][79].

2.2.4 Intrinsic Theory, Variogram

Large though the working field Z is, the variance of a closed random *set* inside it remains necessarily bounded by maximum possible variance

$$sup\{p(1-p), p \in [0,1]\} = 0,25. \tag{2.23}$$

In contrast, certain physical phenomena can exhibit a quasi infinite range of fluctuations, i.e. a variance which increases without limit with the size of the domain of experiments (ore deposits, rains...). Then the estimated variance$[\sigma_{0/Z}^2]^*$ of a point inside the domain Z increases indefinitely with Z, at any scale of analysis. From Kriges formula, this means that the stationary model is just inadequate : $\sigma^2 = C(0)$ being infinite, the covariance no longer exists. However, the increments of f may still exist and have a meaning. By assuming them stationary, we can study their variances, also called *variogram* $\gamma(h)$

$$\gamma(h) = E[f(x) - f(x+h)]^2 \tag{2.24}$$

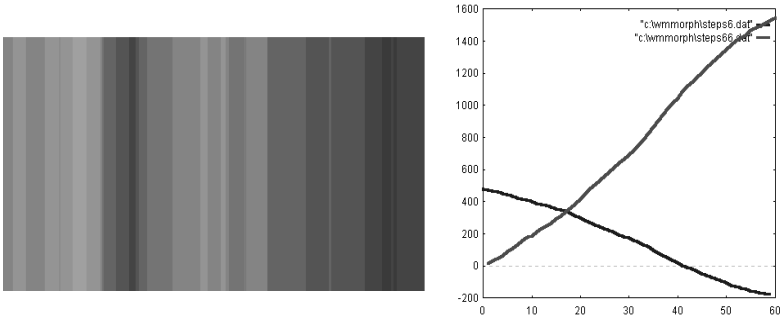

Figure 2.6: Simulation of Poisson steps, that admit only a variogram (ascending curve). The experimental covariance (decending curve) is pure artifact.

Clearly, we always have $\gamma(0) = 0$, and

$$\sigma^2 < \infty \Leftrightarrow \gamma(h) = 2[C(0) - C(h)] \tag{2.25}$$

When $\sigma^2 = \infty$, although the covariance vanishes, the variogram remains defined and new behaviors at infinity appear. Of course, one could argue that numerical data are always finite! We will answer the objection by means of a very suggestive model that lends itself to easy calculations, namely the Poisson steps.

Start from a Poisson point process of variance λ in $\mathbb{R}^1$, and place a jump of amplitude d at each Poisson point. fig. 2.6 The random variable d follows a law of mean 0 and of variance σ^2. In such a model, only the increments are defined, their average is equal to zero and their variogram to

$$\gamma(h) = r\lambda\sigma^2 \tag{2.26}$$

When the data are known along a *finite* segment of length L, the variogram is estimated from experimental data by the relationship

$$\gamma^*(h) = 1/2(L-h)\int_0^{L-h} [f(x+h) - f(x)]^2 dx \tag{2.27}$$

where the right member admits for expectation $E[\gamma^*(h)] = \gamma(h) = r\lambda\sigma^2$. But whereas the mean of the phenomenon does not exists, it is always pos-

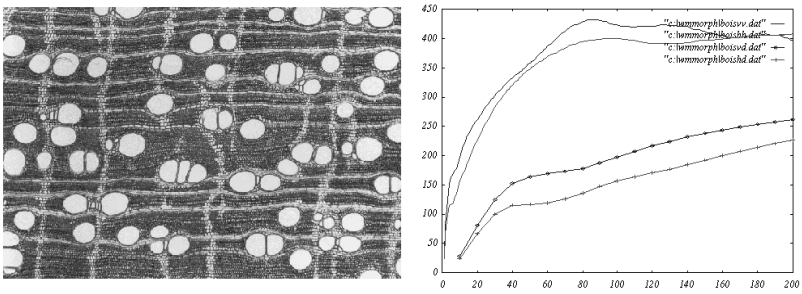

Figure 2.7: Left: thin section of beech, of size 1506 x 1016 pixels, with 1 pixel = 1 micron. Right: the variograms in the two orthogonal main directions, and their beginnings (the lower curves).

sible to put $f_L = 1/L \int_0^L f(x)dx$, and to introduce the pseudo-covariance

$$Cov^*(h) = 1/(L-h) \int_0^{L-h} (f(x+h) - f_L)(f(x) - f_L)dx. \qquad (2.28)$$

Such a pseudo-covariance admits for expectation

$$E[Cov^*(h)] = L/3 - 4/3.h + 2/3.h^2/L \qquad (0 \leq\ h \leq\ L) \qquad (2.29)$$

where the actual phenomenon (behaviors at the origin and at infinity, parabolic increasingness instead of a linear one) is completely distorted (fig. 2.6) .

To conclude on this point, we will say that when different scales interfere, even when the structure under study is binary, it is always preferable to investigate it by variograms rather than by covariance. The wood specimen depicted in figure 2.7 illustrates such a situation. It is a thin section of beech taken normally to the axis of the trunk . The horizontal direction is that of the the radii that start from the center of the tree; the vertical one is that of the annual rings . Its stucture combines fibers of a few microns with vessels that are twenty times larger but both more or less elliptic. In superimposition, two orthogonal directional structures appear: horizontally they are the radii that start from the centre of the tree, and vertically some elements of the annual ring. Both horizontal and vertical variograms show a finite variance at 0.4 (the ordinate of the sill). Nevertheless, if we want to

see acurately the fiber structure that governs the physical properties of the wood, we must magnify ten times more, and then the sill is far from being reached fig.2.7. We are typically in the situation of an infinite a priori variance, so that covariance measurement would provide a wrong quantization of the structures.

2.3 Linear erosion

2.3.1 Moment P(h)

As previously, symbol h denotes a vector of origin 0, of modulus r and of direction α in $\mathbb{R}^n$, but the structuring element B now becomes the whole segment $[0, h]$ so that

$$X \ominus B = \{X_{-u}, u \in [0, h]\}. \tag{2.30}$$

The eroded $X \ominus B$ is the set of those points common to set X and to the family of its translates by all vectors contained between 0 and h .

The *moment P(h)* of set X is the Lebesgue measure of $X \ominus B$, it is denoted by

$$P(h) = P_a(r) = P_{\alpha+\pi}(r) = Mes[X \ominus B] \tag{2.31}$$

and the integral St of moment $P(h)$, divided by $P(0)$, is called the star of X

$$St = (1/P(0)) \int P(h)dh = (1/MesX) \int P(h)dh \tag{2.32}$$

An Example Linear Erosion is given in fig. 2.8. Near the origin, the behavior of $P(h)$ is identical to that of the non-centred covariance, at least for non-fractal Euclidean sets and for digital ones

$$\begin{aligned} P(0) &= K(0) = MesX \\ -P'_\alpha(0) &= -K'_\alpha(0) = \textit{diametral variation of } X. \end{aligned}$$

The rotation averages also admit the same interpretations as for covariance. As vector h increases $P(h)$ becomes smaller than $K(h)$ since the requirement of having the whole segment $[x, x+h]$ included in set X is more demanding than having the two extremities only included in X

$$\forall a : K_\alpha(r) \geq P_\alpha(r) \geq 0 \text{ and } r_1 \leq r_2 \Rightarrow P_\alpha(r_1) \geq P_\alpha(r_2) \geq P_\alpha(\infty) = 0. \tag{2.33}$$

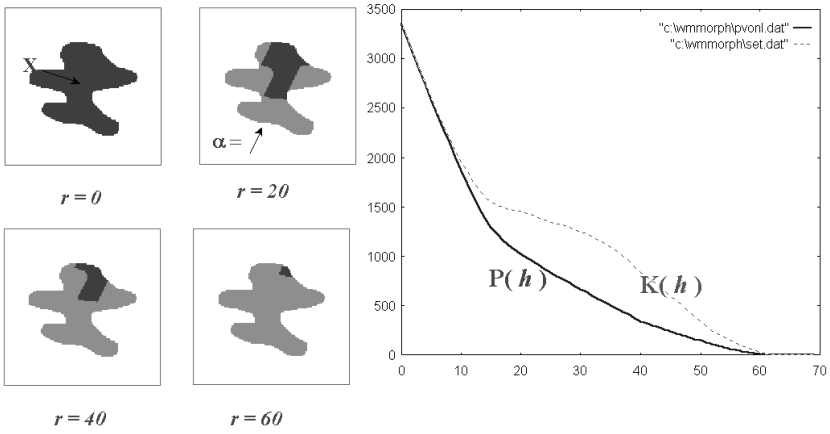

Figure 2.8: Linear erosion comparated with the covariogram.

Granulometries Unlike covariograms and covariances, the moments $P_\alpha(r)$ are associated to *granulometric* measures. Here a preliminary comment is worthwhile. There exist two different ways for weighting a size distribution. Recall the story of the butcher who sells lark pie, and advertises "Excellent mixed pie : 50% lark, 50% horse", because he guarantees the proportion of one horse to one lark. As well, when one deals with statistics about sizes of objects, it is advisable to clarify whether each individual is counted for one such as blood formula, in medecine, or in proportion of its volume (or any increasing parameter) such as sieving techniques. One speaks of analysis in number in the first case, and in measure in the second.

Coming back to the linear erosion, suppose direction α fixed, and consider the chords that intersect set X. Their distribution function is expressed by

$$\text{proportion of the chords } \geq h \ = 1 - F(h) = P'(h)/P(0) \tag{2.34}$$

as shown in fig 2.9. In such a formalism, all chords have the same weight, hence they are counted in number. Now, what about the granulometry in measure G, where each chord is weighted by its own length? Consider the adjunction opening $X \circ B = X \ominus B \oplus B$ of set X by segment $B(r, \alpha)$, and its measure. We see form figure 2.9 that

$$[1 - G(h)]MesX = Mes[X \circ B] = P(h) - hP'(h) \tag{2.35}$$

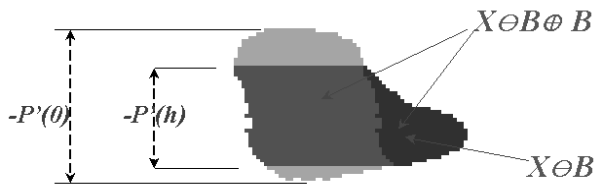

Figure 2.9: Geometrical interpretation of the area of the opening $X \circ B$.

Hence the granulometry by openings derives from $P(h)$, which contains all the information necessary to calculate the distribution function in measure $G(h)$.

Weights, individuals, sampling, and Stereology The distinction between various ways of weighting allows a pertinent approach to questions such as sampling or stereology. When the space is sampled according to a regular grid, the sampling process weights automatically in volume, for the probability of finding a vertex in a grain is proportional to its area (or its volume in 3-D). For the same reason, when extracting the grain which contains the origin, one implicitly introduces a measure weighting in the drawing lots. Similarly again, a random section on a 3-D material weights the individual objects according to their diametral variation normal to the section plane. If in addition the grains on section are themselves weighted by a grid, then the product of the two operations is a weighting in volume.

Moments in Number and in Measure We will draw the moments in number from relation $1 - F(h) = P'(h)/P'(0)$ that implies

$$E[h] = \int_0^\infty [1 - F(h)]dh = -P(0)/P'(0) \tag{2.36}$$

and more generally

$$E[h^n] = [n(n-1)/ - P'(0)] \int_0^\infty h^{(n-2)} P(h)dh. \tag{2.37}$$

Concerning the moments in measure, we suppose for the simplicity that both distributions F and G admit densities f and g respectively. Then we

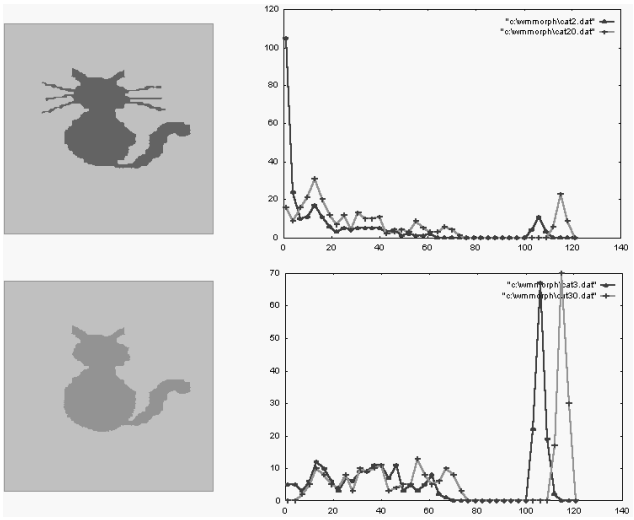

Figure 2.10: $f(h)$ sees that the whiskers of the cat have been cut ...but $g(h)$ sees that it ate a mouse !

draw from the definition $g(h) = hf(h)/E[h]$ the expression of the moment in measure $\mathcal{M}[h^n]$

$$\mathcal{M}[h^n] = \int_0^\infty h^n g(h)dh = [n(n+1)/P(0)] \int_0^\infty h^{n-1} P(h)]dh \qquad (2.38)$$

An Example of Densities $f(h)$ and $g(h)$(??)

2.3.2 Stationary Random Approach

Just as previously with the covariance, the stationary random version of $P(h)$ is obtained by replacing the measure of the linearly eroded set by the volume *proportion* of the erosion, i.e. by dividing $P(h)$ by the unitary volume (or area, or length). Since this unit is a constant, all above interpretations remain true. Therefore, for the sake of simplicity, we keep the same symbol $P(h)$ in the following. The stationary version allows one to make play symmetrical roles to P(h) and to the eroded Q(h) of the pores. If h_1

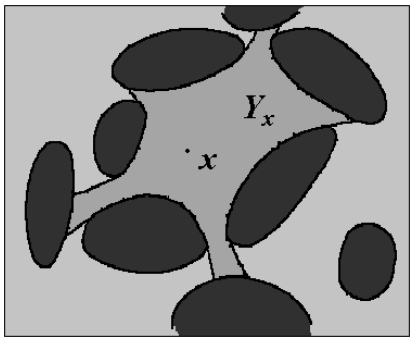

Figure 2.11: Star Y_x of the pores at point x.

stands for the grain chords and h_0 for the pore ones, we can write

$$\begin{aligned} P(0) &= p = L_L(X) = E[h_1]/E[h_0 + h_1] \\ Q(0) &= 1 - p = L_L(X^c) = E[h_0]/E[h_0 + h_1] \\ -P'(0) &= -Q'(0) = N_L(X) = N_L(X^c) = 1/E[h_0 + h_1] \end{aligned}$$

The Star Consider the pores for set X, and assign to each point $x \in X$ the set Y_x of all points $y \in X$ that are seen directly from x. The mathematical expectation of integral

$$Mes(Y_x) = \int_{\mathbb{R}^n} Ind_x(y)dy \qquad [Ind_x(y) : indicator\ function\ of\ Y_x] \tag{2.39}$$

defines the *star St(X),* of set X. Interestingly, this n-dimensional measurement turns out to be stereological, in that it depends on the linear moment $P(h)$ only; we have

$$\begin{aligned} St(X) &= E[Mes(Y_x)] = \int_{\mathbb{R}^n} prob\{[xy] \in X \mid x \in X\}dy \\ &= 1/P(0) \int_{\mathbb{R}^n} P(y - x)dy = \int P(h)dh/MesX. \end{aligned}$$

since by stationarity $P(y - x)$ does not depend on point x. In the isotropic case, the connection between star and moments in measure is more obvious,

since the orientations are eliminated by integration in α, and we obtain

$$\begin{aligned} St_3(X) &= 4\pi/V_V \int_0^\infty h^2 P(h)dh = \pi/3\mathcal{M}[h^3] \qquad \text{in } \mathbb{R}^3 \\ St_2(X) &= 2\pi/A_A \int_0^\infty hP(h)dh = \pi/3\mathcal{M}[h^2] \qquad \text{in } \mathbb{R}^2 \end{aligned}$$

When set X is a population of disjoint convex sets the star admits a nice stereological interpretation. Each point x of grain X_i sees the totality of its own grain, and nothing else. Hence the latter is weighted in measure in the star, i.e.

$$\begin{aligned} St_3(X) &= \mathcal{M}[V] = \pi/3\mathcal{M}[h^3] \qquad \text{in } \mathbb{R}^3 \\ St_2(X) &= \mathcal{M}[A] = \pi/3\mathcal{M}[h^2] \qquad \text{in } \mathbb{R}^2 \end{aligned}$$

In contrast, when X is arbitrary, such as a porus medium for example, the zone of direct vision Y_x varies from point to point. The star then allows one to define a mean volume of the pores, even if they are connected, and to calculate it from plane sections .

2.3.3 Curvatures

We conclude the chapter by some comments about curvatures that are applicable to both covariance and linear erosion, since they involve behaviors near the origin of these curves. We will approach them via limited expansions of the chord distribution, and treat successively the 2-D and 3-D cases.

Mean curvature in $\mathbb{R}^2$ Let $X \in \mathbb{R}^2$ be a set which admits a finite curvature C in each point of its boundary ∂X. Consider a point $x \in \partial X$, of radius of curvature $R = 1/C$ and of tangent direction α. Its contribution to $F_\alpha(r)$ is proportional to $R - \sqrt{R^2 - (r/2)^2} \approx r^2/8R$, hence, if $N_{+A}(\alpha)$ stands for the convexity number of the grains direction α we have

$$N_L(\alpha)F_\alpha(r) = r.\frac{N_{+A}(\alpha)}{4}E[\frac{1}{R}], \quad r \ \ small \tag{2.40}$$

As a varies, $N_{+A}(\alpha)d\alpha = du/R$ when $R > 0$ and 0 when not ; so that the directional average $f_1(r)$ of the $N_L(\alpha)F_\alpha(r)$ becomes

$$f_1(r) = \frac{r}{4}L(\partial X)\int_{R>0} du/R^2. \tag{2.41}$$

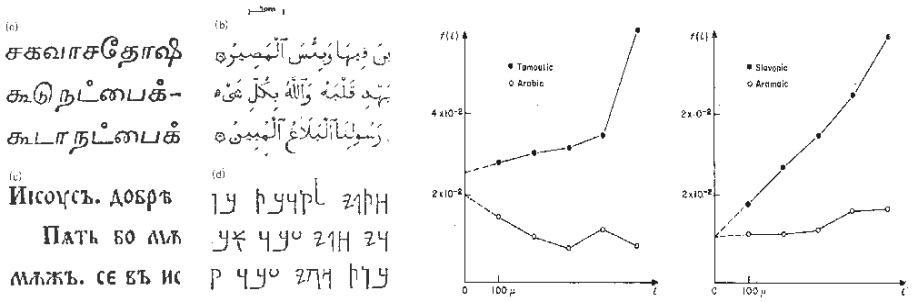

Figure 2.12: Roughnesses of handwritings.

By combining this result with the symmetrical one for the pores, we obtain

$$f(r) = \frac{f_1(r) + f_0(r)}{2} = \frac{r}{8}.L(\partial X) \int_{\partial X} du/R^2 = \frac{rE(C^2)}{8} \tag{2.42}$$

So, for r small, the chord histogram $f(r)$ is linear and its slope is equal to the quadratic mean of the curvature of X divided by eight .

We see in figure 2.12 a use of roughness measurents for comparing various handwritings. The aramean (d), the tamoulic (a) and the slavonian (c), do satisfy the model of finite curvatures (up to a nugget effect du to graphical noise); the slope of $f(h)$, practically zero for the aramean, increases from tamoulic to slavonian, whose curvatures are more and more narrow. In contrast, the model is not satisfied for classical arabic, with its surfeit of punctuation.

Mean and Total Curvatures in $\mathbb{R}^3$ The previous model extends from $\mathbb{R}^2$ to $\mathbb{R}^3$and brings into play, at each point, the average curvature C and the total curvature C' associated with the main radii of curvature R_1 and R_2 by the relations $2C = 1/R_1 + 1/R_2$ and $C' = 1/R_1R_2$. The limited expansion of $f(r)$ near the origin becomes now

$$f(r) = r\frac{E(3C^2 - C')}{8}. \tag{2.43}$$

Two cases are interesting :

- Set X is made of N_v disjoint grains homeomorphic to balls, then $f(r) = rE(3C^2 - 4\pi N_v)/8$.

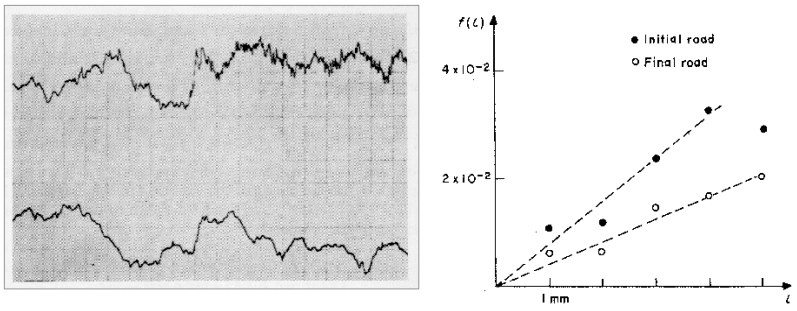

Figure 2.13: Roughnesses of two roads, from profiles of their surfaces.

- Set X is the sub-graph of a numerical function; in this case the term in C' vanishes and $f(r)$ reduces to

$$f(r) = r3/8E(C^2). \tag{2.44}$$

This last relation has been succesfully applied to roughness characterisation of roads, from profiles of their surfaces 2.13.

Two series of 1.000 and then 10.000 passages of 6,5 tons trucks going at 65km/h have been emulated on a test ring. By measuring $f(h)$ in six directions and applying the above formula, we find

$$\begin{aligned} E(C^2) &= 2,210^{-2}mm^{-2} \quad before\ wear; \\ E(C^2) &= 10^{-2}mm^{-2} \quad after\ \ wear. \end{aligned}$$

Remarkably, such a regular model (curvatures at each point are assumed!) still provides pertinent information here.

2.4 Exercises

2.4.1 Distribution function of the diameters of spheres from the law of their intercepts

When set X is made of disjoint spheres, one can go back from the granulometry $F_1(r)$ of the intercepts to that $F_3(r)$ of their diameters. The contribution of a sphere of diameter D to the chords $\geq r$ is $(\pi/4)(D^2 - r^2)$, which yields,

after integration over the diameters

$$N_L[1 - F_1(r)] = N_V \int_r^\infty (\pi/4)(D^2 - r^2)F_3(dD). \tag{2.45}$$

By differentiating both members with respect to r we obtain the equation

$$N_L f_1(r) = N_L F_1'(r)] = N_V(\pi/2)r[1 - F_3(r)] \tag{2.46}$$

from which we deduce the specific number of the spheres

$$N_V = 2/\pi N_L F_1'(0) \tag{2.47}$$

and their moments E_3, $\mathcal{M}_3$ as functions of the chords moments E_1, $\mathcal{M}_1$, namely

$$E_3(D^n) = [n/f\prime_1(0)]E_1(D^{n-2}) \ \ and \ \ \mathcal{M}_3(D^n) = (n+3/3)\mathcal{M}_1(D^n). \tag{2.48}$$

2.4.2 Poisson tesselations

The random function which is studied here-below comes from the "turning band method", a method from G. Matheron [81], and is constantly used in fractals construction. It is instructive for several reasons, not only as an application of Poisson lines, but also as a mean and variance-free example of a model, and that can only be reached through its increments. Consequently, we will also wonder about the meaning of the induced experimental covariances (critics also from G. Matheron, in his theory of regionalized variables[79]).

1. In R^1, a Poisson tesselation is defined as follows. Given a realization of Poisson points $\{x_1, i \in I\}$, we consider the function f, constant betwen two consecutive points, and which jump by s_i at point x_i , where the s_i are independent random variables, with a mean 0 and a variance σ^2.

Simulate f when the jumps value ± 1 with a probability 1/2, and when Poisson density varies from 1 to 10.

[*Procedure* **steps**, *with* $n \leq 40$ *; when n increases, notice the fluctuations for larger and larger ranges*].

2. Prove that the random function f has no mean nor variance, whereas the increment $|f(x+h) - f(x)|$ is stationary , with a zero mean and with a variance equals to $2\sigma^2 |h|$ so that the variogram of f is $\gamma(h) = \sigma^2 |h|$

[*We find* $2\sigma^2 |h|$ *by poissonizing the number of jumps on* $[0, h]$].

3. For h > 0, we know that the variogram of order one, $\gamma_1(h)$, is given by

$$\gamma_1(h) = E\,|f(h) - f(0)| = 2/\pi \int_0^\infty \{[1 - \exp \lambda h(\cos u - 1)/u]\}\, du \quad (2.49)$$

By a direct proof, show that

$$\textit{for small } h \quad \gamma_1(h) \ \sim 2\lambda h - 4\lambda^3 h^3 + \varepsilon(h^3) \quad (2.50)$$

$$\textit{for large } h \quad \gamma_1(h) \sim (\lambda h/\pi)^{1/2} \quad (2.51)$$

Measure the γ_1's for the above simulations of ex. 7.1. Why does the observed linear behaviour continues on quite long distances ?

[*In order to set the limited expansion near the origin that appears in rel.(2.50), assign the probabilities* P_n *to the upwards jumps and* P'_n *to the downwards ones, with* $P_n = P'_n = e^{-\lambda h}(\lambda h)^n/n!$. *For small h, we have*

$$\gamma_1(h) = P_0P_1' + P_1P_0' + 2\left[P_0P_2' + P_2P_0' + P_1P_1'\right] + ... \quad (2.52)$$

which leads to relation (2.50). The lack of second order terms explains the quasi-linear experimental behaviour. For large values of h, set $\theta = (\lambda h/2)^{1/2}$. *The sum of the positive jumps tends towards the variable* $\theta^2 + Y\theta$, *and the negative jumps one towards* $-\theta^2 + Y\theta$, *where Y is the reduced normal variable, hence*

$$\gamma_1(h) \ \sim \theta E\,|Y_1 - Y_2| = (\lambda h/\pi)^{1/2}\ . \quad (2.53)$$

Thus, γ_1, *which was initially proportional to* γ, *is finally proportional to its square root*].

4. Build rectangular Poisson tessalations, by summing the simulations of horizontal and vertical bands of the first question (two different densities λ_1 and λ_2 have to be considered). Measure the $\gamma_1(h)$ in the direction $\pi/2$. Interpret. What happens when these directions increase ?

[*We come back to the previous case, and note that jumps on a diagonal segment of length h admit a decomposition into two independent families of positive and negative jumps, with the same Poisson parameter* $(\lambda_1 + \lambda_2)h/2\sqrt{2}$. *Up to factor* $\sqrt{2}$, *this results in the sum of an horizontal and a vertical component for* γ, *as well as for* γ_1 *when h is small and h large. Finally, as these characteristics do not depend upon the number of*

directions, they remain valid under averaging of Poisson bands in all directions of the space : numerous fractal reliefs are simulated on this principle].

5. Critics of the "finitary" mathematician to the above approach : " What does a infinite random function f mean ? You will ever have finite means to build it, which will lead to finite numbers as well. So, please, keep your subtleties and variograms for yourself, and use a covariance as everyone else does".

Well, let's try for a realization f of vertical Poisson bands, that we intersect by a segment of lenght L, and whose direction is orthogonal to the banding.

(a) Estimate the hypothetical covariance $C(h)$, which in fact does not exist here, from the experimental quantities

$$m^* = (1/L)\int_0^L f(x)dx \quad \text{and} \quad C^*(x,y) = (f(x)-m^*)(f(y)-m^*). \tag{2.54}$$

By putting

$$C^*(h) = (1/L-h)\int_0^{L-h} C^*(x+h,x)dx \tag{2.55}$$

Show that for h>0

$$E\left[C^*(x+h,x)\right] = 2L/3 + (x^2+(x^2+h^2))/L - 2x - 2h \tag{2.56}$$

and, by integrating in x, derive

$$E\left[C^*(h)\right] = L/3 - 3/4h + 2h^2/3L \tag{2.57}$$

Calculate the mean of the experimental variogram and covariance on several band simulations. Comment on the results.

[*An apparent variance* $E\left[C^*(0)\right] = L/3$ *is found, depending on the length L of the segment considered. It is a pure artefact, since the true variance is infinite. Although there is no covariance (the variogram is linear), the biases introduced by this procedure of estimation result in an apparent confirmation of the existence of a covariance (with a range!). It will be noted also that the stucture of the phenomenon is extremely distorded: not only is the straight line replaced by a parabola, but even the* slope at the origin is changed (3/4 instead of 1) *Thus* $C^*(h)$ *represents almost nothing of the true structure*]

(b) Show that the experimental variogram

$$2\gamma^*(h) = (1/L - h) \int_0^{L-h} [f(x+h) - f(x)]^2 \, dx \tag{2.58}$$

has an expectation

$$E[\gamma^*(h)] = \gamma(h) = |h| \tag{2.59}$$

and does not run into the same bias problem as $C^*(h)$.Comment

[*We observe that the experimental variogram of relation (2.58) does not involve any cumbersome mean value (so that* $E(\gamma^*(h) = \gamma(h))$*; it is linked to* $C^*(h)$ *by the expression.*

$$2C^*(h) = -2\gamma^*(h) + (L/L - h)m^* + (1/L - h) \int_h^{L-h} [(f(x) - m^*]^2 \, dx \tag{2.60}$$

which introduces a variance in right member. When the experimental variance of a phenomenon increases with the size of the zone investigated, without tending towards a horizontal asymptote, it is not wise to fit the structure under study with a stochastic model possessing a covariance. However, in such a case, the variogram still exists and its estimation is significant. Consequently it provides a safer *method than the covariance.*]

.

Chapter 3

Boolean Model and Random Sets

3.1 Introduction: a counterpoint

The quantitative description of random sets has to be carried out at two different levels. First of all, we have to define them properly, i.e., provide them with adequate axiomatics, and then derive their main mathematical properties (characterization of random sets by their Choquet functionals, infinite divisibility, etc.). However, a purely mathematical approach would not be sufficient, and must be complemented with a forthright description of the random sets, i.e., by effectively giving recipes for the construction of random sets possessing desirable morphological properties. For the sake of pedagogy, it is better to start with this second aspect, and to concentrate on one particular model. We propose the Boolean model, since it is especially interesting in itself, and lends itself to many attractive derivations. Moreover, the model, and its derivations, are for a large part due to the Centre de Morphologie Mathematique of Fontainebleau.

The counterpoint between the Boolean model and the general properties of random sets results in the following sections :

Boolean model	*Random sets*
2 Construction	3 Definition and Basic Properties
4 Functional Moments	5 Infinite Divisibility
6 Convex Primary Grains	7 Semi-Markov RACS
8 Specified Boolean RACS	9 Derived models

3.2 Construction of Boolean Sets

The first outline of the Boolean model appears in the literature with Solomon [148]and B. Matern [74] ; the latter took a disk with a constant radius as primary grain, and calculated the covariance of the model in this particular case. A few years later, G. Matheron [76] gave the general definition of the model, that we adopt here, and calculated the key formula 3.6. The literature on Boolean models and on their uses is copious, a non exhaustive list on the subject inludes the books of D. Jeulin [60] (*use in physics)*, G. Ayala [3] (*statistical inference)*, I. Molchanov [102] (*estimations in the general case*), and the papers of A. Greco and Al [37] (*Multiphased model*), J. Goutsias [34] (*discrete approach*), M. Schmitt [144] (*density estimation in the general case*), J. Serra [128] (*overview and derivated models*) and S. Stoyan [151] (*spherical primary grains*).

The definition of the Poisson point process in $\mathbb{R}^n$ is well known. This random set of points is characterized by the following two properties :

(a) If B and B' are two sets such that $B \cap B' = \phi$, the numbers $N(B)$ and $N(B')$ of points falling in B and B' are two independent random variables.

(b) The elementary volume dv contains one point with probability $\theta\,(dv)$ and no points with probability 1- $\theta\,(dv)$. The measure θ is called the density of the process. Here we will take θ = constant, because it leads to more geometrically interpretable results.

Suppose we take a realization of a Poisson process of constant density θ, and consider each point as the germ of a crystalline growth. If two crystals meet each other, we suppose that they are not disturbed in their growth, which stops independently for each component. Let us transpose this description in terms of random sets. The I points of the Poisson realization are at the points $x_1\,(i \in I)$ in $\mathbb{R}^n$. The elementary grain is an almost surely compact random set X' ; we pick out various realizations X'_i of X' from its space of definition, and implant each X'_i at the corresponding point $x_{i.}$ The different X'_i are thus independent of each other.

We shall call the realization X of a Boolean model, the union of the various X'_i after implantation at the points x_i :

$$X = \underset{i \in I}{\cup} X'_i \tag{3.1}$$

The Boolean model is extremely flexible : it is a first step, where one admits only negligible interactions between the particles X'_i . Figure 1 represents a typical Boolean structure.

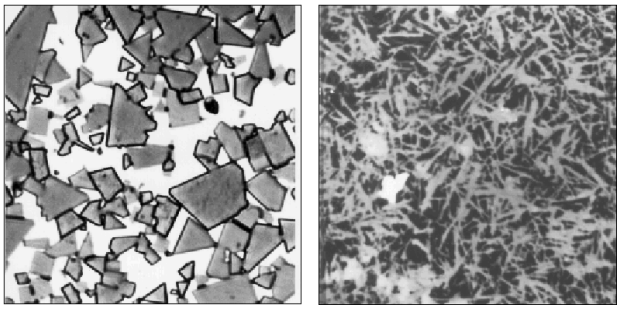

Figure 3.1: Natural objects that fit with Boolean RACS: wolfram carbide (on the left) and ferrite crystals (on the right).

3.3 Random Sets

We have just introduced a random closed set X (in brief, a RACS) via the technique which allows us to construct it (in the following, we use the same symbol X for denoting a RACS and its realization). However, just like a random variable, a RACS is mathematically defined from a collection of events, namely the relationships "K misses X", where K describes the class of compact sets. These events are governed by the classical axioms of probability, which require first a σ-algebra, call it σ_f and then a probability P on the measurable space $(\mathcal{F}, \sigma_f)$, where $\mathcal{F}$ denotes the set of closed sets in $\mathbb{R}^n$. The σ-algebra σ_f is generated by all countable unions of the events and by their complements. To define P we associate with any event V of σ_f the probability that this relation V is true.

Here, a few topological comments are necessary. To handle the random sets correctly, we must be able to express how a sequence $\{X_i\}$ of sets tends towards a limit X. On the other hand, we have to restrict the class $\mathcal{P}(\mathbb{R}^n)$ of all possible subsets of $\mathbb{R}^n$. Indeed the Euclidean space is too rich for our purpose. For example, a set such as "all the points with irrational coordinates in the plane" has absolutely no physical meaning. In order to make this simplification, define the distance ρ, from point x to set X, as follows :

$$\rho(x, X) = \inf_{y \in X} d(x, y), \qquad x \in \mathbb{R}^n, \qquad X \in \mathcal{P}(\mathbb{R}^n), \tag{3.2}$$

where d is the Euclidean distance. With respects to ρ, there is no difference

between a set X and its topological closure ∂cX (i.e., X plus its boundary), since $\rho(x, X) = \rho(x, \partial cX), \forall x, \forall X$. In other words, all the notions derived from ρ will not be related to the parts $\mathcal{P}(\mathbb{R}^n)$ of $\mathbb{R}^n$, but to the equivalence classes of sets which admit the same closure. For example, the points with irrational coordinates of $\mathbb{R}^2$, and the whole plane itself, will be considered as *identical*. Hence, from now on it suffices to concentrate upon the class of the closed sets of $\mathbb{R}^n$. The distance ρ generates a topology, called the hit-or-miss topology. Matheron [78] [82] and Kendall [63] exhaustively studied it in a more general frame than $\mathbb{R}^n$. By definition a sequence $\{X_i\}, X_i \in \mathcal{F}$, converges towards a limit $X \in F$ if and only if, for any $x \in \mathbb{R}^n$, the sequence$\rho\{x, X_i\}$ converges towards $\rho(x, X)$ in $\mathbb{R}_+$. From this standpoint, we can derive all the basic topological notions, such as neighborhoods, continuity, semicontinuity, etc. We quote only one result, for it will be useful below.

Proposition 3.1 *An increasing mapping Ψ from $\mathcal{F}$ into itself (or more generally from $\mathcal{F} \times \mathcal{F} \to \mathcal{F}$) is upper semi-continuous (u.s.c.) if and only if $X_i \downarrow X$ in $\mathcal{F}$ implies $\Psi(X_i) \downarrow \Psi(X)$ in $\mathcal{F}$*

Here, "$X_i \downarrow X$ " means that $X_{i+1} \subset X_i$ and $X = \bigcap_i X_i$. It is not obvious that, if X is a RACS and Ψ an arbitrary set transformation, the transform $\Psi(X)$ is still a RACS. However, if Ψ is a *semi-continuous* mapping from $\mathcal{F} \to \mathcal{F}$ (or $\mathcal{F} \times \mathcal{F} \to \mathcal{F}$), the resulting set $\Psi(X)$ is always a RACS. Hence, $X \cup X'$, $X \cap X'$, ∂X, X^c, $X \oplus K$, $X \ominus K$, and the finite iterations of these transformations provide RACS (Note that a mapping may be semi-continuous and *not* increasing, e.g., the boundary mapping $X \to \partial X$). Similarly, the volume, $V(X)$, in $\mathbb{R}^3$; and the area $A(X)$, in $\mathbb{R}^2$ which are semi-continuous mappings $\mathbb{R}^3 \to \mathbb{R}^+$ (or $\mathbb{R}^2 \to \mathbb{R}^+$) provide random variables.

It is well known that the probability distribution associated with an ordinary random variable is completely determined if the corresponding distribution function is given. There is a similar result for RACS. If X is a RACS and P the associated probability on σ_f define

$$Q(B) = P\{B \subset X^c\} \tag{3.3}$$

to be the probability that X misses a given compact set $B \in \mathcal{K}$. That is, we obtain a function Q on $\mathcal{K}$, called the functional moment, associated with the probability P. Conversely, the probability P is completely determined

if the function Q on $\mathcal{K}$ is given (Matheron-Kendalls'theorem [80, 63]). It is interesting to find the necessary and sufficient conditions for a given function Q to be associated with a RACS :

(i) One must have $0 \leq Q(B) \leq 1$ (Q is probability) and $Q(\phi) = 1$, since the empty set misses all the other ones.

(ii) If $B_i \downarrow B$ in $\mathcal{K}$, we must have $Q(B_i) \uparrow Q(B)$.

(iii) Let $S_n(B_0; B_1...B_n)$ denote the probability that X misses the compact set B_0, but hits the other compact sets $B_1...B_n$. These functions are obtained by the following recurrence formula :

$$\begin{aligned} S_1(B_0; B_1) &= Q(B_0) - Q(B_0 \cup B_1), \\ S_n(B_0; B_1...B_n) &= S_{n-1}(B_0; B_1...B_{n-1}) - S_{n-1}(B_0 \cup B_n; B_1...B_{n-1}). \end{aligned}$$

These S_n, which are probabilities, must be ≥ 0 for any integer n and any compact sets $B_0, B_1...B_n$.

The last two prerequisites make the quantity $1 - Q$ an *alternating Choquet capacity* of infinite order. The three requirements (i), (ii), (iii) must obviously be satisfied by the function Q. Choquet [20] proved that they are also sufficient. His basic theorem orients us toward the calculations to perform in order to characterize a RACS. The morphological interpretation of rel (3.3) is clear. When B is centered at point $x, Q(B)$ is nothing but the probability that x belongs to the pores of the dilate $X \oplus \check{B}$, i.e. the porosity $q_B(x)$ of $X \oplus \check{B}$ at point x.

3.4 Moments of the Boolean Sets

We now apply Matheron-Kendall's theorem, which has just been stated, to the case of the Boolean model. By definition, the primary grain X' is known, and the question is to express the $Q(B)$'s of X as functions of those of X'. Consider an arbitrary point a. Denote by $\eta(a)$ the probability that point a lie in grain X, and look for the probability that a be not in set X. In the elementary zone dz, two mutually exclusive favorable events may occur

- either no germ, with a probability $1 - q(dz)$

- or one germ, but the grain X_i does not reach a : Probability $q(dz)[1 - \eta(a - z)]$.

By composition of these two probabilities and integration of z over $\mathbb{R}^n$,

we find for porosity q

$$q = Q(a) = Prob.\{a \in X^c\} = exp[-\theta \int_{\mathbb{R}^n} \eta(a-z)dz] = exp\{-\theta MesX\} \tag{3.4}$$

More generally, if B_a stands for a compact set centered at point a, then

$$B_a \subseteq X^c \Leftrightarrow a \in X^c \ominus B \Leftrightarrow a \in (X \oplus \check{B})^c = \cup\{X_i \oplus \check{B}, \ i \in I\}^c \tag{3.5}$$

Hence, B_a is included in the pores of the boolean RACS X iff point a belongs to the pores of the boolean RACS of primary grain $X\prime \oplus B$, i.e.

$$P\,(B \subset X^c) = Q(B) = Prob\{B \subseteq X^c\} = exp\{-\theta\overline{Mes}(X\prime \oplus B)\} \quad \forall B \in \mathcal{K} \tag{3.6}$$

Now, according to Matheron-Kendall theorem, a RACS is characterized by the probabilities $Q(B)$ as B spans the class $\mathcal{K}$ of the compact sets. Thus, relation (3.6) describes completely the RACS X , and shows, among others, that it is stationary. This relation, which links the functionals of X to those of X', is the *fundamental* formula of the model [76][82]. One derives from it a series of important properties and formulas.

3.4.1 Set Properties

α.We see from 3.6 that $Q(B)$ does not depend on the location of B. Hence the Boolean model is *stationary*. One can also prove that it is *ergodic*, i.e. the spatial averages for one realization tend toward the corresponding $Q\,(B)$. Thus, we can speak of porosity of a specific surface, covariance, etc., without referring to a particular portion of the space.

β. RACS X *is closed under dilation*. We derived from 3.6 that the dilate of X by K (K a deterministic compact set) is still boolean with primary grain $X' \oplus \check{K}$.

γ. *The cross-sections of* X *are Boolean*, since 3.6 does not depend on the fact that B belongs to a subspace of R^n. Similarly, if we cut a thick slice of X, limited by two parallel planes, of normal ω, and if we project the slice on a plane normal to ω, the projection set is still Boolean.

δ. The Boolean model is *infinitely divisible* (this basic property in fact implies all the other ones of this section). "Infinitely divisible" means the following : if one picks out two realizations of the model, and superimposes them, taking the set union of phases X, then the result is again a model of the same family.

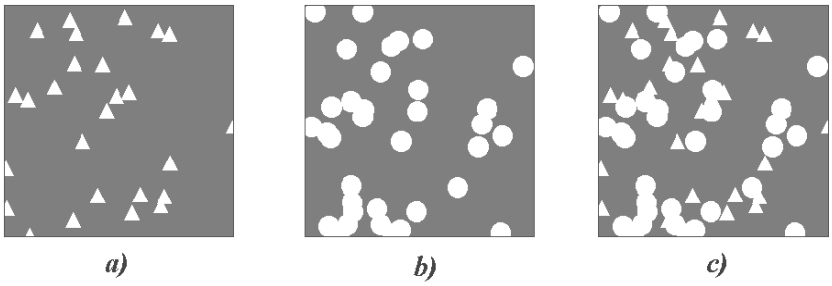

Figure 3.2: The union of two Boolean sets is still Boolean

ϵ. *Domain of attraction.* Just as the normal law appears as the limit of an average of independent random variables, the Boolean model also turns out to be the final term of an infinite union of *other* random sets. One says that it has a certain domain of attraction. The following result ([27], [129]) illustrates this point.
Let X be a random partition of the space, arbitrary but stationary and ergodic. From X, construct a set Y by assigning each class X' of the partition to the phase "grain" with a probability p, independently from one class to another . Now superimpose n realizations of Y, and let Y_n denote the intersection of the grains of the n realizations. Assuming that $np \to \theta\,(0 < \theta < \infty)$ as $n \to \infty$ (if not, $Y \downarrow$ is trivially equal to $\emptyset$!), and denoting by $Q_n(B)$ the functional moments of Y_n, we have

$$\lim_{n\to\infty} Q_n(B) = \exp\left(-\theta\ \overline{Mes}\ X'\right)^{-1\cdot} \overline{Mes}\left(X' \oplus B\right), \tag{3.7}$$

i.e., according to Matheron-Kendall's theorem, a Boolean model of density $\theta(\overline{Mes}\ X')^{-1}$ and with primary grains the class X' of the initial partition.

ζ. The number of primary grains hitting B follows a *Poisson distribution* of parameter $\theta\overline{Mes}\,(X' \oplus \check{B}B)$. This is a direct consequence of the infinite divisibility. D.Stoyan [151] enlarged this result to the case of a density $\theta(x)$ variable over the space.

3.4.2 Applications of the Fundamental Formula

α. *Porosity.* Reduce the structuring element B to one point ; then

$$B = \{.\} \Rightarrow Q(B) = q = \exp\left(-\theta\,\overline{Mes}\ X'\right) \tag{3.8}$$

β. *Covariance.* Take for B two points that are vector h apart

$$B = \left\{ . \overset{h}{\leftrightarrow} . \right\} \Longrightarrow Q(B) = C_{00}(h) = q^2 e^{K(h)}, \tag{3.9}$$

where $K(h) = \overline{Mes}(X' \cap X'_h)$ is the geometric covariogram of set X. The covariance $C_{00}(h)$ represents the probability that the two points of B lie in the pores. For the covariance $C_{11}(h)$ of the grains (i.e., $P(B \in X)$), we have

$$C_{11}(h) = 1 - 2q + C_{00}(h) = 1 - 2q + q^2 e^{\theta K(h)} \tag{3.10}$$

γ. *Law of the first contact.* Suppose a random point x in the pores is chosen uniformly, and let R be its distance to the grains. Denoting by $F(r)$ the distribution function of the random variable R, we obtain

$$1 - F(r) = \frac{Q(Br)}{q}, \tag{3.11}$$

where B_r is the ball of radius r (or the disk in $\mathbb{R}^2$).

δ. *Specific surface and perimeter.* To avoid some pathological anomalies, such as fractal sets, we assume X' to be regular enough (a finite union of compact convex sets, for example). Then the specific surface of X, i.e., the surface S_V of ∂X per unit volume, in $\mathbb{R}^3$, and the specific perimeter U_A of X, in $\mathbb{R}^2$, are the derivative of $Q(Br)$ in $r = 0$, that is

$$\begin{aligned} S_V &= \theta.\text{Pcs}\left(X'\right).e^{-\theta\overline{V}(X')} \qquad \text{in } \mathbb{R}^3, \\ U_A &= \theta.\overline{U}\left(X'\right).e^{-\theta\overline{A}(X')} \qquad \text{in } \mathbb{R}^2. \end{aligned} \tag{3.12}$$

Before going on with the Boolean model for more specific cases, we now resume the analysis of the general properties suggested by this section.

3.5 Infinite Divisibility

The key notion we met in the preceding section is that of *infinite divisibility.*

Definition 3.2 *We say that a RACS X is infinitely divisible with respect to the union, if for any integer $n > 0$, X is equivalent to the union $\cup Y_i$ of n independent RACS Y_i, $i = 1...n$, equivalent to each other.*

This property depends only on the functional Q. The following theorem, from G. Matheron [82], characterizes the infinitely divisible RACS.

Theorem 3.3 *A function Q on $\mathcal{K}$ is associated with an infinity divisible RACS without fixed points, if and only if there exists an alternating capacity of infinite order φ satisfying $\varphi(\phi) = 0$ and $Q(B) = \exp\{-\varphi(B)\}$.*

This theorem opens the door to the Boolean sets, but not only to them. Imagine, for example, the union in $\mathbb{R}^3$of a Boolean set and trajectories of Brownian motions. The result is infinitely divisible, but not reducible to Boolean structures. For random variables, a classical theorem of P. Levy states that an infinitely divisible variable is a sum of independent Gaussian and Poisson variables. It seems that the equivalent of such a theorem does not exist for random sets, although the Boolean sets and the Poisson flats are in fact the major representatives of this type of model.

Beyond the infinite divisibility is another more demanding structure, namely, that of the RACS *stable with respect to union.* A RACS X belongs to this category when, for any integer n, a positive constant λ_n can be found, such that the union $X_1 \cup X_2 ... \cup X_n$ of n independent RACS equivalent to X is itself equivalent to $\lambda_n X$. Obviously a stable RACS is necessarily infinitely divisible, but the converse is false. The following theorem (Matheron [82]) characterizes stable RACS. A RACS X without fixed points is stable with respect to union if and only if its functional $Q(B) = \exp(-\varphi(B))$ for a capacity of infinite order φ satisfying $\varphi(\phi) = 0$ and homogeneous of degree $\alpha > 0$, i.e.,

$$\varphi(\lambda B) = \lambda^{\alpha} \varphi(B) \qquad (\lambda > 0, B \in \mathcal{K}) \tag{3.13}$$

The Poisson lines (in $\mathbb{R}^2$) or planes (in $\mathbb{R}^3$), and the Brownian trajectories (in $\mathbb{R}^3$), are stable RACS. Indeed it results from their definition that the stable RACS are self-similar, and model the sets described by B. Mandelbrot [70].

3.6 Convex Primary Grains

We go back to the Boolean thread of ideas. For the results we derived from rel.(3.6) until now, we did not need to make explicit the quantity $\overline{Mes}$ $(X' \oplus \check{B}_x)$. If we want to go further in the analysis, we now must try to exploit it. There is a particular, but particularly important case, where $\overline{Mes}$ $(X' \oplus B)$ admits a simple expression ; it is when both X' and B are convex. Then Steiner's formula is applicable (J. Steiner (1840) reedited in Miles and Serra [100], Blaschke [13]), and provides several new fruitful results. Consequently, we now assume the compact random set X' to be almost

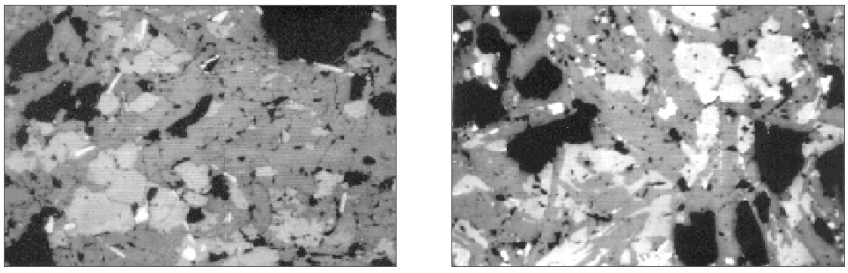

Figure 3.3: Two Caucasian dolerites of the same volcano, but from two different eruptions.

surely convex. For the sake of simplicity we also assume that the various X' which constitute X are uniformly oriented. This latter hypothesis is not compulsory, but allows us to reduce the notation without substantially modifying the meaning of the results. (For more detailed expressions, see [76] and [129]).

3.6.1 Stereology

Start from a Boolean set X_3 in $\mathbb{R}^3$, with a Poisson density θ_3, and primary grain $X'_3$of volume v'; surface s'; mean width d'. On any test plane Π , X_3 induces a Boolean set $X_2 = X_3 \cap \Pi$ of density θ_2, of primary grain area a' and perimeter u'.

Since the covariance is the same for both RACS of $\mathbb{R}^3$ and of $\mathbb{R}^2$, we can write

$$\theta_3 v' = \theta_2 a' \quad ; \quad \pi\theta_3 s' = 4\theta_2 u' \quad ; \quad \theta_3 d' = \theta_2 \tag{3.14}$$

The primary grains X'_2 induced on Π are related to X'_3 by the following formula :

$$v' = \frac{1}{2\pi} \cdot a' \cdot d' \tag{3.15}$$

(Formulas (3.14) and (3.15) can be generalized to the nonconvex case; [129]). The relations involved in (3.14) allow us to set and to solve the classical problem of "Nucleation versus Growth", that we introduce here by means of an example.Figure 3.3 depicts rocks micrographs from two eruptions of the same volcano. The second one displays more pores (in black) . Did the physical process generate more 3D pores, or larger ones ?

Now, the average pore number in section is the product of the 3D number of pores by their mean width, which prevent us from separating the effect of nucleation from that of growth, unless we use a model. Assume that both textures are modeled by boolean RACS where the grains of the model are the physical pores. Let $(\theta_3'; v'; s'; d')$ be the parameters of the first one, and $(\theta_3"; v"; s"; d")$ those of the second one. A pure growth would imply that

$$\theta_3"v"/\theta_3'v' = k^3 \;\; ; \;\; \theta_3"s"/\theta_3's' = k^2 \;\; ; \;\; \theta_3"d"/\theta_3'd' = k \tag{3.16}$$

whereas in a pure nucleation, these three ratios are equal. Now, we draw from the stereological relations (3.14) that

$$\theta_3"v"/\theta_3'v' = \theta_2"a"/\theta_2'a' = 1.227 \quad \text{and} \quad \theta_3"s"/\theta_3's' = \theta_2"u"/\theta_2'u' = 1.224. \tag{3.17}$$

Therefore, in the present case, the physical process may be considered as a nucleation.

3.6.2 Convex erosions

Consider a 2-D Boolean set X_2, with parameters (θ_2, X_2'), and take for B's, first the segments of length l and second the families λB of sets similar to a given plane convex set B, having nonzero area. According to Steiner's formula we can write

$$Q(l) = \exp\left(-\theta_2\left[\overline{A}\left(X_2'\right) + (l/\pi)\,\overline{U}\left(X_2'\right)\right]\right), \tag{3.18}$$

$$Q\left(\lambda B\right) = \exp\left(-\theta_2\left[\overline{A}\left(X_2'\right) + (\lambda/2\pi)\,U\left(B\right)\overline{U}\left(X_2'\right) + \lambda^2 A\left(B\right)\right]\right). \tag{3.19}$$

We immediately derive from (3.18) the pore traverse length distribution $G\left(l\right)$,

$$1 - G\left(l\right) = \frac{Q'\left(l\right)}{Q'\left(O\right)} = \exp\left(-\theta_2\left(\overline{U}\left(X_2'\right)/\pi\right)\cdot l\right), \tag{3.20}$$

and from (3.19) and (3.11), the law $F\left(r\right)$ of the first contact;

$$1 - F\left(r\right) = \exp\;\left(-\theta_2\left[r\overline{U}\left(X'\right) + \pi r^2\right]\right). \tag{3.21}$$

Now we can perfectly well consider X_2 as the plane cross section of a Boolean set X_3 in space. What knowledge of X_3 can we get from X_2 ? Obviously not an exhaustive one (take, for example, the union of X_3 and a 3-D Poisson point process Z; X_3 and $X_3 \cup Z$ induce the same X_2). However,

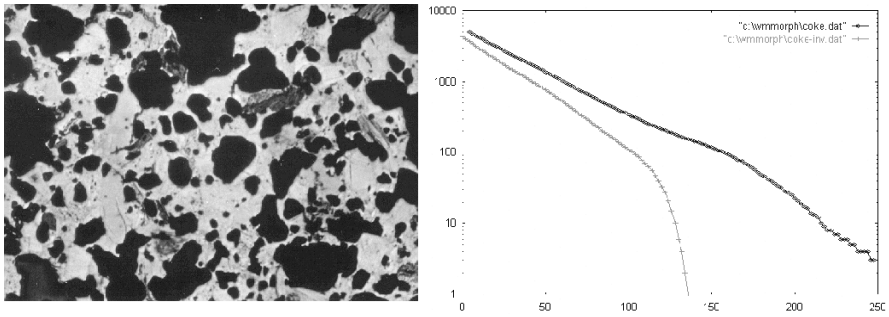

Figure 3.4: Left: polished section of formed coke G×10^4 (pores in black); right: linear erosions of the pores (in black) and of the carbon (in grey) plotted in semi-Log coordinates.

using (3.14), (3.15) and (3.29), we can interpret the functionals (3.18) and (3.19) in terms of $\mathbb{R}^3$, i.e.,

$$Q(l) = \exp\left(-\theta_3\left[\overline{V}\left(X_3'\right) + (l/4)\,\overline{S}\left(X_3'\right)\right]\right), \tag{3.22}$$

$$Q(\lambda B) = \exp\left(-\theta_3\left[\overline{V}\left(X_3'\right) + (\lambda/8)\,U(B)\,\overline{S}\left(X_3'\right) + \left(\lambda^2/2\pi\right)A(B)\,\overline{M}\left(X_3'\right)\right]\right). \tag{3.23}$$

Comparison of (3.19) and (3.23) is instructive. In $\mathbb{R}^2$ we see that when B describes the class of compact convex sets, $Q(B)$ involves only three parameters of X, namely θ_2, $\overline{A}\left(X_2'\right)$ and $\overline{U}\left(X_2'\right)$, which can easily be estimated from (3.19). However, these three parameters do not exhaustively characterize X, since B only spans the class of compact *convex* sets. In other words, the morphological notions related to the convexity of B, such as size distributions, can easily be studied, but others, angularities, for example, cannot. In $\mathbb{R}^3$ we have a similar result, since RACS X turns out to be described by the four parameters θ_3, $\overline{V}\left(X'\right)$, $\overline{S}\left(X'\right)$ and $\overline{M}\left(X'\right)$. Unfortunately, when the structuring element B moved in $\mathbb{R}^3$ is planar, it does not allow us to access all the parameters, but only their linear combinations given by Log $Q(\lambda B)$ in (3.23), which provide only the three terms $\theta_3\overline{V}\left(X_3'\right)$, $\theta_3\overline{S}\left(X_3'\right)$, and $\theta_3\overline{M}\left(X_3'\right)$. In order to go further, we can alternatively specify the primary grain more completely as we will do below, or calculate the two-dimensional $Q(\lambda B)$ for the projection of the thick sections of X_3. For example, if d is the thickness of the section, and B is a polygon with n

sides, we have :

$$Q(\lambda B) = \exp\left(-\theta_3 \left\{ \begin{array}{c} \text{Þc}V(X_3') + \frac{\lambda}{8}[U(B) + d(n-2)]\,\text{Þc}S(X_3') \\ +\frac{\lambda^2}{4}[2A(B) + dU(B)]\,\text{Þc}M(X_3') + \lambda^3 dA(B) \end{array} \right\}\right) \tag{3.24}$$

which enables us to estimate the four characteristics of X_3 ([129] ; see also [98]).

Take for example the form coke depicted in fig.3.4. We see from the plot on the right that the pores may be considered as Boolean, but that the solid phase cannot. The we draw from the plot that

$$\theta_2 a' = -Log\ 0.58 = 0.54 \qquad \text{and} \quad v' = \theta_2 u' = -8/Log\ 0.58 = 14.8 \tag{3.25}$$

and from the stereological relations (3.14) that $\theta_2 a' = \theta_3 v' = 0.54$ and $\theta_2 u' = (\pi/4)\theta_3 s' = 11.6$. Nevertheless, one cannot extract θ_3 and v' from these only pieces of information.

3.7 Semi-Markov RACS

The underlying concept which governs Boolean textures with convex primary grains is the semi-Markov property. As soon as the chord distributions for the pores are exponential (3.18), we can suspect the model to be somehow Markov. Nevertheless the grain chords are *not* exponential , and thus X never induces a 1-D Markov process on any linear cross section. Such an asymmetry leads us to the Matheron definition of the semi-Markov property [80].

Definition 3.4 *Two compact sets B and B' are said to be separated by a compact set C if any segment (x, x') joining a point $x \in B$ to a point $x' \in B'$ hits C. Then a RACS X is said to be semi-Markov if for any B and B' separated by C the RACS $X \cap B$ and $X \cap B'$ are conditionally independent, given $C \cap X = \emptyset$.*

Proposition 3.5 *The RACS X is semi-Markov if and only if its functional Q satisfies the relationship*

$$Q\left(B \cup B' \cup C\right) \cdot Q(C) = Q(B \cup C) \cdot Q\left(B' \cup C\right), \tag{3.26}$$

where B and B' are separated by C.

In particular, if the union $B \cup B'$ is compact and convex, then they are separated by their intersection $B \cap B'$ and the semi-Markov property implies

$$Q\left(B \cup B'\right) \cdot Q\left(B \cap B'\right) = Q\left(B\right) \cdot Q\left(B'\right). \tag{3.27}$$

Moreover, if X is indefinitely divisible, the converse is true, and rel (3.27) implies that X is semi-Markov. One can rediscover this result intuitively in the following way. Intersect X by the straight line Δ, and pick up one point x in the pores of $X \cap \Delta$. x separates Δ into two half-lines Δ_1 and Δ_2. A primary grain X' of X which hits Δ_1 cannot hit Δ_2 since X' is convex ; moreover, the various primary grains are independently located, thus any event on $X \cap \Delta_1$ is independent of any other one on $X \cap \Delta_2$, given $x \in X^c$.

The characterization relation (3.12) points out that it is interesting to combine the three properties of stationarity, infinite divisibility and semi-Markovianness. Indeed, according Matheron [82], any RACS of $\mathbb{R}^3$ satisfying these three conditions is equivalent to the union of three stationary independent RACS, $X_1 ... X_3$. X_1 is a Boolean set with convex grains; X_2 and X_3 are the unions of cylinders the bases of which are 2-D and 1-D Boolean sets with convex grains. Note that if these two latter Boolean models have points as primary grains, the associated cylinders become Poisson lines and planes, respectively. In other words, the Poisson plane and line networks and the Boolean models are the two prototypes from which any stationary, infinitely divisible semi-Markov set may be constructed (the same comment applies to the RACS in $\mathbb{R}^2$). If we now replace infinite divisibility by the stability condition, then we restrict the possible class of sets. Indeed the only RACS which are stationary, stable and semi-Markov are the Poisson flat networks (planes and lines in $\mathbb{R}^3$, lines in $\mathbb{R}^2$).

Unlike the classical Markov chains, the semi-Markov concept does not require any ordering relation in $\mathbb{R}^2$, and thus is isotropic. Defined in the continuous space, it can lend itself to digital sampling, and defined in $\mathbb{R}^2$ or $\mathbb{R}^3$, it is connected with spatial textures directly, and not via line sections. Its natural field of application is textures presenting a limited number of phases, which can thus be modeled by sets.

3.8 Testing Boolean RACS

3.8.1 Test approach

Again we go back to the Boolean thread of ideas and we wonder how to test whether a texture is Boolean. Altough general approaches have been proposed by M. Schmitt [144], and by I. Molchanov [102] for the general case, it is mainly the convex (and most frequent) case that lends itself to efficient tests, based on the Steiner formula. Indeed by making varying the planar shapes of the structuring element B (e.g. segments, squares, hexagons), one obtains :

- various functions $LogQ(\lambda B)$ to be fitted with straight lines, parabolae, etc;

- and, if the fits are satisfactory, various estimates of $\theta a'$, $\theta u'$ and θ (in $\mathbb{R}^2$) and of $\theta v'$, $\theta s'$ and $\theta d'$

These tests hold on both Boolean hypothesis and convexity of X'. One can design other more or less sophisticated tests, based on the variance of X' for example, that avoid convexity assumption. The one which follows is just based on porosity and on number of intercepts. Start from the Choquet functional $Q(l, \alpha)$ for B a small segment of length l and direction α. As $l \to 0$ we have at the origin

$$\begin{aligned} \text{porosity } q &= Q(0) = exp\{-\theta a\} \\ \alpha - \text{specific diameter} &= Q'_\alpha(0) = -\theta d'_\alpha Q(0) \end{aligned}$$

which provide two relations to estimate q a and q da from the experimental data (note that no convexity assumption for the primary grain has been made at this level). We will check the soundness of the approach on a simulation, where the actual data are the following

Data of the simulation X	*Parameters to estimate*
field area 800×600 *pixels*	$\theta = 4/4800 = 8.33 \times 10^{-4}$
mean area $a' of\ X' = 622$	$\theta a' = 8.33 \times 0.0622 = 0.518$
diameter $d' of\ X' = 24.9$	$\theta d' = 24.88 \times 8.33 \times 10^{-4}$
mean number of germs $= 400$	$= 2072 \times 10^{-5}$

The experiments made on the simulation shown in fig.3.5 (left) yield the following values

Measured values in field Z	*Estimated parameters*
pores area $X^c \cap Z = 273191$	$(\theta a')^* = ln(1/q^*) = 0.564$
diametral variation of $X \cap Z = 5635$	$(\theta d')^* = 1953 \times 10^{-5}$

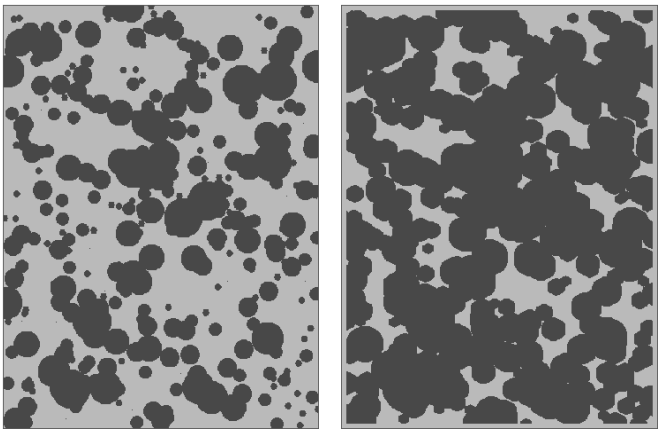

Figure 3.5: Left: simulation to be tested ; right: dilate of the simulation by an haxagon of size 10.

A result which is acceptable. It remains to estimate θ. We will proceed by dilating the simulation according to an hexagon H of size 10 (hence of a vertical diameter 21), which results in a new boolean RAC of same density θ as previously but of vertical diameter $d'' = d' + 21$. Hence we obtain $\theta = (\theta d'' - \theta d')/21$, an equality which provides the basic relation of the test. Numerically speaking, we have to measure the area of the pores of set $X \oplus H$ and also its diametral variation in the eroded field $Z \ominus H$ (i.e.100 331 and 3643 respectively), so that

$$\theta^* = [(\theta d'')^* - (q d')^*]/21 = (3631 - 1953)/21 = 7.98.10^{-4}. \qquad (3.28)$$

Without being as precise as the two estimates $(\theta a)^*$ and $(\theta d)^*$, the estimate θ^* is still acceptable.

3.8.2 Heuristic approach

The Boolean model provides several relationships between accessible parameters and indirect ones . The Central Limit Theorem suggests to use them a priori, i.e. in situations where the model is possibly not satisfied. The counting algorithm for partly covering objects is a typical example of suh a heuristic use. If a_Z stands for the area of the field Z under study and a' for the mean area of the primary grain X' (estimated from a few isolated grains

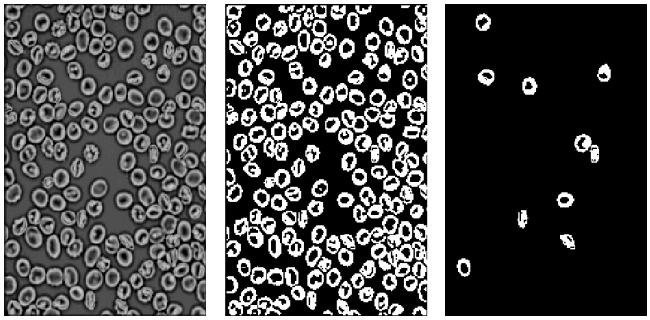

Figure 3.6: Heuristic use of the Boolean RACS for counting red blood cells.

in Z), then, if the structure is boolean, functional Q(A) implies that

$$\{\text{number of objects in Z}\} = -(aZ/a')Log\ q \tag{3.29}$$

Now, even when the structure is not boolan, rel.(3.29) is generally still verified with an accuracy $\leq 15\%$. For example, start from the left micrograph of 204 (non convex!) red blood cells depicted in fig.3.6, threshold it between 100 and 255 (porosity q = 0.640 for a field of 39360 pixels), and extract ten isolated cells (right image), whose avearge area is 93.0 pixels.Then by applying rel.(3.29) we find

$$N = -(39360/93)\ Log\ 0.640 = 188 \tag{3.30}$$

The estimate is robust: if the low threshold is replaced by 90, we obtain

$$a = 100.1\ \ ;\ \ q = 0.609\ \ ;\ \ N = 195 \tag{3.31}$$

3.9 Specified Boolean RACS

Coming back to the Boolean model, we now present three more specific models, which rather often appear in applications. Note that in all these cases the 3-D density is accessible from 2-D sections.

3.9.1 Isovolume Primary Grains

Let X be a Boolean model of density θ_3 and primary grain X' such that $V(X')$ is constant and not random. Then from the pore covariance $C_{00}(h)$,

accessible from line sections, we get

$$\begin{aligned} \log C_{00}(0) &= \log q = \theta_3 V\left(X'\right), \\ \frac{1}{g^2}\int_{\mathbb{R}^3} \log C_{00}(h)\, dh &= \theta_3 V^2\left(X'\right), \end{aligned}$$

which allows us to estimate θ_3 and $V(X')$. One can also test the hypothesis "$V(X')$ is constant" from more sophisticated measurements performed on 2-D sections ([129]).

3.9.2 Spherical Primary Grains

The 3-D primary grains are balls. Denote the distribution function of their radii by $F_3(r)$. The model is completely determined by the covariance $C_{00}(h)$.We have

$$\frac{1}{2\pi r}\left[\log C_{00}(2r)\right]^{(ii)} = \theta_3\left[1 - F_3(r)\right] \tag{3.32}$$

and in particular when $r \to 0$

$$\frac{1}{\pi}\left[\log C_{00}(2r)\right]_{r=0}^{(iii)} = \theta_3 \tag{3.33}$$

[In practice, using the left-hand side to estimate θ_3 would result in a large estimation variance, so it seems wiser to open the model with a small ball of radius r_0,i.e., essentially replace θ_3 by $\theta_3\left[1 - F_3(r_0)\right]$ given by 3.32].

3.9.3 Poisson Polyhedron Primary Grains

In a partition of the space by isotropic Poisson plane networks, pick out the polyhedron containing the origin, and take is as a primary grain X'. This compact random set depends on one parameter only, namely, the intensity ρ of the Poisson planes ([97], [99]). The geometric covariogram $K(h)$ of X' is given by the formula

$$K(h) = \mathbb{E}V\left(X \cap X_h\right) = \frac{6}{\pi^4\lambda^3} e^{-\pi\rho|h|}. \tag{3.34}$$

The two basic quantities used for estimation are $Q(l)$ of (10) and the covariance $C_{00}(h)$. Putting $\theta' = 6\theta/\pi^4\rho^3$, we obtain

$$Q(l) = qe^{-\pi\rho\theta' l} \qquad \text{with} \qquad q = e^{-\theta'}, \tag{3.35}$$

$$C_{00}(h) = q^2 e^{\theta'} e^{-\pi\rho|h|} = q^2 e^{\theta K(h)} \tag{3.36}$$

which allows us to estimate the two parameters θ and ρ of the model.

3.10 Derived Models

The Boolean model is the seed for a considerable number of random sets. In what follows, we give only a short presentation of a few of them (more detailed information and examples may be found in Jeulin [54] and in Serra [129]). We hope that these few derivations will suggest ideas to the reader for inventing his own models.

3.10.1 Three-Phased Structures

There are many ways of building up models for multiphased textures. Depending upon whether or not we wish to emphasize the dependence between two phases, we could use either the following metallographic or petrographic models.

3.10.1.1 Metallographic model.

We developed this model in conjunction with Greco and Jeulin [37] in order to describe the morphology of sinter textures. It often happens, in metallography, that one type of crystal, say X_2, wipes out all others, which can survive only in places left by X_2 (i.e., in X_2^c). For example, assume that X_1 and X_2 are two independent Boolean sets, and that X_2 wipes out X_1. This leads to a three-phase texture X_2, X_3, X_4, with

$$X_2, \qquad X_3 = X_1 \cap X_2^c, \qquad X_4 = X_1^c \cap X_2^c = X_3^c \cap X_2^c. \tag{3.37}$$

If the primary grains X_1' and X_2' are convex the intercept histographs of X_{2^c}' and of X_3 should be negative exponentials (tests for the model result). An interesting piece of information for the three-phase structures is given by the co-occurrence matrix, which is equivalent here to the three covariances C_1, C_2 and C_3 of the three phases that are present. We have

$$\begin{aligned} C_2(h) &= C_2(h) \qquad \text{(unchanged)} \\ C_3(h) &= C_1(h)\left[1 - 2q_2 + C_2(h)\right], \\ C_4(h) &= \left[1 - 2q_1 + C_1(h)\right]\left[1 - 2q_2 + C_2(h)\right]. \end{aligned}$$

3.10.1.2 Petrographic model.

This RACS was proposed by Serra to model synthetic soils in which the clay partly surrounds the quartz grains, and partly spreads out in the pores, looking like small spots. A Boolean model is chosen, whose primary grain is

- with probability p, a ball of quartz of radius r_1 surrounded by a spherical crown of clay of thickness $r_2 - 2$, which we call contour clay,

- with probability 1-p, a ball of clay of radius r'_2, which we call isolated clay.

We Booleanize and rule that when quartz and clay overlap, the quartz obliterates the clay. As in the former case, two phases exhibit intercept histograms which are negative exponential (the pores and the pore-clay union). The cooccurrence matrix is easily calculable, and constitutes the main piece of information on the model. The 3-D characteristics p, r_1, r_2 and r'_1 are derived from these covariances.

3.10.2 Dead Leaves Model

This other variation of the Boolean model that we now present is due to Matheron [77] and has been extended by D. Jeulin to multiphased structures as well as to numerical functions [58][59]. It has the dual advantage that it provides us with a tessellation of the space, as well as a model for non-overlapping particles.

Dead leaves partition. When one looks at a cloudy sky, one sees only the lowest clouds, which hide those above. The dead leaves model is just a quantitative description of this type of superposition. Although the basic relation 3.38 is independent of the dimension of the space, we will take our realizations to be in $\mathbb{R}^2$, and develop the model in this space.

Let X' be a primary grain in $\mathbb{R}^2$. Place the origin of time t in the distant past, at -∞. From the origin to the present (i.e., $t = 0$) take the realization of Boolean sets, independent of each other, with identically distributed primary grains X' at time instants given by a constant spatial Poisson density θdt. The grains appearing between $-t$ and $-t+dt$ *hide* the portions of the former grains.

At time zero the plane is completely covered (since the origin of t is -∞), giving a *random stationary partition* of the space. The probability $Q(B)$ that a given compact set B is included in one class of the partition is

$$Q(B) = \frac{\overline{Mes}\,(X' \ominus \check{B})}{\overline{Mes}\,(X' \oplus \check{B})} \tag{3.38}$$

This relationship completely characterizes the partition, and opens the way to the classical measurements (size distribution, convex erosion, covariance, etc.).

Relief grains. From now on, the assumption of connexity of X' is very essential ; however, our restriction to a 2-D isotropic analysis is only for pedagogical reasons. Imagine that the observer is now able to decide whether or not a given class of the final partition corresponds to an *entire* primary grain X_1 that has not been partially obscured by another. The union of all these classes generates a stationary random set X made up of disjoint compact convex grains.

Denote by A' and U' the random area and perimeter of the primary grain X', let $F(dA', dU')$ be the law of these two variables, and $\mathbb{P}_{\mathrm{conv}}[B; A', U']$ be the probability that $B \subset X'$, where X' is a primary grain with functionals A' and U' and located at the origin of $\mathbb{R}^2$. If B is a *connected* compact set (and only in this case), we have

$$Q(B) = \int_{\mathbb{R}^2} dx \int \frac{\mathbb{P}_{\mathrm{conv}}(B_{-x}; A', U')\, F(dA', dU')}{A' + \mathbb{P}_{\mathrm{conv}} A' + U' \mathbb{P}_{\mathrm{conv}} U'/2\pi} \tag{3.39}$$

From this relation, we can derive the specific number N_A and the distribution $F_1(dA_1, dU_1)$ of the areas A_1 and the perimeters U_1 of the relief grains X_1 :

$$N_A = \int \frac{F(dA', dU')}{A' + \mathbb{P}_{\mathrm{conv}} A' + U' \mathbb{P}_{\mathrm{conv}} U'/2\pi}, \qquad N_A F_1(dA_1, dU_1) = \frac{F(dA', dU')}{A' + \mathbb{P}_{\mathrm{conv}} A' + U' \mathbb{P}_{\mathrm{conv}} U'/2\pi} \tag{3.40}$$

We see in the denominator the bias affecting the size distributions of the areas and perimeters ; i.e., large values appear with a lower frequency in the relief grains X_1 than in the primary grains X'.

3.10.3 Hierarchical Models

By hierarchical models (Serra [127]) we mean the following. During the time interval $(0, dt)$ we generate an initial Boolean model with density θdt and primary grain X'_0 ; at the instant dt we generate a second elementary process that will interact with the first, etc. The resulting set at time t is denoted by X_t. In both particular cases that we present below (α and β), the primary grains are assumed to be deterministic sets.

α.*Separated grains* Any primary grain X'_{t+dt} appearing during the interval $[t, t+dt]$ is suppressed if it touches X_t; this will generate a random set with

separate grains (Fig.10a). Then, denoting by $Q_t(B)$ the probability that $B \subset X_t^c$, and by $Q_t'(B)$ its derivative with respect to t, we have

$$Q_t'(B) = -\theta \text{ Mes } \left(B \oplus \check{X}_t'\right) \cdot Q_t\left(X_t'\right) \tag{3.41}$$

β. Gypsum crystals Each primary grain X'_{t+dt} that does not touch X_t is suppressed. If it does touch X_t, we take its union with X_t for constructing X_{t+dt}. This will generate a random set with clusters of interpenetrating crystals, as in a gypsum crystal, for example. We now have

$$Q_t'(B) = -\theta \text{ Mes } \left(B \oplus \check{X}_t'\right)\left[1 - Q_t\left(X_t'\right)\right]. \tag{3.42}$$

The integral equations 3.41 and 3.42 cannot be solved in general, but only computed by numerical means.

However, when the number of steps of the hierarchy is finite, they can effectively be calculated. One particularly interesting case happens when there are only two steps. Starting from a first Boolean model (θ_1, X_1'), we generate a second one (θ_2, X_2') and allow them to interact in one of the two ways described above. The "separate grains" model now becomes a three-phased model (X_1, X_2, and the background) where X_1 and X_2 are *disjoint* from each other. The probability $Q(B)$ is

$$\exp\left\{ \begin{array}{c} -\theta_1 \overline{\text{Mes}}\left(\check{X}_1' \oplus B\right) - \theta_2 \overline{\text{Mes}}\left(\check{X}_2' \oplus B\right). \\ \exp\left[-\theta_1 \overline{\text{Mes}}\left(\check{X}_1' \oplus X_2'\right)\right] \end{array} \right\} \tag{3.43}$$

(For the gypsum crystal type model, replace exp[ ] by 1 - exp [ ].

3.10.4 Boole-Poisson Model

Although Conrad and Jacquin [22] constructed the following model (3.7) to describe aerial photographs of geological cracks, by using Poisson polygons and Boolean fissures, their "mixed random set" is extremely general. For simplicity, we will present it as it was originally. Start from an anisotropic Poisson line process in $\mathbb{R}^2$, with density ρ and denote it as X_1. Intersect each polygon Π of the partition with a stationary random set X_2 in the following special way. For each polygon of the given realization of X_1 use a *different* realization X_2 of X_2^*. The union of all these portions of X_2, together with X_1, makes up the set we shall call Y. If $Q_1(B)$, $Q_2(B)$ and $Q(B)$ denote the functional probabilities with X_1, X_2 and Y, respectively, we have

$$Q(B) = Q_1(B) \cdot Q_2(B) = \exp\left(-[\rho U(B) + \theta \overline{A}\left(X_2' \oplus B\right)]\right), \tag{3.44}$$

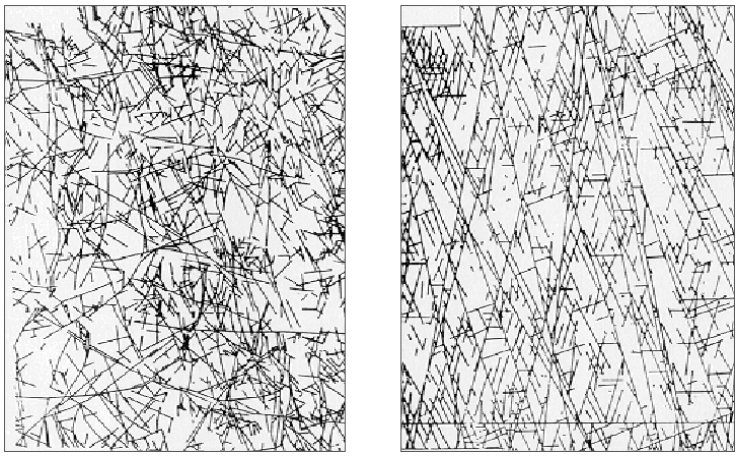

Figure 3.7: Left: set of faults observed from aerial photographs ; right: simulation of a Boole-Poisson RACS admitting the same parameters.

3.11 Exercises

3.11.1 Boolean simulations

This exercice, which is mainly visual, is aimed at highlighting the general aspects and construction flexibility of boolean models ; it will also give an idea about the variability (very large, sometimes) from one realization to the other when the parameters of the model are determined. Some of these simulations shall be saved and will be used for the exercice about tests.

1. Simulate boolean sets with square, hexagonal or circular grains, with a fixed or variable size.

[*For the first ones, one only has to dilate Poisson points, for the second ones, to consider the union of several dilations of various sizes. Two procedures-***isobool** *and* **isobool 2** *- may also be applied*].

2. The previous simulations are isotropic, at least on their definition grid. Carry out now some anisotropic simulations from segments or ellipses.

[*As previouly, make a union with Poisson points dilations with different size and orientation segments, or with ellipses (procedures* **eldil** *and* **elbool***)*]

3. Simulate boolean sets with primary asymmetric grains, as for instance a mixture of equilateral upwards and downwards triangles.

[*Use the procedure* **tribool**. *The shapes catalogue may also be grown with* **dropdil**, *which dilates according to asymmetric droplets of the eight possible orientations*].

4. As a last example of non convex primary grains, we will use doublets of disjoint disks which centers are d apart (cell division model)

[*Make a union of a first realization of Poisson points with its horizontal translate of distance d, then a second one with its translate at angle 4500xb0 and of distance d, etc ... Make a union of all the points you got, and dilate them with a small disk*].

5. Start from a Poisson points simulation with a regionalized density g (cf. exercise 9-5), and pass to the boolean system with small homogranular circles. Explain.

[*We get a* binarization *technique of the function g*].

6. Simulate conic boolean functions (we will use the cones sizes and heights whether to isolate the islets or whether to invade space). Simulate a cones doublets realization.

[*Use procedures* **conedil 1 and 2,** *applied to Poisson points, consider the sup for several points density, matching several cones sizes. In case of doublets, act as for question 4 to get the points, and dilate with a cone*].

3.11.2 Boolean tests

1. Symbols $a\prime$ and $u\prime$ denote the mean area and perimeter of the primary grain respectively, and q and u the porosity and specific perimeter after a booleanization. We know that

$$q = \exp\{-\theta a'\} \quad \text{and} \quad u = \theta u' \exp\{-\theta a'\}$$

Check both relations on several simulations of the previous exercise, and particularly on the disks doublets. What about the boarder effects ?

[*Use the function* **perim**. *Note the generality of the approach, which does not imply that the primary grain is connected. Note also that, only the products* $\theta u'$ *and* $\theta a'$ *are accessible, but neithert* u' *nor* a']

2. When the primary grain is supposed to be convex, the first boolean test is based on linear erosions, which must be negative exponentials. If K is the segment with length L and direction α, we indeed have

$$logQ(K) = logQ_1(L, \alpha) = -\theta(Ld'_\alpha + a') \tag{3.45}$$

where d'_α is the mean diameter of the primary grain in direction α. Test relation (3.45) on one of the convex grains simulations of exercise 1, and apply it successively to grains and pores. Test it afterwards for circles doublets, and for primary grains with regionalized density.

[*Use the procedure* **pvonl** *(which corrects boarder effects) and report the measurements on semi-log paper. Note that θ is still inaccessible*].

3. Use the images of the previous question, and erode them now by hexagons or squares. Prove that the logarithm of $Q(K)$, for a square with side L and directions α, β, is

$$\log Q(K) = \log Q_2(L, \alpha) = -\theta \left[L^2 + L(d'_\alpha + d'_\beta) + a'\right] \tag{3.46}$$

which yields estimator θ such that

$$\theta L^2 = \log Q_1(L, \alpha) + \log Q_1(L, \alpha + \pi/2) - \log Q_2(L, \alpha) - \log q \tag{3.47}$$

Discuss the experimental results. Does the formula remain admissible when the primary grain is not convex anymore ?

4. Measure the covariance of the disks doublets realization. Interpret the results.

[*The mean distance between two primary grain disks turns out to appear as a hole effect in the covariance*].

5. Develop the questions (2) and (3) for Boolean islands.

[*Start from the simulations of conic Boolean functions of the previous exercise. The function is Boolean if and only if all sections are Boolean sets. Tests arising from relations (3.45) and (3.46) are applied to each grey level t. By integrating over the gray levels t, we obtain*

$$-\int_T \log Q_1(t; L, \alpha)dt = \theta \left[L\rho'_\alpha + v'\right] \tag{3.48}$$

with ρ'_α and v' integral of the directional gradient and volume of the primary grain respectively (similar extension for relation(2))]

6. Check that the specific number $\nu(t)$ of the maxima at altitude t of a random boolean function simulation fulfills the relation :

$$\nu(t) = \theta q(t) \varpi(t) \tag{3.49}$$

where $\varpi(t)$ represents the probability that the primary grain has a height t.

3.11.3 Boolean model and counting

The Boolean model allows to calculate explicitly a number of relations between observable characteristics of the primary grain. These relations can be used as tests (cf exercise above), or, on the contrary, can be admitted in a heuristic fashion, without further discussion.

For instance consider, in R^2, a random primary grain with a mean area a' and a mean perimeter u'. After booleanization, the number θ of grains per unit area is linked to the porosity q and to the specific perimeter s by the two relations

$$\theta a' = -\log q \quad \text{and} \quad \theta u' = s/q \tag{3.50}$$

1. Simulate a succession of boolean R.A.C.S. with circular grains (for the sake of simplicity) of variable densities, homogranular or not. Once s and q have been measured on the simulations (whose parameter θ is given), check the relevance of the first relation (3.50) and of the following relation

$$u'/a' = -s/q \log q \tag{3.51}$$

[*Use procedures* **isobool** *and* **isobool2**. *Define, for $\theta^* = n$ fixed, for instance, at 50, the validity scope of relations (3.50) and (3.51) with respect to a'*]

2. Simulate hierarchical R.A.C.S. (therefore non boolean), for which all variables taking place in relations (3.50) and (3.51) are known. To what extent are these relations still correct? Explain.

[*You can start from the procedure* **rose**, *or directly from* **isobool**, *when a realization is intersected with a Poisson points set, followed with a circular dilation. The first relation (3.50) implies that we have quite a precise idea*

about the mean size of the primary grain ; the relation (3.51) rather implies that its shape is known, and that its size changes very little. Therefore rel.(3.51) may be better for the low values of q. Formulae (3.50) and (3.51) are anyhow satisfied as long as the object under study can be locally modelled by a boolean model, that allows free covering]

3. Extend the first relation (*3.50*) to Boolean random functions, and test it by simulating boolean islets.

[*Dilate Poisson points by cones, by considering the sup of two or three realizations with different densities or sizes of cones. The relation (3.50) must now be integrated with respect to grey levels :*

$$\theta v' = -\int \log q_t dt \tag{3.52}$$

Check numerically the ranges of validity of the various parameters]

3.11.4 Hierarchical models

The adjective "hierarchical" indicates here the implementation of a second boolean generation (θ_2, X_2'), conditionally to a first one (θ_1, X_1'). The second grains mays lean on the first ones or avoid them. This leads to aggregates in the first case, and to separate sets in the second one. Although these models are rapidly incalculable, they can nevertheless be developed in easy and instructive simulations.

1. Simulate hierarchical models for each of both types, and choose $\theta_1 \neq \theta_2$ and primary grains of different sizes.

[*Procedure* **rose***(as in desert rose) and* **hard**]**.**

2. Iterate the hierarchies in order to construct a sequence. Boolean models will be considered with respect to smaller and smaller disks.

[*Procedure* **flake** *(as in Von Koch "snow flake") and* **disjoint**].

3.11.5 Boolean domain of attraction

Choose half a dozen ordinary tesselations. For instance, the starting point may be the watershed lines of images such as *electrop* or *barrier* (after a small preliminary filtering in order to avoid too many classes). Skeletons may also to drawn according to influence zones or even Poisson lines. In each partition, assign the value 1 or 0 to each class with a low probability p

for the 1s. Consider the union of the results, and test if it can be considered as boolean. Draw the conclusions.

3.11.6 Poisson lines in the plane

1. Use a square grid and simulate Poisson points (density λ) on the axes O_x and O_y.Take the perpendiculars on these points. This leads to a family of Poisson anisotropic lines, that segment the space into rectangles.

Convert the previous drawing into an approximately isotropic process, by incorporating lines with slopes ± 1, ± 2 and $\pm 1/2$. Simulate several realizations for both methods and note the important size variability.

[*The procedure* **lines** *creates Poisson rectangles, and* **diags**, *Poisson polygons in the six other directions. In* **lines**, *n is the effective number of points on each axis ; in diags,* $n\sqrt{2}$ *points are implemented on each diagonal, and* $n\sqrt{5/2}$ *points on each axis with* ± 2 *and* $\pm 1/2$ *gradient. These operations can be deconditionalized when extracting beforehand n values in Poisson law with parameters* λL *(L being the unit length of the axes)*].

2. Prove that Poisson lines induce, on each line, a Poisson points process, with a density 2λ in the isotropic case. Compare this result with the previous eight directions approximation.

[*Isotropic case : the lines with directions* $(\alpha,\ \alpha + d\alpha)$ *induce a small Poisson with a density* $\lambda \sin\alpha d\alpha$, *which implies, through a summation over* π, *a total density of* 2λ. *In digital case, the points induced on the axis* O_x *(for instance) have a density of* $(1 + \sqrt{2} + 6\sqrt{5})/\pi = 1,62$].

3. Conditional sections. Suppose K and K' be two compact convex sets with respective perimeters u and $u\prime$, and K'$\subseteq$ K. Prove that if one and only one line intersects K, then, the probability it also intersects K' equals the perimeters ratio u'/u.

[*If a line has a direction* $(\alpha, \alpha + d\alpha)$, *such a probability equals the diameters ratio* D'_α/D_α *in the direction* α. *As and varies the searched conditional probability is then given by*

$$\int_0^\pi \frac{D'_\alpha}{D'_\alpha}\frac{D_\alpha}{u}d\alpha = \frac{u'}{u}] \tag{3.53}$$

4. Mean chord. Knowing that a line intersects K with an area a, prove that the conditional expectation of the intersected length is $\pi a/u$.

[*In direction α, this expectation equals a/D_α ; when deconditionalizing in α, we get $\pi a/u$*].

5. Specific number of peaks. Prove that if two lines intersect a disk of radius r, there is one chance out of two they intersect inside the disk. Infer that the number of intersections per surface unit equals $\nu = \pi\lambda^2$.

[*1st point : if the intercepted chord on the first line has a length l, the second one intersects it with the probability $2l/2\pi r$ (question 3). But the conditional expectation of l is $\pi r/2$ (question 4), which leads to the result.*

2nd point : the a-priori probability that two lines intersect the disk equals $\frac{(2\pi r\lambda)^2}{2}\exp\{-2\pi r\lambda\}$. When $r \to r_0$, half the number equals $\pi\lambda^2$].

6. Determine the relative variance $var(\mathrm{A})$, in number, of the polygons size,by means of their average in measure M(A). It is reminded that

$$var(A) = \frac{\sigma^2(A)}{[E(A)]} = \frac{M(A)}{E(A)} - 1 \tag{3.54}$$

[*Let Y_0 be the polygon including the origin. The probability it also contains the small area $r\ dr\ d\alpha$ equals exp $\{-2\lambda r\}$, which leads to :*

$$M(Y_0) = \int_0^{2\pi} d\alpha \int_0^{\infty} \exp(-2\lambda r) r dr = \pi/2\lambda \tag{3.55}$$

On the other hand, since each peak labels one and only one polygon, we have $E(A) = 1/v$, and (3.54) induces $var(A) = \pi^2/2 - 1 \ \sim 4$. This particularly high value explains the large disparity of the sizes considered in simulation].

3.11.7 Poisson partitions

The model here-under was initially proposed by F. Conrad ([22]) in order to describe aerial photographs of geological cracks as those presented in the course. But the approach by "mixed" random set, on which the model is based, is extremely general and applies to any set or random function in R^n. We shall limit ourselves here to R^2.

1. Let X_1 be a tesselation and X_2 a R.A.C.S. of the euclidian plane. Let us build a realization X_1^* of X : each polygon is kept or rejected, independently of the others, with a probability p. Affect the restriction of a distinct realization in X_2 to each remaining polygon Π. The union of these portions,

together with X_1^*, may be considered as the realization of a random closed set A.

Denoting by Q the characteristic functional of A, prove that the following relation (1) is satisfied for any connected compact set K

$$Q(K) = Q_1(K)\,[q + p\;Q_2(K)] \tag{3.56}$$

where q = 1-p, and where Q_1 and Q_2 stand for the characteristic functionals of X_1 and X_2 respectively.

[*If K misses X_1^*, then it is contained in a single polygon* Π, *therefore we can equivalently say that K misses A, or misses the restriction* $X_2^* \cap \Pi$, *or again misses* X_2^*. *This leads to the relation (3.56)*].

2. Let X_1 and X_2 be two tesselations of isotropic Poisson lines in the plane, with respective densities λ_1 and λ_2. The relation (*3.56*) becomes

$$Q(K) = \exp\{-\lambda_1 u(K)\}\,[q + p \exp\{-\lambda_2 u(K)\}] \tag{3.57}$$

where u is the perimeter. Simulate A in a square grid, and check relation (*3.57*). When p = 1, is Q(K) different from the Poisson lines functional ? What is the explanation ?

[*We can use the procedure* **lines 2**, *which directly builds A according to the square grid isotropy, or start as well from a simulation* **diags**, *richer in directions, and then simulate A polygon after polygon. Take a* λ_2 *at least twenty times larger than* λ_1, *and for K a square or an hexagon with side k. Q(k) is estimated by the procedure* **binerotest**. *Denote, when setting on semi-logarithmic coordinates, that log Q(k) looks like two successive segments, whose angle is all the larger as p is small*].

3. Similarly, draw a simulation A where X_2 is a boolean R.A.C.S., and another one where X_2 is a random function of Poissons tubes.

[*In the latter case, we will get* X_2 *by dilating the simulations* **diags** *by cones*].

3.11.8 A few point models

1. Order two analysis. The points models that follow are stationary and generally admit a covariance *measure* C(dx), which can be decomposed into the sum of a Dirac measure and a *function* g(x)

$$C(dx) = m\delta(dx) + g(x)dx \tag{3.58}$$

The mean number of points Z_B in the borelian set B is

$$m(Z_B) = m\ a(B) \tag{3.59}$$

and the covariance between the numbers in B and in B' is

$$C(Z_B, Z_{B'}) = m\ a\ (B \cap B') + \int_{R^2}\int_{R^2} 1_B(x) 1_{B'}(y) g(x-y) dx\ dy \tag{3.60}$$

In the isotropic case, there is a simpler way to reach g from experiments. Note H(r), the average number of points which are included in the disc of radius r, centered on a point x_i (not counted), which is itself part of the set model. By taking for B' the disc of radius ds centered x_i,and for B the disc (r, x_i) minus B', relation (*3.60*) becomes :

$$C(Z_B, Z_{B'}) = 2\ \pi\ dx \int_0^r g(s)\ s\ ds \tag{3.61}$$

But, this covariance is nothing else than the centered version of $mH(r)$

$$C(Z_B, Z_{B'}) = E\left[Z_B - m(Z_B)\right]\left[Z_{B'} - m(Z_{B'})\right] = m\left[H(r) - \pi r^2 m\right] dx \tag{3.62}$$

where the primitive $\left[H(r) - \pi r^2 m\right]$ of sg(r) is experimentally accessible.

Write a computing procedure for H(r)

[*Procedure* **pp**, *for "point packing"*].

2. Anisotropic Poisson points. Work again with procedure **points** and divide the simulation by setting in a memory the random points (x_i, y_i) and in the other (x_i, y_i/2). To which extend does the affinity of ratio 1/2 make the simulation more anisotropic from a visual point of view ? Interpret by calculating the number of points which are included in the flat (sides 2,1) and long (side 1,2) rectangles.

[*Only the density varies, here doubles. Such thing as Poisson points cannot be anisotropic !*]

3. Measure the primitive H(r) for Poisson points simulations, and for the centres in the model of disc doublets. Derive g(s) and explain. Calculate H(r) for the germs centers in the hierarchical sets derived from the boolean model.

[*For Poisson points with a density* λ, *we find, in square grid* $H(k) \sim \lambda(k + r)^2$ *and in hexagonal grid* $H(k) \sim \lambda(3\ k^2 + 3\ k + 1)$, *which duly corresponds to Poisson law variance, and implies* $g(s) \equiv 0$. *In case of doublets*

*from d apart, H(r) undergoes a thrust, at distance d. In hierarchical cases, clustering situations (***rose, flake***) lead to an additional increase of H(r), and repulsive ones (***hard, disjoint***) to a decrease, followed an asymptote in both cases. The range of function H(r) - $\pi r^2 m$ corresponds to the average size of the interactions between points*].

4. Calculate H(r) for the set of points generated by the crossing of isotropic Poisson lines, with an intensity λ. Derive the measure $g(r) = 4\lambda^3/r$. Simulate such a process and calculate its H(r). Give an interpretation.

[*We will simulate a process wich is close to the model, but easier to implement, by considering two realizations of* **lines** $\cup$ **diags**, *and by intersecting them. A linear increase of H(r) is noticed, unlike all the other point processes considered until now. In theory, if x_i is a point of the set, the disk B(r, x_i) includes, on the one hand, lines intersections different from those which define x_i (average number $\pi r^2 \lambda^2$, see "Poisson lines" exercice), and, on the other hand, the points of the two lines that intersect at point x_i (average number $8\lambda r$). Consequently, $H(r) = \pi r^2 \lambda^2 + 8\lambda r$, and*

$$\int_0^r sg(s)\, ds = 4\lambda^3/r \qquad \text{therefore} \qquad g(r) = 4\lambda^3/r \;] \tag{3.63}$$

5. Regionalized density. In this last exercice, we come back to image processing. Let f be a numerical function of the plane. Simulate Poisson points with a variable density f. Apply the simulation by chosing for f a grey tone image. Explain.

[*Procedure* **regpoints**. *This simulation is explained as the binarization of the numerical grey image, whose quality is all the smaller since the involved gradients are steeper and steeper*].

.

Chapter 4

BOOLEAN RANDOM FUNCTIONS

4.1 Introduction

The very starting point of the theory of Boolean functions lies in a theorem of G.Matheron dating from 1969 [78], which proves that the upper semi-continuous functions, considered via their sub-graphs, form a compact space with respect to the hit-or-miss topology (a result that allows one to construct probabilities). But Matheron did not continue in this direction and his main book [82] does not even mention the theorem. In fact the generalisation of the Matheron-Kendall theorem to numerical functions is due to Serra [129], chapter XII. This second starting point arose during the eighties, and after a relatively slow begining the theory has spread in different directions. It is now applied in geostatistics, for calculating isofactorial models and change of supports [83],[113], in material sciences for modelling the physics of rupture [57], and for characterizing the roughness of steel plates [56], in medical radiology of the bone [111] and also for simulating textures that satisfy given properties [19]. An exhaustive presentation of the method can be found in [134]. The current chapter follows the same plan, but in a simpler style.

The idea to threshold roughness profiles and to consider the resulting sections as Boolean appears in D. and P. Jeulin [55]. The first formal study is due to Serra ([129]), who defines a restricted version of Boolean functions (called hereafter basic Boolean functions (BBF) or Boolean islands), gives its characteristic functional $Q_t(B)$ and develops $Q_t(B)$ for B, a flat com-

pact convex set. Later on, the same author [133] improved the analysis of Boolean islands by studying integrals of $\log Q_t(B)$. Jeulin [56] calculated a series of polyhedral primary grains, which are useful in electron microscopy, and established several useful stereological results. Prêteux & Schmitt [111] simulated Boolean islands in order to check the experimental access to $Q(B)$, using a three-dimensional approach, and have used the model to describe vertebral spongy bone textures in scanner imagery. The initial BBF model led to a second particular model, namely the rocky deeps, and to the generalized Boolean functions (called below Boolean functions) in [131], chapter 15. Mathematical aspects concerning the measurability of the primary grain f'_t acccording to variable t, and also the determination of Boolean functions have been approached by Prêteux and Schmitt (in[131], chapter 18).

4.2 Morphological Random Functions

The topology of the semi-continuous functions has already been introduced section 4.2.2, when space E is metric. Here we briefly sketch G. Matheron's approach to the upper semi-continuous functions from an L.C.D space E into $\overline{\mathbb{R}}$. Just as in chapter 4, they are considered, via their subgraphs, as closed sets in $E \otimes \overline{\mathbb{R}}$. In this approach, the familly $\mathcal{C}$ of those sets $C \in \mathcal{F}\left(E \otimes \overline{\mathbb{R}}\right)$ that satisfy the two conditions

i/ $C \supset E_{-\infty}$

ii/ $\forall x \in E, \forall t \in \overline{\mathbb{R}}, (x,t) \in C \Rightarrow \{x\} \otimes [-\infty, t] \subset C$

is identified with the class F of the u.s.c. functions $E \to \overline{\mathbb{R}}$, and it is proved to be a *compact family* in $\mathcal{F}\left(E \otimes \overline{\mathbb{R}}\right)$. The topology on F is obtained as the restriction to $\mathcal{C}$ of the topology on $\mathcal{F}(E \otimes \overline{\mathbb{R}})$. Consequently, the open sets in F are generated by the parts of F whose elements f satisfy the two conditions:

$$\overline{X}_f(G) = \sup\{f(x), x \in G\} > b \quad \text{and} \quad \inf\left\{\overline{X}_f(G), G \supset K\right\} < a \quad (4.1)$$

as G spans the open sets of E, and K its compact sets ($a, b \in \overline{\mathbb{R}}$). This results in the following criterion of convergence [theorem 3.2.1 in [78]]

Proposition 4.1 *A sequence f_n converges towards f in F if and only if it satisfies the two following conditions: 1/ for all $x \in E$, there exists a sequence $x_n \to x$ in E such that the sequence $f_n(x_n) \to f(x)$ in $\overline{\mathbb{R}}$. 2/ If a sequence x_{n_k} converges towards x in E, then the sequence $f_{n_k}(x_{n_k})$ satisfies*

$\overline{\lim} f_{n_k}(x_{n_k}) \leq f(x)$.

The next step consists in equipping F with the σ-algebra generated by its topology, i.e. by the events $\overline{X}_f(G)$ introduced in rel.(4.1). Finally a random u.s.c. function f is defined by providing the measurable space (F, σ) with a probability P. The compactness of set F ensures that there actually exist probabilities on σ.

Just as a random variable is characterized by its distribution function, a random function $f \in (F, \sigma, P)$ is completely determined by the joint probabilities

$$\Pr\{\sup\{f(x), x \in B_1\} < \lambda_1 \quad ; \ldots \quad \sup\{f(x), x \in B_n\} < \lambda_n\} \tag{4.2}$$

for every finite sequence $B_1 \ldots B_n$ of compact sets in E and of real values $\lambda_1 \ldots \lambda_n$. Formula (4.2), due to by J.Serra [129], expresses a general theorem on random sets due to G. Choquet [21] and G. Matheron [82], which is interpreted here for random functions .

4.3 Definition of a Boolean function

To make the transition from Boolean sets to Boolean functions, it suffices to dilate Euclidean Boolean sets by a half straight line. More precisely, consider a σ-finite measure $\theta(\mathrm{d}t)$ on $\mathbb{R}$ (i.e. such that the measure of any bounded interval is finite). Associate with the Euclidean space $\mathbb{R}^n \times \mathbb{R}$ the measure $\theta(\mathrm{d}t)\mathrm{d}x$ which represents the intensity measure of a Poisson point process $\mathcal{J}$ over $\mathbb{R}^n \times \mathbb{R}$, where $\mathrm{d}x$ stands for the elementary volume in the "horizontal" space $\mathbb{R}^n$, and $\mathrm{d}t$ for the elementary length along the "vertical" axis $\mathcal{R}$. The measure $\theta(\mathrm{d}t)\mathrm{d}x$ is assumed to be constant on horizontal slices, and variable along the t-axis. The horizontal stationarity which results is not necessary for the theory, but it allows a more expressive formalism, and suffices in practice. It will be implied for the rest of this paper, except for Section 5.

Suppose we take a realization of the Poisson point process with intensity measure $\theta(\mathrm{d}t)\mathrm{d}x$ and consider each of its points as the germ of a crystalline growth, the crystal being the umbra, or subgraph, of a function $f'(x)$. We call f' the "primary grain", by analogy with the set case and use the notation $f'(x)$ for both umbra *and* function. The random function f' is u.s.c., almost surely bounded and with compact horizontal cross-sections for all $t > -\infty$.

It is, by construction, implanted at the origin, and its translate to point y, $t \in \mathbb{R}^n \times \mathbb{R}$ is $f_{y,t}$.

Consider the $I(\mathrm{d}t)$ Poisson points located in the slice $(t, t+\mathrm{d}t)$, and generate $I(\mathrm{d}t)$ realizations of a *same* random primary grain f'_t, which are shifted to the points of the slice. Repeat then the same procedure for all horizontal elementary slices. The primary grain $f'_t(x) = f'(x/t)$ may vary as a function of the depth t. The Boolean function f is finally obtained by taking the sup of all the $f'_{y,t}$ for all slices. In other words, we can state the following.

Definition 4.2 *Let $\mu_n(dx)$ be the Lebesgue measure in $\mathbb{R}^n$ and $\theta(dt)$ be a $\sigma-$finite measure on $\mathcal{R}$. Consider the Poisson point process $\mathcal{J}$ in $\mathbb{R}^n \times \mathbb{R}$, whose intensity mesure is $\mu_n(dy) \otimes \theta(dt), y \in \mathbb{R}^n, t \in \mathbb{R}$. Let $\{f'(x/t)\}$ be a family of u.s.c., independent random functions from $\mathbb{R}^n$ into$\mathbb{R}$, which are parameterized by t and such that all cut-off sets Y_u if $\mathbb{R}^n \times \mathbb{R}$*

$$Y_u = \{x, f'(x/t) : f'(x/t) \geq u\} \qquad u > -\infty \tag{4.3}$$

are a.s. compact. The $f'(x/t)$ are called primary grains centred at the origin. Then the Boolean function f, of primary grain $f'(x/t)$ and of intensity $\theta(dt)$ is obtained by taking the following sup :

$$f(x) = Sup\{f_{y,t}(x/t); (y,t) \in \mathcal{J}\} \tag{4.4}$$

The simulations depicted in figure 4.1, due to J.M Chautru [19], illustrate this definition by showing two types of Boolean functions that we will study later on. In equation (4.4) we implicitly admit some measurability conditions of $f'(x/t)$ with respect to t, which will no longer be developed here (for theoretical developments on this point, see [112]).

4.4 The Characteristic Functional $Q(B)$

Let B be a compact set contred at point $(0, t_0)$ on the t-axis. According to the Matheron-Kendall theorem ([82], p.30), the probabilities $Q(B)$ that B lies in the pores (i.e. misses all the f') as B spans the class of the compact sets of $\mathbb{R}^n \times \mathbb{R}$ and as t_0 spans the t-axis, *characterize* the Boolean function f.

In the case of Boolean functions, the functional $Q(B)$ can be calculated easily (Serra,[131], p.321) and allows a rather simple expression. Indeed, we may state as follows.

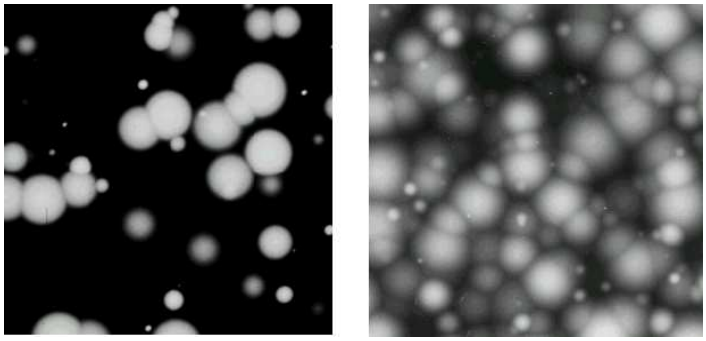

Figure 4.1: Simulations of the two major types of Boolean functions: Boolean islands (left, cone grains) and Rocky deeps (right, paraboloids grains)

Theorem 4.3 *The characteristic functional $Q(B)$ of the Boolean function $f = [f'(x/t), \theta(dt)]$ is*

$$Q(B) = \exp\left\{-\int_{-\infty}^{+\infty} \theta(dt)\, \check{c}\mu_n\left[\left(f'(x/t) \oplus \check{c}B\right) \cap \Pi_{-t}\right]\right\}; \qquad (4.5)$$

it shows that the random function f is stationary.

In this formula, B has been centred at the origin and $\check{c}B$ denotes the symmetric of B with respect to the origin in $\mathbb{R}^n \times \mathbb{R}$. When B is shifted up or down by t_0, we just have to replace t by $t - t_0$ in rel.(4.5). Π_{-t} denotes the horizontal plane at level t. We can illustrate these various parameters by taking an example. Suppose that $\theta(\mathrm{d}t) = \theta_1\delta_{t1} + \theta_2\delta_{t2}$ is the sum of two Dirac measures at levels $t_1 < 0$ and $t_2 > 0$. Take $f'(x/t_1) = f'_1(x)$ and $f'(x/t_2) = f'_2(x)$ to be the two primary functions and the disc B as structuring element. If $\check{c}I_1$ (resp.$\check{c}I_2$) designates the average length of the section L_1 of $f'_1(x) \oplus B$ by the horizontal line Π_{-t1} (resp, the section L_2 of $f'_2(x) \oplus B$ by Π_{-t2}), then the probability $Q(B)$ that B is above the graph of the Boolean function f is, according to rel.(4.5)

$$Q(B) = \exp\{-\theta_1\check{c}I_1 - \theta_2\check{c}I_2\} \qquad (4.6)$$

The example shows how some parameters of the primary grain, or more precisely, of its dilated versions, are reached via quantities that we can experimentally access (left member of rel.(4.6)).

4.4.1 Decompositions and uniqueness

But this example also exhibits a certain ambiguity. Consider the Boolean function f^* obtained by only *one* Dirac measure, namely $(\theta_1 + \theta_2)\,\delta_{t1}$, and whose primary grain is either f'_1 with a probability $\theta_1\,(\theta_1 + \theta_2)^{-1}$, or $f'_2 + (t_2 - t_1)$ with a probability $\theta_2\,(\theta_1 + \theta_2)^{-1}$. Clearly $f = f^*$, whereas both densities and primary grains differ from each other. A same Boolean function turns out to admit several *decompositions*. The range of this ambiguity is given by the following proposition, due to Prêteux & Schmitt ([112], p. 382).

Proposition 4.4 *Let $f = [f'(x/t), \theta(dt)]$ be a Boolean function. Every decomposition of f yields an intensity measure $\phi(dt)$ such that*

$$\int_{\mathbb{R}} \theta(dt) = \int_{\mathbb{R}} \varphi(dt) \tag{4.7}$$

(i) If $\int_{\mathbb{R}} \theta(dt) < \infty$, then there exists a decomposition of f of the form $[g'(x), a\delta_0]$ i.e. as Boolean islands.

(ii) If $\int_{\mathbb{R}} \theta(dt) = \infty$, then there exists a decomposition of f of the form $[g'(x/t), \mu^-]$, where μ^- is the Lebesgue measure on the negative t- axis.

In type (i), which is the more often used in practice, the Poisson points are concentrated in the plane Π_0. In type (ii) the intensity measure admits a uniform density. Here the simplest case occurs when the corresponding primary function $g'(x/t)$ is independent of the altitude of its location. We then find the rocky deep model ([131] chapter 15).

In the previous chapter, we had to assume the compacity of the primary grain X' of the Boolean RACS X for avoiding a full covering of the space. Here the corresponding notion consists in taking primary functions f' all of whose horizontal cross sections $X_t(f')$, $t < \infty$ are compact. We still have to associate an origin, i.e. a characteristic point, with each f'. In case of Rocky deeps, we can pin them up by their tops, but for Boolean islands it is preferable to fix the characteristic point at a centroid of their support, in order to have all the bases (rather than all the tops) located in the same horizontal plane [112].

4.5 Spatial law

Among others, the characteristic functional $Q(B)$ given by (4.5) allows us to calculate the *spatial law* of the model, i.e. the joint distribution of $f(x)$ at n

points x_1 ... x_n, n finite. As an example, we will determine the probabilities of order one and a moment of order two.

We start by choosing B as the point $(0,t)$, located at altitude t on the t- axis, and by setting $q = Q(0,t)$. q_t is the porosity of the section of f at altitude t. Relation (4.5) implies

$$\Pr\{f(x) < t\} = q_t = \exp\left\{-\int_{-\infty}^{+\infty} \theta(\mathrm{d}u)\, c\mu_n\left[(f'(x+u))_{-t} \cap \Pi_{-u}\right]\right\}. \tag{4.8}$$

Thus, the probability distribution of f involves only the $n-$volumes of the horizontal cross-sections of the primary grains, which are weighted by $\theta(\mathrm{d}t)$. When it exists, the mathematical expectation of $f(x)$ derives immediately

$$m = \int_0^{\infty} (1 - q_t)\, \mathrm{d}t - \int_{-\infty}^{0} q_t\, \mathrm{d}t. \tag{4.9}$$

The probabilities of order two, and the associated moments (covariance, variogram) may be calculated in a similar way. But their implementation involves a double integral in t. In the present case the variogram of order *one*, i.e. $2\gamma_1(h) = E|[f(0) - f(h)]|$ better suits the computational aspect of the model. γ_1 does not have the statistical properties of the covariance of the variogram and cannot serve to predict variances. However, morphologically speaking, it reveals the same features of $f(x)$ as those detected by the usual variogram γ_2 (anisotropies, periodicities, superimposition of scales, hole effects, nugget effects, ranges, etc). We will obtain $\gamma_1(h)$ by noticing that

$$|f(0) - f(h)| = \sup\{f(0), f(h)\} - \inf\{f(0), f(h)\}, \tag{4.10}$$

and that

$$Sup\{f(0), f(h)\} = f(0) + f(h) - \inf\{f(0), f(h)\}, \tag{4.11}$$

thus

$$|(f) - f(h)| = f(0) + f(h) - 2\inf\{f(0), f(h)\}. \tag{4.12}$$

Now, if B stands for the horizontal doublet $[(0,0),(h,0)]$ and if

$$Q_t(B) = \Pr\{f(0) < t; f(h) < t\}, \tag{4.13}$$

then

$$E[\inf\{f(0), f(h)\}] = \int_{-\infty}^{+\infty} -1 - q_t(B)]\mathrm{d}t \tag{4.14}$$

and finally:

$$\gamma_1(h) = \frac{1}{2}E|f(0) - f(h)| = \int_{-\infty}^{+\infty}[q_t - Q_t(B)]. \tag{4.15}$$

4.6 Divisibility under Supremum

Boolean random functions satisfy two major structural properties, namely divisibility under the sup operation , and semi Markovization. In this section, we present some results concerning only the first aspect. The second one is studied in ([131], ch.15), where the reader will also find the proofs which are missing here.

Before presenting these results it should be noted that first, the horizontal stationarity, which was necessary to formulate relation (4.5) and the spatial law, is no longer required here, and propositions 5-9 remain valid without this assumption. Secondly, concerning the fact that a random set approach to functions via their subgraphs is applied: all these random subgraphs share a *fixed* part, which is made of all the points $(x, -\infty)$, $x \in \mathbb{R}^n$.Similarly, when we transform the subgraphs by an anamorphosis such as e^t , we yield new subgraphs, (associated with the *positive* random function) which all contain the half $\mathbb{R}^{n+1}$ space of $t \leq 0$, as a fixed part. Indeed, the properties associated with infinite divisibility are valid only when the random sets under study have *no* fixed points ([82], p. 55). For this reason, we have restricted ourselves, in the definition equation (4.3), to the parts of the primary subgraphs which are above all the thresholds $t_0 \neq -\infty$. In the same way, when positive Boolean functions are concerned, we have to use exclusively compact structuring elements B of $\mathbb{R}^{n+1}$ which miss the half space of the negative or null t. This approach comes to work on the subgraphs minus their fixed points. Under these constraints, we may state the following.

Proposition 4.5 *The Minkowski sum of a Boolean random function f by an arbitrary compact set $K \subset \mathbb{R}^n \times \mathbb{R}$ is still a Boolean random function. (The Minkowski addition $f \oplus K$ of function f by set $K \subset \mathbb{R}^n \times \mathbb{R}$ is, by definition, the function whose subgraph is the Minkowski sum of the subgraph of f by K.)*

Corollary 4.1 *Let f be a Boolean function in $\mathbb{R}^n \times \mathbb{R}$. The cross-section of f by any subspace H is a Boolean function when H is parallel to the t-axis, and a Boolean set when it is orthogonal to the t-axis.*

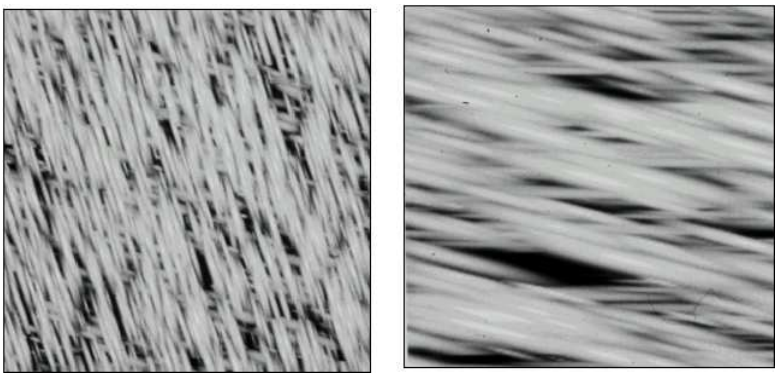

Figure 4.2: Suprema of Boolean Functions, involving anisotrpic conic and cylindric islands, and paraboloidic rocky deeps.

It suffices, for proving the corollary, to consider the horizontal cross-sections of f and of $f \cap H$. These induced Boolean functions will be investigated with more details for the Boolean Islands, when H is parallel to the t-axis (Section on stereology).

Proposition 4.6 *If* $\{f_j\} = \left\{f'_j, \theta_j(dt)\right\}, j \in \mathcal{J}$ *is a family of Boolean functions whose sum* $\theta = \sum_j \int_{\mathbb{R}} \theta_j(dt)$ *is finite, then* $f = Sup\{f_i\}$ *is a Boolean function of intensity* θ.

Figure 4.2 illustrates proposition 4.6. Now, what about the converse point of view, i.e. that of the infinite divisibility under supremum? A random closed *set* X is said to be infinitely divisible under $\cup$ if, for any integer $k > 0$, X is equivalent to the union $\cap X$ of k independent random closed sets $X_i, i = 1, 2, ..., k$, which are equivalent to one another. In particular, any Boolean random closed set is infinitely divisible under $\cup$. Moreover, owing to a Matheron theorem ([82], p. 56) and to equation (4.5) we can state the following.

Theorem 4.7 *Any random Boolean function* f *from* $\mathbb{R}^n$ *into* $\mathbb{R}$ *is infinitely divisible under Sup; i.e. for each integer* k*, it can be written as*

$$f = Sup\{f_i, i \in [1, ..., k]\}, \tag{4.16}$$

in which f_i *are* k *equivalent independent Boolean random functions.*

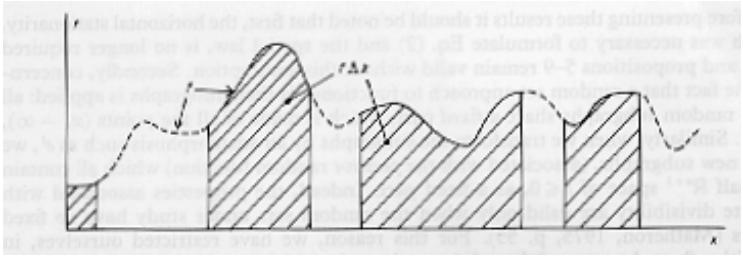

Figure 4.3: The function $k_i \wedge f_i$. The random function f_i is piecewise replaced by zero.

Note that there exist infinitely divisible random functions which are *not* Boolean (e.g. the Poisson functions (in [129], p. 471), whose horizontal sections are Poisson hyperplanes).

The following instructive property derives from infinite divisibility and shows that Boolean functions, just as Boolean sets, admit a domain of attraction. Consider m realizations $\{f_i\}, 1 \leq i \leq m$, of a stationary random function f of $\mathbb{R}^n$ which is non-negative, u.s.c., and a.s. bounded. Furthermore, let there be m realizations $\{X_i\}$ of a stationary random partition of $\mathbb{R}^n$ into a.s. bounded classes of non-zero measures.

All points of the topological closure $\overline{X_i}(j)$ of each class $X_i(j)$ of the realization X are coded with the value -∞ or $+\infty$ with a probability p which is independent of the class. This results in the function $k_i(x)$. Next, construct the random function

$$\varphi_m = v\{k_i \wedge f_i, 1 \leq i \leq m\}; \tag{4.17}$$

Fig.4.3 illustrates $k_i \wedge f_i$ in $\mathbb{R}^1$. Denote by k' the random function which assigns the value 1 to the closure of the class of X which contains the origin, and the value 0 everywhere else. This gives us:

Proposition 4.8 *When $p \to 0$ and $m \to \infty$ such that $mp \to \theta < \infty$, then the random function φ_m defined in equation (4.17) converges to the stationary Boolean islands with primary grain $f \wedge k'$ and with $\theta(dt) = \theta'\delta$, where δ is the Dirac measure located in $t = 0$, supp stands for the support, and*

$$\theta' = \theta\left\{\overline{\mu_n}\left[supp\left(f \wedge k'\right)\right]\right\}^{-1}. \tag{4.18}$$

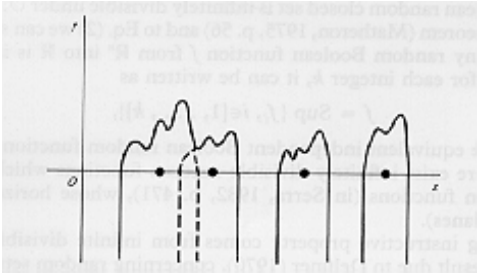

Figure 4.4: In Boolean islands, the Poisson points are concentrated in the horizontal plane Π_0 and the primary grains are positive functions: the study of the Boolean islands may be restricted to the positive t.

We thus discover a domain of attraction for the Boolean model and this is, without doubt, a strong reason why this model is so well-suited to the description of various physical phenomena.

4.7 The Boolean Islands

The Boolean islands model is obtained by taking for $\theta(\mathrm{d}t)$ a Dirac measure implanted at the origin of the t-axis, i.e. by putting $\theta(\mathrm{d}t) = \theta\delta_0(\mathrm{d}t)$. The germs turn out to be an n-dimensional stationary Poisson point process located in Π_0 and having an intensity θ (see Fig.4.4). Clearly, this designs the simplest Boolean function that can be imagined; indeed, it has been the first to be proposed in the literature.
If we replace $\theta(\mathrm{d}t)$ in rel.(4.5), the characteristic functional becomes

$$Q(B) = \exp\left\{-\theta \,\text{Þc}\mu_n\left[\left(f' \oplus \text{Þc}B\right) \cap \Pi_0\right]\right\}. \tag{4.19}$$

When B is moved by a vertical translation of vector t, ÞcB is replaced by ÞcB_{-t} and

$$\left(f' \oplus \text{Þc}B_{-t}\right) \cap \Pi_0 = \left(f' \oplus \text{Þc}B\right)_{-t} \cap \Pi_0 = \left[\left(f' \oplus \text{Þc}B\right) \cap \Pi_t\right]_{-t'} \tag{4.20}$$

thus

$$Q(B_t) = \exp\left\{-\theta \,\text{Þc}\mu_n\left[\left(f' \oplus \text{Þc}B\right) \cap \Pi_t\right]\right\}, \tag{4.21}$$

which is Serra's original formula ([129], p. 470). For the sake of simplicity, the primary grain f' is considered to be a *non-negative* function: it is always

possible to modify the t-axis by the anamorphosis $t' =$ (principal value of $\tan^{-1} t) = \Pi/2$. Since the B are compact we can also consider that the expression "B is implanted at the origin" means "the origin is the highest point of B" (or one of the highest points in case of non-unicity). Then, $f' \oplus \hat{\jmath} cB$ is still non-negative.

To say that point (x,t) belongs to $(f' \oplus \hat{\jmath} cB) \cap \Pi_t$ is equivalent to saying that $(f' \oplus \hat{\jmath} cB)(x) \geq t$. Such an event occurs with a probability 1-$F_x(t, f' \oplus \hat{\jmath} cB)$ where $F_x(t, f' \oplus \hat{\jmath} cB)$ is the distribution function of the random variable $f' \oplus \hat{\jmath} cB$. We know from Matheron ([82], p.47) that we can invert integration over $\mathbb{R}^n$ and mathematical expectation, and write:

$$\begin{aligned} M(k,B) &= -\int_0^\infty t^{k-1} \log Q(B_t)\, dt \\ &= \theta \int_{\mathbb{R}^n} dx \int_0^\infty t^{k-1} \left[1 - F_x\left(t, f' \oplus \hat{\jmath} cB\right)\right] dt, \\ &= \frac{\theta}{k} E\left[\int_{\mathbb{R}^n} \left(f' \oplus \hat{\jmath} cB\right)^k (x)\, dx\right]. \end{aligned}$$

Thus there is a one to one and onto correspondence between the moments of $\log Q(B_t)$ and the average space integrals of the powers of $f' \oplus \hat{\jmath} cB$. In particular, for $k = 1$, one finds (Jeulin, 1985; Serra, 1985):

$$M(1,B) = -\int_0^\infty \log Q(B_t)\, dt = \theta E\left[\int_{\mathbb{R}^n} \left(f' \oplus \hat{\jmath} cB\right)(x)\, dx\right]. \qquad (4.22)$$

Let us summarize these results by stating :

Theorem 4.9 *A Boolean islands model is a Boolean function with measure $\theta(dt)$ being θ times a Dirac measure concentrated in $t = 0$, and with a non-negative primary grain $f'(x)$. It allows the following characteristic functional*

$$Q(B_t) = \exp\left\{-\theta\, \hat{\jmath} c \mu_n\left[\left(f' \oplus \hat{\jmath} cB\right) \cap \Pi_t\right]\right\}, \qquad (t>0)$$

such that

$$-\int_0^\infty t^{k-1} \log Q(B_t)\, dt = \frac{\theta}{k} E\left[\int_{\mathbb{R}^n} \left(f' \oplus \hat{\jmath} cB\right)^k (x)\, dx\right]. \qquad (4.23)$$

We will now complete the study of this model by calculating θ and various measurements on f' from the $Q(B)$. By simplifying the notation, we consider that

- $v(f')$ and $h(f')$, i.e. volume and maximal height,
- q_t, s_t, porosity and specific surface of $f \cap \Pi_t$,
- s'_t, surface of $f \cap \Pi_t$,

are always mathematical expectations.

4.7.1 Volume of f' and its support

First, we take B to be the origin. By applying rel.(4.22) we find

$$M(1, \{\sigma\}) = -\int_0^\infty \log q_t \mathrm{d}t = \theta \int_{\mathbb{R}^n} E\left[f'(x)\right] \mathrm{d}x = \theta v\left(f'\right). \tag{4.24}$$

Consider now the support $\mathrm{supp}(f')$ of f' (i.e. the set of points $x \in \mathbb{R}^n$ where $f'(x) \neq 0$), and take B to be the vertical segment of length τ whose top point is the origin. Formula (4.22) gives

$$M(1, B) = \theta v\left(f'\right) + \theta\tau \, \mathbb{E}c\mu_n\left[\mathrm{supp}\left(f'\right)\right]. \tag{4.25}$$

In digital imagery, the dilation by an elementary vertical segment consists in adding one to the function f under study. More simply, the above procedure comes to work on the set $X_1 = \{x : f(x) \geq 1\}$ and to compute its porosity q_{t0}. The Boolean assumption implies that :

$$\log\ q_1 = \theta \, \mathbb{E}c\mu_n\left[\mathrm{supp}\ \left(f'\right)\right]. \tag{4.26}$$

4.7.2 Pseudo-covariance

Choose B to be a pair of points distant from the horizontal vector h, of modulus $|h|$ and direction α. Let $Q_t(h) = Q_t(|h|, \alpha)$ be the probability that B misses the umbra of f. The equation (4.22) now takes the following form

$$-\int_0^\infty \log Q_t(h) \, \mathrm{d}t = 2\theta v' - \theta \int_{\mathbb{R}^n} \inf\left[f'(x), f'(x+h)\right] \mathrm{d}x, \tag{4.27}$$

or, if $K'_t(|h|, \alpha)$ denotes the n-dimensional geometric covariogram of section X'_t of the primary grain f' by the hyperplane Π_t, equivalently

$$-\int_0^\infty \log Q_t(h) \, \mathrm{d}t = \theta \int_0^\infty \left[2K'_t(0; \alpha) - K'_t(|h|, \alpha)\right] \mathrm{d}t. \tag{4.28}$$

We may consider this integral as a sort of pseudo-covariance because it can exhibit nugget effects, hole effects, or more or less periodic oscillations,

etc. just like the true covariance ([129], chapter 9). Note that the variogram of order one which can be drawn from rel.(4.27) concerns function f' and not function f, as was the variogram $\gamma_1(h)$ of Section 4.

Furthermore, it is a functional which is directly related to the primary grain f', and which can be calculated theoretically when one wants to test a specific model.

4.7.3 Gradient

Suppose that the primary grain function $f'(x)$ is regular enough so that we can take the derivative with respect to $|h|$ under summation in rel.(4.27) (this implies that the primary grain is not fractal). We obtain for $h = 0$:

$$\int_0^\infty Q'_t(0;\alpha)/Q_t(0)\,\mathrm{d}t = \theta \int_0^\infty \left|\partial K'_t(|h|;\alpha)/\partial|h|\right|_{h=0} \mathrm{d}t. \tag{4.29}$$

Here, $Q'_t(0;\alpha)$ is the (specific) variation of the diameter of the Boolean set $X_t = f \cap \Pi_t$ in the direction α, and K'_t is the (global) covariogram of the primary grain $X'_t = f' \cap \Pi_t$. By averaging over the directions α perpendicular to the t-axis, equality (4.29) becomes a relationship between the specific surface s_t (of n, not $n+1$, dimensions) of the set X_t and the (non-specific) surface s'_t of its primary grain section X'_t :

$$\int_{\Omega n} \mathrm{d}\alpha \int_0^\infty Q'_t(o;\alpha)/Q_t(o)\,\mathrm{d}t = \int_0^\infty s_t/q_t \mathrm{d}t = \theta \int_0^\infty s'_t(\mathrm{d}t), \tag{4.30}$$

a relationship whose left member is experimentally accessible. This set relation, which is informative in itself, can be interpreted in terms of functions. By introducing the module $\ell'(x)$ of the gradient of the primary grain function $f'(x)$ and using proposition (14-4) in [131] we obtain

$$\int_0^\infty s_t/q_t \mathrm{d}t = \theta E\left[\int_{\mathbb{R}^n} \ell'(x)\,\mathrm{d}x\right]. \tag{4.31}$$

4.7.4 Number of maxima

We will end with a result about the maxima [56]. Take for primary grain a random function f' that has (a.s.)only one maximum value, h' say, and locate conventionally the maximum at the vertical of the origin. The probability that the random variable h' lies in the interval $(t, t+dt)$ is $\overline{\omega}(dt)$ and $\nu(dt)$ stands for the specific number of maxima of f (i.e.after booleanization) in

the interval $(t, t+dt)$. Then the elementary zone dV of size $dx \times dt$ contains a maximum of f if there is a germ in dx, if the corresponding grain as a height h', and finally if this maximum is not covered by an other grain, which occurs with a probability $Q(dV) \simeq q_t(1-\theta dxdt)$. Therefore the specific number $v(dt)$ of maxima of f (i.e. the average number of maxima per unit volume in $\mathbb{R}^n$) between the altitudes t and $t+dt$ is given by

$$v(dt) = \theta.q_t.\overline{\omega}(dt), \tag{4.32}$$

a relation that allows to estimate the unknown probability $\overline{\omega}(dt)$ from the experimental data.

4.8 Convexity and Boolean Islands

Generally, convexity occurs in Boolean models (sets or functions) for two reasons. Via the Steiner relationship, it provides a means for calculating $\mu_n(f' \oplus \check{B})$ for various B, and consequently for *testing* the model; moreover it allows us to formulate and solve *stereological questions*. In testing problems, three levels of assumptions have to be distinguished:

(i) the support $\text{supp}(f')$ of f' is compact convex (in $\mathbb{R}^n$)
(ii) all the horizontal cross-sections of f' are compact convex (in $\mathbb{R}^n$)
(iii) the subgraph of f' is compact convex in $\mathbb{R}^n \times \mathbb{R}^+$.

Each hypothesis contains the preceding ones. Below, we develop the first two cases only. As a matter of fact nothing really new is reached within the framework of assumption (iii) (for further discussion see [131], pp. 334 and 398).

Before comparing the first two assumptions, we recall the classical Steiner formulae ([129], p.111). In $\mathbb{R}^3$, when B is successively a segment of length l, a disc of radius r or a ball of radius λ, the average volumes of the dilates of a compact convex set A by lB, rB and λB are given by :

$$\begin{cases} v(A \oplus lB) = v(A) + \frac{l}{4}s(A) \\ v(A \oplus rB) = v(A) + \frac{\pi}{4}rs(A) + \pi r^2 d(A) \\ v(A \oplus \lambda B) = v(A) + \lambda s(A) + \frac{\pi\lambda^2}{2}d(A) + \frac{4}{3}\pi\lambda^3 \end{cases} \tag{4.33}$$

$(v, s \text{ and } d \text{ denote the volume, surface and mean width respectively})$.

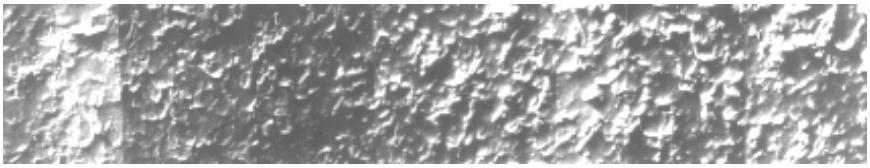

Figure 4.5: Synthetic image obtained from roughness profiles of an iron plate (D. Jeulin).

In R^2, when B is successively a segment of length l, then a disc of radius r, we find similarly :

$$\begin{aligned} a(A \oplus lB) &= a(A) + \frac{u(A)}{\pi} l \\ a(A \oplus \lambda B) &= a(A) + \lambda u(A) + \pi\lambda^2 \end{aligned} \tag{4.34}$$

(a = area, u = perimeter). This said, averaging according to the rotations of the space is not a dogma. We can alternatively perform cylindrical dilations. In the case of a primary grain f' of $\mathbb{R}^2 \times \mathbb{R}^+$, this technique comes to averaging with respect to the rotations of $\mathbb{R}^2$; the volume of the dilate is then given by a Steiner polynomial of $\mathbb{R}^2$ (in which B is the circular basis of the cylinder) multiplied by the thickness τ of the cylinder.

Lastly, we can remark that the linear structure of the rel.(4.33) may subsist in practice even when none of the three convexity assumptions is stricly satisfied. A classical example is given by Jeulin's study on the roughness of iron plates ([56]). The rolling process has torn up small "crescents of moon" which are visible on the photograph in 4.5.This relief of an iron plate is reconstructed from a series of roughness profiles, where the t-axis is strongly emphasized. Whereas the primary functions are obviously non-convex, D. Jeulin succeeded in proving the Boolean structure of the relief by using non-isotropic Steiner formulae ([56]).

Although these primary functions are not convex, the volumes of their dilations by horizontal segments of length λ can be fitted with linear functions of λ.

4.8.1 Convexity of the support supp (f')

Assumption (i) concerns above all the calculation of θ. When it is satisfied, the probability $Q(\lambda B)$ that a ball λB of $\mathbb{R}^n$, lying in Π_0, misses the support

$\text{supp}(f)$ is such that

$$\log Q(\lambda B) = -\theta \, \text{Pc}\mu_n \left[\text{supp}\left(f'\right) \oplus \lambda \, \text{Pc}B\right]. \tag{4.35}$$

By taking $\text{supp}(f')$ for A in the third rel.(4.33) (resp. the second rel.(4.34)) we obtain a polynomial of degree 3 (resp. 2) in λ, whose coefficient of the term of highest degree allows one to estimate θ. Then the other terms give the Minkowski functionals of $\text{supp}(f')$. The reader will find a more detailed presentation of this technique in Serra ([129], pp. 495-502).

Notice that this procedure tests the Boolean structure of supp (f) and, at the same time, determines θ and the major characteristics of $\text{supp}(f')$. However, there is no certainty that f itself is Boolean but only presumptions.

4.8.2 Convexity of the horizontal cross-sections of f'

As far as convexity is concerned, assumption (ii) is an important one. First, if we extend the previous procedure to the series of the cross-sections f, we can test whether all these sections are Boolean, and have strong presumptions that f is Boolean.

Secondly, if the section at level t is Boolean with a density θ_t, then θ_t is θ multiplied by the probability that the primary function f' is higher than t. Denoting by $G(t)$ the distribution function of the maximum height of f' we have:

$$\theta_t = \theta \left[1 - G(t)\right], \tag{4.36}$$

a relation which can be used to estimate $G(t)$ from experimental values of θ_t.

Thirdly, using Steiner's formulae we access the average Minkowski functionals of the section as functions of the level t. If we want to express them more synthetically, we can use functionals of $M(B)$ type rel.(4.22). For example, in $\mathbb{R}^2 \times \mathbb{R}^+$, for B a compact convex set with an area $a(B)$ and a perimeter $u(B)$, we can write

$$-\int_0^\infty \log Q(\lambda B_t)\, \mathrm{d}t = \theta \left\{ v\left(f'\right) + \lambda \frac{u(B)}{2\pi} E\left[\int_{\mathbb{R}^2} \ell'(x)\, \mathrm{d}x\right] + \lambda^2 a(B)\, h\left(f'\right)\right\}, \tag{4.37}$$

where $h(f')$ is the mathematical expectation of the maximal height of f', i.e.

$$h\left(f'\right) = \int_0^\infty \left[1 - G(t)\right] \mathrm{d}t. \tag{4.38}$$

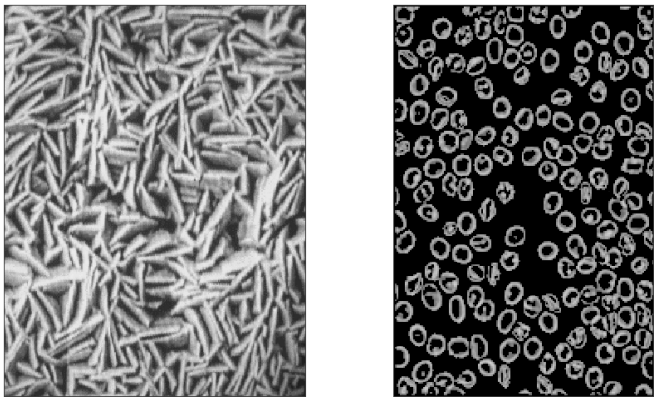

Figure 4.6: Two natural textures that can be modelled by Boolean islands. The elementary crystals of ferrite (left) are convex. In contrast, neither the red blood cells, not their supports (right) are convex.

(In rel.(4.37), the Boolean function is assumed to be isotropic. When not, one must average the left member with respect to the rotations of B in $\mathbb{R}^2$.)

Notice that the average integral $v(f')$ of f', and that of its gradient ℓ' could be calculated directly, see rel.(4.24) and (4.31) without assuming convexity, but also without any guarantee that the Boolean model, hence the formalism, is valid.

4.8.3 Heuristic use of Boolean islands

In the previous chapter, we draw from the Boolean RACS a counting algorithm that proved to be efficient even when the structure under study was not Boolean at all. The Boolean islands lend themselves to the same use. The algorithm derive now from the integral (4.24), which allow us to estimate θ_2 as soon as we know a priori $v(f')$, or by direct measurements on isolated grains . The number of red blood cells (estimated by 188 in the binary approach of the previous chapter) is now given by the above formula (4.24) :

$$-\int_0^\infty \log q_t \mathrm{d}t = \theta_2 v\left(f'\right). \tag{4.39}$$

which results in $N =$ - (*field area* . $-\int_{90}^{255} \log q_t \mathrm{d}t$) / $v(f') = 39360 \times 70{,}055$ / $14.020 = 197$.

4.9 Stereology for Boolean Islands

The situations which require a stereological approach are, in general, of two types. First, they can concern a (3-D) material with a variable grey tone at each point. For example, in radiology we could consider the X-rays or the NMR tomography of an organ. (We assume here that we have access only to individual planar cross-sections of the material, and not to series of sections.) Secondly, the material under study may be two-dimensional and is accessed by vertical profiles (e.g. roughness measurements). The block diagram representation of Fig. 7 clearly shows the two situations, since it exhibits one vertical section, and is itself the cross-section of a 3-D grey tone function.

If a 3-D function is a Boolean island f_3 of intensity θ_3 and with primary grain f_3', then it is easy to see that it induces a 2-D Boolean island function f_2 on each planar cross-section of the space. Let $\Pi(\varpi)$ be one of the planar cross-sections, with orientation ϖ; let $\theta_2 = \theta_2(\varpi)$ and $f_2' = f_2'(\varpi)$ denote respectively the induced intensity and the induced primary grain. To f_2 and f_2' there correspond sets in the 3-D space $\mathbb{R}^2 \times \mathbb{R}$ and to f_3 and f_3' there correspond sets in the *four*-dimensional space $\mathbb{R}^3 \times \mathbb{R}$.

We first show that θ_2 is proportional to θ_3. A grain $f'(x)$ at the point x in $\mathbb{R}^3$ induces another grain in the section $\Pi(\varpi)$ if and only if the support $\text{supp}[f(x)\ ]$ of $f(x)$ hits $\Pi(\varpi)$. This leads us to a problem concerning the supports of Boolean sets. We know ([76], p.70; [129], p.489) that

$$q_2 = \theta_3 D_3'(\varpi), \tag{4.40}$$

where $D_3'(\varpi)$ is the average apparent diameter, or width, of $\text{supp}[f_3'(x)]$ in direction ϖ. Likewise, we can go from the function f_3 to the function f_1 induced on the linear cross-section $\Delta(\varpi)$ in the direction ϖ using the following relation:

$$\theta_1 = \theta_3 S_3(\varpi), \tag{4.41}$$

in which θ_1 is the induced intensity on $\Delta(\varpi)$ and $S_3(\varpi)$ is the average apparent 2-D surface of $\text{supp}[f_3'(x)]$ perpendicular to the direction ϖ.

We obtain a second relationship between the parameters of f_3 and of f_2 by noting that the porosity q_t is the same if it is measured in R^3 or in any vertical cross-section, i.e.

$$-\int_0^\infty \log q_t dt = \theta_3 v_3\left(f_3'\right) = \theta_2 v_2\left(f_2'\right) = \theta_1 v_1\left(f_1'\right) \tag{4.42}$$

and by combining with rel.(4.40):

$$v_3\left(f_3'\right) = v_2\left(f_2'\right) D_3'\left(\varpi\right) = v_1\left(f_1'\right) S_3'\left(\varpi\right). \tag{4.43}$$

This asserts that the mathematical expectation of the integral of the original primary grain is equal to the product of the expectation of the integral of the induced grain and the measurement of the apparent contour of its support in the complementary sub-space of the section.

By applying similar reasoning in $\mathbb{R}^2 \times \mathbb{R}^+$. We obtain

$$\begin{cases} \theta_2 v_2\left(f_2'\right) = \theta_1\left(\alpha\right) v_1\left(f_1'\right) \\ \text{and} \\ v_2\left(f_2'\right) = v_1\left(f_1'\right) D_2'\left(\alpha\right), \end{cases} \tag{4.44}$$

where $\alpha \in (0, 2\pi)$ is the normal to the vertical cross-section under study (e.g. vertical profiles on a rough metallic surface). We can state the following.

Theorem 4.10 *Let f be a Boolean island function in $\mathbb{R}^3 \times \mathbb{R}$. The cross-sections of f_3 by 3-D and 2-D sub-spaces parallel to the $t-$axis are still Boolean islands in $\mathbb{R}^2 \times \mathbb{R}$ and in $\mathbb{R} \times \mathbb{R}$ respectively. The corresponding intensities and mean volumes are given by rel.(4.42) and (4.43). Similar statements and results exist from $\mathbb{R}^2 \times \mathbb{R}$ to $\mathbb{R} \times \mathbb{R}$, see rel.(4.44).*

Comments :

(1) Obviously, the theorem could be stated in $\mathbb{R}^n$.

(2) These results remain rather general in the sense that they do not assume convexity nor isotropy for the primary functions.

(3) However, these results suffer from the inevitable stereological limitation that measurements in sub-spaces of $\mathbb{R}^3$ can give all Minkowski functionals of the space, except the last one, i.e. the countability. Here, it is θ_3 [or $v\left(f_3'\right)$] which remains inaccessible. In rel.(4.40) and (4.42) the left members may be estimated by experiments. So we only know the *product* $\theta_3 v_3\left(f_3'\right)$.

(4) Instead of *sections* we could also consider slices S with a non-zero thickness $\mathrm{d}\varpi$, and parallel to the t-axis. The sup of the grey intensity taken at each point $x \in S$, along $\mathrm{d}\varpi$, generates a Boolean island. The technique for studying it is that presented for Boolean sets in Serra ([129], pp. 496-497).

4.9.1 Use of stereology

What can we gain from these stereological calculations ?

(a) First, we can use them for studying evolutions. For example, in $\mathbb{R}^3$, if we wish to know if θ_3 has increased by 10% from one state to another, it is not necessary to know v_3' : we simply assume that it is constant.

(b) During an evolutionary process, we can also separate the part due to the nucleation of new grains from the part due to the increase (or reduction) in size of the already existing grains. Here again we must assume that the grains are convex. Let us denote the parameters of the final state by capital letters. If variation by simple growth has occured (in $\mathbb{R}^3 \times \mathbb{R}^+$ for example), then

$$\begin{aligned} \left(\theta_3 V_3'\right) / \left(\theta_3 v_3'\right) &= k^3, \\ \left(\theta_3 S_3'\right) / \left(\theta_3 s_3'\right) &= k^2, \\ \left(\theta_3 H_3'\right) / \left(\theta_3 h_3'\right) &= k, \end{aligned}$$

since $\theta_3 = \theta_3'$. On the contrary, these three ratios are equal if there is nucleation without modification in the probability distribution of the primary grain. In the same way, we can test the increase in volume with constant intensity (change of scale of the primary grain in $\mathbb{R}^3$ only), etc.

$$-\int_0^\infty \log q_t \mathrm{d}t = \theta_2 v_2' = \theta_3 v_3' \tag{4.45}$$

we can deduce a *counting algorithm*. If we know v_3' and v_2' a priori, or from direct measurement of isolated grains, then from (4.45) it suffices to calculate *the proportion of surface* q_t on each level to deduce an estimate of θ_2 (or θ_3). It turns out that even when the Boolean model fails, for large distances in particular, (4.45) remains a good estimate (within 10 %) of the number of objects in a scene. Furthermore, this estimate is quite insensitive to noise (as opposed to the Euler-Poincaré constant) and is *well* adapted to the case of partial coverings. Finally, a threshold is unnecessary because (4.45) asserts that all levels are examined.

In conclusion, note that one can also decide to reject stereology, and choose a sequence of planar cross-sections which are close to each other. This is often the best solution in X-ray tomography and in nuclear magnetic resonance images. It then suffices to dilate the function by several simple polyhedrons in order to obtain a reasonable estimate of θ_3 from a few cross-sections. The measurement of the remaining parameters can be obtained from planar and linear structuring elements, and the list of parameter estimates of the model is therefore complete. Note that the hypothesis of convexity is still indispensable for the calculation of the intensities θ_3 and θ_2 (it involves the Steiner formula).

4.10 The Rocky Deeps Model

When one contemplates the view of a submarine coral reef, where the deeper the rocks the darker they appear, one has the impression of diving into infinite deeps. The theory of Boolean functions allows one to model such a relief as follows [131]:

(a) the elementary Poisson point intensity is

$$\begin{cases} \theta(\mathrm{d}t) = 0 & \text{when } t > 0 \\ \theta(\mathrm{d}t) = \theta\,|\mathrm{d}t| & \text{when } t \leq 0; \end{cases} \tag{4.46}$$

(b) the primary grain f' is independent of t

$$f'(x/t) = f'(x) \qquad (t \leq 0)\,. \tag{4.47}$$

Figs.4.1 and 4.7 give an idea of the model, that we shall call "rocky deeps". In fact it is a Boolean random function of the general type, and even the simplest one, since the primary grains exhibit the same shape and size everywhere. So, we can reasonably expect simple expressions for the characteristic functionals.

Let $B(h)$ be a compact set implanted at height h. The probability $Q(B_h)$ that B(h) misses the rocks is given by the characteristic functional (4.5), which becomes in the present case:

$$\begin{aligned} Q(B_h) &= \exp\left\{-\theta \int_{-\infty}^{0} \mathrm{d}\mu_n \left[\left(f' \oplus \check{B}(-h)\right) \cap \Pi_{-t}\right] \mathrm{d}(-t)\right\}, \\ Q(B_h) &= \exp\left\{-\theta \int_{0}^{\infty} \mathrm{d}\mu_n \left[\left(f' \oplus \check{B}\right)_{-h} \cap \Pi_t\right] \mathrm{d}t\right\}, \\ Q(B_h) &= \exp\left\{-\theta \int_{h}^{\infty} \mathrm{d}\mu_n \left[\left(f' \oplus \check{B}\right) \cap \Pi_u\right] \mathrm{d}u\right\}. \end{aligned} \tag{4.48}$$

Example of Boolean rocky deeps; the Poisson density is uniform over the negative half space and null for positive t. The primary grain (here a cone) is the same for all depths, and has the origin located at its top.

This relationship is the fundamental formula of the model. The derivation and the integral of $\log Q(B_h)$ are instructive. Indeed,

$$\frac{1}{Q(B_h)} \cdot \frac{\mathrm{d}Q(B_h)}{\mathrm{d}h} = \theta \mathrm{d}\mu_n \left[\left(f' \oplus \check{B}\right) \cap \Pi_h\right], \tag{4.49}$$

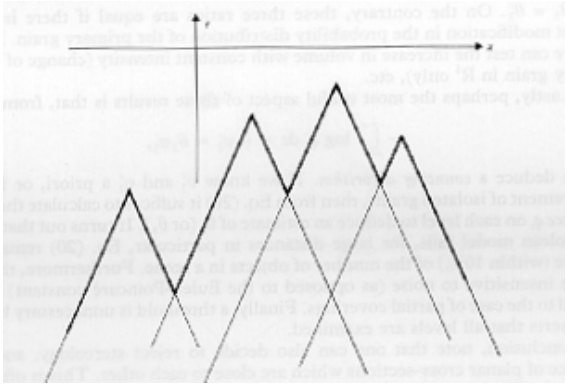

Figure 4.7: Example of Boolean rocky deeps; the Poisson density is uniform over the negative half space and null for positive t. The primary grain (here a cone) is the same for all depths, and has the origin located at its top.

i.e. the logarithmic derivative of $Q(B_h)$ equals θ times the average measure of the cross-section of $f' \oplus \check{B}$ at level h. So the left member of Eq.(4.49) must be positive and decrease as h increases, and these two properties can be tested from the estimates of $Q(B_h)$. If we now calculate the moment of order p of $\log Q(B_h)$, $(p > 1)$, we obtain, by integrating by parts :

$$-\int_0^\infty h^{p-2} \log Q(B_h)\, \mathrm{d}h = \frac{\theta}{p-1} \int_0^\infty h^{p-1} \mu_n \left[\left(f' \oplus \check{B} \right) \cap \Pi_h \right] \mathrm{d}h. \tag{4.50}$$

We have already interpreted the right member of this equality in terms of integrals of $(f' \oplus \check{B})^p$ when studying the Boolean islands. This leads to the following basic formula of the Rocky deeps model:

$$-\int_0^\infty h^{p-2} \log Q(B_h)\, \mathrm{d}h = \frac{\theta}{p(p-1)} E\left\{ \int_{\mathbb{R}n} \left(f' \oplus \check{B} \right)^p (x)\, \mathrm{d}x \right\}, \qquad p > 1. \tag{4.51}$$

It exhibits the same structure as the corresponding relation for Boolean islands (see Eq (4.23)) but with different integrands.

4.11 Exercises

4.11.1 Random ω-continuous functions

This exercise aims to provide a random status to the ω-continuous classes introduced in chapter 4.

1. Construct the class of the random ω-continuous functions

[Given a modulus of continuity ω, the lattice L_ω is compact as a closed subset of the (compact) set F of the upper semi-continuous functions from E into $\overline{\mathbb{R}}$. The events (4.1) that generate the σ-algebra σ on F admit a similar meaning in L_ω, and the compactness of L_ω ensures that there do exist probabilities on the σ-algebra of the measurable space (L_ω, σ). Moreover, we draw from Theorem 4.14 that the dilations (and the erosions) acting on L_ω, as well as their finite sup, inf, and compositions preserve class L_ω in the stationary case, and then are continuous.

The random functions which will be obtained from $(L_{\omega,}\sigma)$ will result in relatively regular realizations. For example, a Lipschitz Boolean function will accept sharp valleys, but without strict verticalities.]

2. Establish first the following lemma :

Lemma 4.11 *: A function $f : E \to \overline{\mathbb{R}}$, E a metric space, is $\omega-$continuous if and only if for all $x \in E, t \in \mathbb{R}$ and $h > 0$, we have*

$$f(x) < t \qquad and \qquad y \in B_{\theta(h)} \Longrightarrow \qquad f(y) < t + h \tag{4.52}$$

where function θ designates the largest inverse of modulus ω, i.e.

$$\theta(h) = \sup\{d : \omega(d) \leq h\} \qquad h, d \in \mathbb{R}_+ \tag{4.53}$$

and where $B_{\theta(h)}(x)$ is the closed ball centered at x and of radius $\theta(h)$.

[Suppose f to be ω-continuous, and $f(x) < t$ for some $x \in E$ and some $t \in \mathbb{R}$. Fix the value h. If point $y \in B_{\theta(h)}(x)$, then $d(x, y) = \theta(h)$,i.e. $\omega[d(x, y)] \leq h$. Since f is ω-continuous, we have

$$f(y) \leq f(x) + \omega[d(x, y)] < t + h \tag{4.54}$$

Conversely, suppose that implication (4.52) is true for all $x \in E, t \in \mathbb{R}$ and $h > 0$. If there is no pair (x, t) such that $f(x) < t$, then $f = +\infty$, hence

is ω-continuous. If not, $f(x)$ admits finite upper bounds t and rel.(4.52) implies, for any point y at distance $\theta(h)$ from x apart, that

$$f(y) < h + t \qquad \Longrightarrow \qquad f(y) \leq h + \bigwedge \{t, t > f(x)\} = h + f(x) \quad (4.55)$$

and finally $|f(y) - f(x)| \leq h = \omega[d(x,y)]$.

Now point y may, in turn, play the role of starting point for an arbitrary point z, since $f(y) < \infty$, and this achieves the proof.]

In more geometrical terms, the lemma says that when a point (x,t) is strictly above the subgraph of the $\omega-$continuous function f, in the product space $E \times \overline{\mathbb{R}}$, then the whole cone of summit (x,t), of generator $\omega(d)$ and oriented upwards, is strictly above the subgraph of f.

3. How does the ω-continuity affect the characteristic functional rel.(4.5)?

In terms of Random Sets, the property depicted by the previous lemma has a meaning of a *condition* : when we know that compact set K misses the subgraph of f, then all the sections of the cone generated from K, miss it too. Prove that this result can be stated as follows :

Proposition 4.12 *Let f be a random u.s.c. function from a metric space E into $\overline{\mathbb{R}}$. Function f is almost surely $\omega-$continuous if and only if there exists a function $\omega : \mathbb{R}_+ \to \mathbb{R}_+$ continuous at the origin, and such that we have for all $K \in \mathcal{K}, t \in \mathbb{R}$ and $h \geq 0$:*

$$\Pr\left\{\sup\left\{f(x), x \in \delta_{\theta(h)}(K)\right\} < t + h / \sup\{f(x), x \in K\} < t\right\} = 1 \quad (4.56)$$

where $\theta(h) = \sup\{d : \omega(d) \leq h\}$.

[Observe that implication (4.52) extends to compact sets K, since the dilate of set $\delta_{\theta(h)}(K)$ of set K by the closed ball $B_{\theta(h)}$ is the union of the balls $B_{\theta(h)}(x)$, as x spans K. Hence we have

$$\sup\{f(x), x \in K\} < t \qquad \Longrightarrow \qquad \sup\{f(x), x \in \delta_{\theta(h)}(K)\} < t + h \quad (4.57)$$

Therefore the event of the left member of Eq.(4.56) is almost sure, which yields Eq.(4.56). Conversely, the datum of Eq.(4.56) means almost surely implication (4.57), hence the a.s. ω-continuity of f.]

Bibliography

[1] **R. Alberny, J. Serra and M. Turpin**, Use of covariograms for Dendrite Arm Spacing Measurements, *Trans.* AIME 245, 55-59,1969.

[2] **C. Arcelli and G. Saniti di Baja**, "Width-independent fast thinning algorithms", *IEEE Trans. Pattern Anal. Machine Intell.,* vol. 7, pp. 463-474, 1985.

[3] **G. Ayala** *Inferencia in modelos Booleanos.* Thesis Doc. Sci. Universitat de Valencia, Spain;1988.

[4] **G.J.F. Banon, and J. Barrera,** Minimal representation for translation-invariant set mappings by mathematical morphology. SIAM J. Appl. Math. 1991,vol.51, pp.1782-1798.

[5] **G. Bertrand**, "Simple points, topological numbers and geodesic neighborhoods in cubic grids", *Pattern Rec. Letters*, vol. 15, pp. 1003-1012, 1994.

[6] **S. Beucher**, Interpolation of sets, of partitions and of functions, *Mathematical Morphology and its applications to image and signal processing*, H.Heijmans and J. Roerdink eds Kluwer,1998,

[7] **S. Beucher & C. Lantuejoul,** Use of watersheds in contour detection, *Proc. Int. Workshop on image processing, real-time edge and motion detection/estimation,* Rennes (France), September 1979.

[8] **S. Beucher,** Analyse de diagraphies électriques par morphologie mathématique, int. report, CMM, School of Mines, Paris, January 1989.

[9] **S. Beucher & L. Vincent,** Introduction aux outils morphologiques de segmentation*, J. de Spectroscopie et de Microscopie Electronique,* 43 p., September 1989.

[10] **P. Bhanu Prasad, J.P. Jernot, M. Coster, J.L. Chermant**, "Analyse morphologique tridimensionnelle des matériaux condensés", *in Proc. PIXIM,* 1988, pp. 31-42.

[11] **P. Bhanu Prasad, J.P. Jernot** Three dimensional homotopic thinning of digitized sets, *Acta Stereologica,* vol. 9, pp. 235-241, 1990

[12] **G. Birkhoff,** *Lattice theory,* 3^{rd} edition, A.M.S. Colloq. publ., vol. 25, 1983.

[13] **W. V. Blasckhe**, Vorlesungun über integral Geometrie, Teubner, Leipzig, 1939.

[14] **T.S. Blyth & M.F. Janowitz,** *Residuation theory* Pergamon Press, Oxford, 1972

[15] **G. Borgefors** Distance transformations in digital space. *Computer Vision, Graphics and Image Porcessing,* vol 34, pp.344-37,1986.

[16] **S. Bouchet** Segmentation et quantification d'images tridimensionnelles. Techn. Report. Ecole des Mines de Paris, June 1999,102 p.

[17] **J.R. Casas,** *Image compression based on perceptual coding techniques*, PhD thesis, UPC, Barcelona, March 1996.

[18] **A.T. Clark, R.J. Young and J.F. Bertram** In vitro studies on the roles of transforming growth factor-beta1 in rat metaphrenic development, *Kidney Int* 59 pp 1641-1653 (2001).

[19] **J.-M. Chautru,** The use of Boolean random functions in Geostatistics. *Third Int. Geostatistics Cong., Avigon.* Reidel Publ., Dordrecht, The Netherland,1989 .

[20] **G. Choquet,** Theory of Capacities, *Ann. Inst. Fourier* 5, 131-295, 1953.

[21] **G. Choquet** *Topologie* Academic Press, N.Y. 1966.

[22] **F. Conrad and C. Jacquin,** Représentation d'un réseau bidimensionnel de failles par un modèle probabiliste. Int. report, Centre de Morphologie Mathématique, Fontainebleau, France, 1972.

[23] **M. Coster & J-L. Chermant,** *Précis d'analyse d'images,* CNRS ed., Paris, 1985 (2nd Edition *1989).*

[24] **J. Crespo**, **J. Serra, R.W. Schafer** Theoretical aspects of morphological filters by reconstruction. *Signal Processing,* 1995, Vol. 47, No 2, pp. 201-225.

[25] **J. Crespo, R.W. Schafer,** Locality and adjacency stability constraints for morphological connected operators. *Journal of Mathematical Imaging and Vision* 7, 1 (1997), 85-102.

[26] **P.E. Danielsson**, Euclidean distance mapping *Computer Graphics and Image Processing,* (1980)14, 227-248.

[27] **P. Delfiner**, Le schéma Booléen-Poissonien. Int. report, *Centre de Morphologie Mathematique,* Fontainebleau, France, 1970.

[28] **E. Dougherty**, Application of the Hausdorff metric in gray scale morphology via truncated umbrae, *JVCIR* **2**(2), 1991, pp. 177-187

[29] **G**. **Fricout** Kidney and Skeletonization Int. report CMM, Ecole des Mines de Paris nov 2000.

[30] **G. Fricout, L.A. Cullen-Mc Ewen, I.A. Harper, D. Jeulin , J.F. Bertram** A quantitative method for analysing 3D branching in embryonic kidneys (7 p.) : development of a technique and preliminary data *Image Anal Sterol* 2001, 20 (suppl 1) pp. 36-41.

[31] **S. Gesbert, C.V. Howard, D. Jeulin and F. Meyer** The use of basic morphological operations for 3D biological image analysis, *Trans. Roy. Microsc. Soc.*, vol. 1, pp. 293-296, 1990.

[32] **G. Gierz et Al.** *A Compendium on Continuous Lattices*. Springer, 1980.

[33] **M.J.E. Golay** Hexagonal parallel pattern transformation. *IEEE Trans. Comput.* (1969) C-18, 733-740.

[34] **J. Goutsias** Morphological analysis of discrete random shapes. *Journal of Mathematical Imaging and Vision*,1992, 2, 193-215.

[35] **C. Gratin and F. Meyer** Mathematical Morphology in three dimensions, *Acta Stereol.* vol. 11, pp. 551-558, 1991.

[36] **C. Gratin**, *De la représentation des images en traitement morphologique d'images tridimensionnelles,* PhD thesis, Ecole des Mines de Paris, 1993.

[37] **A. Greco, D. Jeulin and J. Serra** The use of the texture analyser to study sinter structure, *J. Micr.* 116, pt.2, 1979

[38] **M. Grimaud** A new measure of contrast : dynamics. In Proc. SPIE, *Image Algebra and Morphological Image Processing III*, San Diego, 1992, Vol. 1769, pp. 292-305.

[39] **A. Haas, G. Matheron et J. Serra** Morphologie mathématique et granulométries en place. *Ann. Mines* (1967)11, 736-753 et 12, 767-782 (THE Reference Paper on Set Covariance, and on Linear Erosion)

[40] **H. Hadwiger** *Vorsesungen über Inhalt, Oberfläche und Isoperimetrie,* Springer, 1957.

[41] **P.R. Halmos** *Lectures on Boolean Algebras.* D. Van Norstand Company, Inc., Princeton, 1963.

[42] **R.M. Haralick and L.G. Shapiro** *Computer and robot vision.* Vol. I. Addison Wesley, 1992, pp. 191-198.

[43] **H. Heijmans & C. Ronse** The algebraic basis of mathematical morphology, part one: erosions and dilations, *Computer Vision, Graphics and Image Processing 50* pp 84-102 (1990).

[44] **H.J.A.M. Heijmans and J. Serra** Convergence, Continuity, and Iteration in Mathematical Morphology, *Journal of Visual Communication and Image Representation*, Vol. 3, N°1, March 1992, 84-102.

[45] **H.J.A.M. Heijmans** Morphological image operators. *Advances in Electronics and Electron Physics,* 1994, suppl. 24, Vol. 50, Hawkes P. ed., Boston: Ac. Press.

[46] **H.J.A.M. Heijmans** Connected morphological operators. Tech. Rep. CWI No PNA-R9708, April 1997.

[47] **G. Heygster,** Rank filters in digital image processing, *Computer Graphics & Image Processing* 19 (2), pp 148–164, June 1982.

[48] **V.C. Howard and K. Sandau** Measuring the surface area of a cell by the method of the spatial grid with a CSMLM, *J. of Micr.* vol. 165, pp 183-188, 1992.

[49] **D.P. Huttenlocher, G.A.Klunderman, W.J. Rucklidge** Comparing images using the Hausdorff distance, *IEEE PAMI*, **15**(9), Sept. 1995.

[50] **M. Iwanowski and J. Serra** Morphological Interpolation and Colour Images, *Proc. International Conference on Image Processing* ICIAP'99 Venice, sept 1999.

[51] **M. Iwanowski and J. Serra** The Morphological-affine object deformation, *Mathematical Morphology and its Applications to Image and Signal Processing*, J. Goutsias, L. Vincent, D.S. Bloomberg (Eds.) Kluwer Ac. Publ. 2000, pp.81-90.

[52] **M. Iwanowski** *Application de la Morphologie Mathématique pour l'interpolation d'images numériques* Phd thesis Ecoles des Mines de Paris- Ecole Polytechinque de Varsovie, 15 nov. 2000,

[53] **James and James** *Mathematics Dictionary,* Van Nostrand, 1982.

[54] **D. Jeulin** Multicomponent Random Models for the Description of Complex Microstructures, *Fifth Congress for Stereology*, Salzbourg, Austria, 1979.

[55] **D. Jeulin** & **P. Jeulin** Synthesis of rough surfaces by random morphological models. *Stereol. Iugosl.* 3, Suppl. 1, 239-246, 1981.

[56] **D. Jeulin** Anisotropic rough surface modelling by random morphological functions, Proc. 4th Symp. on Stereology, Göteborg, 1985: *ActaStereol.,* 6 (1987), pp. 183-189.

[57] **D. Jeulin** *Modèles morphologiques et changement d'échelle en statistique de rupture.* Ecole des Mines, Paris, 1988.

[58] **D.Jeulin** Morphological modelling of images by sequential random functions. $SignalProcessing - Special\ Issue\ on\ Mathematical\ Morphology,$ Vol. 16, No 4. April 1989, pp. 403-431.

[59] **D. Jeulin** *Modèles morphologiques de structures aléatoires et de changement d'échelle*, Thèse Doctorat ès Sciences Physiques, Univ. Caen 1991.

[60] **D. Jeulin** (ed.) *Advances in Theory and Applications of Random Sets.* World Scientific, 1997.

[61] **P.P. Jonker** Parallel processing in computer vision and collision free path planning of autonomous systems, in *26th ISATA*, 1993.

[62] **P.P. Jonker**, **A.M. Vossepoel** Mathematical morphology for 3D images : comparing 2D and 3D skeletonization algorithms, *Summer School on morphological image and signal processing,* Delft University, 1995.

[63] **D.G. Kendall** Foundations of a theory of random sets in *Stochastic Geometry* (E.F. Harding and D.G. Kendall, eds), Wiley, 1974.

[64] J.C. **Klein** *Conception et réalisation d'une unité logique pour $\mathcal{L}$'analyse quantitative d'images.* Thesis, University of Nancy, 1976.

[65] **E.N. Kolomenski & J. Serra** Trois études de morphologie mathématique en géologie de l'ingénieur. *Bull Assoc. Int. de Géol. de l'Ing.* 13, Krefeld, pp. 89-97, 1976.

[66] **T. Kong and A. Rosenfeld** Digital topology: Introduction and survey, *Comp. Vis. Image Proc.*, vol. 48, pp. 357-393, 1984.

[67] **Ch. Lantuejoul** *La squelettisation et son application aux mesures topologiques des mosaiques polycristallines.* PhD thesis, Ecole des Mines de Paris, 1978.

[68] **Ch. Lantuejoul** Skeletonization in quantitative metallography. *Issues in Digital Image Processing* (R.M. Haralick and J.C. Simon Edts) Sijthoof and Noordoff, 1980.

[69] **C. Lantuejoul & S. Beucher,** On the use of geodesic metric in image analysis, *J. of microscopy,* 121, pp 39–49, 1981.

[70] **B.B. Mandelbrot**, *Fractals: Form, chance and dimension.* W. H. Freeman, San Francisco-London, 1977.

[71] **P. Maragos & R.W. Schafer** Morphological filters—part I: their set-theoretic analysis and relations to linear shift-invariant filters, *IEEE transactions on acoustics, speech and signal processing*, Vol. ASSP-35 (8), pp 1153–1169, August 1987.

[72] **P. Maragos & R.W. Schafer** Morphological filters—part II: their relations to median, order-statistics, and stack filters, *IEEE transactions on acoustics, speech and signal processing,* Vol. ASSP-35 (8), pp 1170–1184, August 1987.

[73] **B. Marcotegui and F. Meyer** Morphological segmentation of image sequences. In *Mathematical Morphology and its applications to image processing,* Serra J. and Soille P. eds., Kluwer, 1994, pp. 101-108.

[74] **B. Matern** *Spatial variation*, Medd. Statens skogsforskingsinstit, 1960.

[75] **G. Matheron** *Les variables régionalisées et leur estimation,* Paris, Masson, 1965, 302 p.

[76] **G. Matheron,** *Eléments pour une théorie des milieux poreux,* Masson, Paris, 1967.

[77] **G. Matheron** Schéma booléen séquentiel de partitions aléatoires, Int. report, Centre de Morphologie Mathématique, Fontainebleau, France, 1968.

[78] **G. Matheron** *Théorie des ensembles aléatoires.* Cahiers du CMM, fascicule 4. Ecole des Mines Paris,1969.

[79] **G. Matheron** *The theory of regionalized variables and its applications,* Cahiers du Centre de Morphologie Mathématique, Fasc. 5. Paris : ENSMP, 1971, 211 p.

[80] **G. Matheron** Polyèdres poissoniens et ensembles semi-markoviens, *Advances in Applied Prob.*, 1971.

[81] **G. Matheron** The intrinsic random functions, and their applications, *Adv. Appl. Prob.*, Vol. 5, 1973, pp. 439-468.

[82] **G. Matheron** *Random sets and integral geometry,* Wiley, New-York, 1975.

[83] **G. Matheron** Two classes of isofactorial models. *Third Int. Geostatistics Cong., Avignon.* Reidel Publ., Dordrecht, The Netherlands, 1989.

[84] **G. Matheron** Filters and Lattices. Ch 6 in *Image Analysis and Mathematical Morphology.* Vol. 2. Serra J. ed. London: Acad. Press, (1988), pp.115-140.

[85] **G. Matheron and J. Serra** Strong filters and connectivity.Ch 7 in *Image Analysis and Mathematical Morphology.* Vol. 2. Serra J. ed. London: Acad. Press (1988), pp. 141-157.

[86] **G. Matheron** Treillis compacts et treillis coprimaires. Tech. rep. N-23/90/G, Ecole des Mines de Paris, Part 1, 1990, part 2, 1996.

[87] **G. Matheron** Les nivellements. Tech. Rep. Ecole des Mines de Paris, No N-07/97/MM, Feb. 1997.

[88] **F. Meyer** Rapport de stage note interne CMM, (1976).

[89] **F. Meyer** *Cytologie quantitative et morphologie mathématique,* Ph.D. Thesis, School of Mines, Paris, 1979.

[90] **F. Meyer & J. Serra** Contrasts and activity lattice, *Signal Processing, special issue on Math. Morph.,* vol. 16 (4), pp 303–317, April 1989.

[91] **F. Meyer & J. Serra** Filters: from theory to practice, *Acta Stereologica*, 8/2, pp 503-508, 1989.

[92] **F.Meyer & S.Beucher** Morphological Segmentation. *J.of Visual Communication and Image Representation*, 1990, Vol.1 (1), pp.21-46.

[93] **F. Meyer** Mathematical Morphology: from two dimensions to three dimensions, *J. of Micr.,* vol. 165, pp. 5-29, 1992.

[94] **F. Meyer** Minimum spanning forests for morphological segmentation. In *Mathematical Morphology and its applications to image and signal processing,* Maragos P. et al. eds., Kluwer,1996.

[95] **F. Meyer** A morphological interpolation method for mosaic images, in *Mathematical Morphology and its applications to image and signal processing,* Maragos P. et al. eds. Kluwer, 1996.

[96] **F. Meyer** The levelings. In *Mathematical Morphology and its applications to image and signal processing,* H. Heijmans and J. Roerdink eds., Kluwer, 1998.

[97] **R. E. Miles** *Random Polytopes*, Ph.D. thesis, Cambridge, England, 1964.

[98] **R. E. Miles** On estimating aggregate and overall characteristics from thick sections by transmission microscopy, *Fourth Congress for Stereology, NBS spec. pub.* 431, 1976.

[99] **R. E. Miles** Poisson Flats in Euclidean Spaces, Part. I, *Adv. Appl. Prob. 1969,* 1, 211-237.

[100] **R. E. Miles and J. Serra (eds.)** *Geometrical Probabilities and Biological Structures.* Springer Verlag, Lecture Notes in Biomathematics 1978.

[101] **H. Minkowski** Volumen and Oberfläche, *Math. Ann.* 57, 447-495, 1903.

[102] **I. Molchanov** *Statistics of the Boolean model for Practitioners and Mathematicians.* J. Wiley and Sons,1997.

[103] **P. Moreau and Ch. Ronse** Generation of shading-off on images by extrapolations of Lipschitz functions, *Graph. Models and Image Processing*, **58**(6), July 1996, pp. 314-333..

[104] **E.H. Moore** Introduction to a form of general Analysis, *AMS colloq. pub.* vol.2 New Haven 1910.

[105] **J.C. Mullikin** *Discrete and Continuous Methods for Three Dimensional Image Analysis*, Delft: Univ. Press, 1993.

[106] **J. Mukkerjee and B.N. Chatterji**, "Segmentation of three-dimensional surfaces", *Pattern Rec. Letters*, vol. 11, pp. 215-223, 1990.

[107] **N. Nikolaidis & I. Pitas** *3-D Image Processing Algorithms*, Wiley , 2001, 176 p.

[108] **Y. Pomeau and J. Serra** Contacts in random packings of spheres, *J. of Micr.*, vol. 138, pp. 179-187, 1985.

[109] **K. Preston & M. Duff,** *Modern Cellular Automata,* Plenum, New York, 1985.

[110] **C. Ronse** Lattice theoretical fixpoint theorems in morphological image filtering, *Journal of Mathematical Imaging & Vision,* Vol.4, no.1, pp.19-41,1994.

[111] **F.Prêteux, & M.Schmitt**, Fonctions booléennes et modélisation du spongieux vertébral. *Int. Electronic Image Week, Nice, April 1986*, *2,* 476-481.

[112] **F.Prêteux, & M.Schmitt** . *Image Analysis and Mathematical Morphologie. Vol 2: Theoretical Advances* (J. Serra Ed), pp. 377-400. Academic Press, London, 1988.

[113] **J. Rivoirard** Models with orthogonal indicator residuals. *Third Int. Geostatistics Cong., Avignon.* Reidel Publ., Dordrecht, The Netherlands, 1989

[114] **C. Ronse,** Erosion of narrow image features by combining local rank and max filters, *Proc.* 2^{nd} *Int. Conf. on Image Processing and its Applications*, London, pp 77–81, 1986.

[115] **C. Ronse** Set theoretical algebraic approaches to connectivity in continuous or digital spaces. *JMIV*, 1998, Vol. 8, pp. 41-58.

[116] **C. Ronse, J.Serra** Geodesy and connectivity in grids *Fundamenta Informaticae*, Vol 46, issue 4, sept. 2001. 46(4): pp. 349-395.

[117] **A. Rosenfeld** Connectivity in digital pictures *Journal of the assoc.for Comp.Mach.*,Vol.17 (1), 1970, pp. 146-160.

[118] **A. Rosenfeld and A.C. Kak** *Digital picture processing.* Ac.Press, New-York, 1976.

[119] **P. Salembier and A. Oliveras** Practical extensions of connected operators. In *Mathematical Morphology and its applications to image and signal processing,* Maragos P. et al., eds. Kluwer, 1996, pp. 97-110.

[120] **L.A. Santalo** *Integral Geometry and Geometrical Probability*, Encyclopedia of Mathematics and its Applications, Addison Wesley, Reading, Mass., USA.1976.

[121] **J. Serra** L'analyse des textures par la géométrie aléatoire. *Comptes-rendus du Comité Scientifique de l'IRSID*, 2 Nov. 1965, 7 p.

[122] **J. Serra,** Remarque sur une lame mince de minerai lorrain. Bulletin du B.R.G.M. n° 6, Déc. 1966, 26 p.

[123] **J. Serra** Equicontinuous functions: a model for mathematical morphology, SPIE San Diego Conf., Vol. 1769, pp. 252-263, July 1992.

[124] **J. Serra** Hausdorff distance and Interpolations, *Mathematical Morphology and its applications to image and signal processing*, H.Heijmans and J. Roerdink eds Kluwer,1998, pp.107-115

[125] **J. Serra** *Introduction à la Morphologie Mathématique, Cahiers du CMM*, Ecole des Mines de Paris, 1969.

[126] **J.Serra** *Echantillonnage et Estimation locale des phénomènes de transition miniers.* Tomes I et II. Thesis, Univ. de Nancy. Nov. 1967, 670 p.

[127] **J. Serra** Hierarchical random set models, Int. report, *Centre de Morphologie Mathématique*, Fontainebleau, France, 1974.

[128] **J. Serra** The boolean Model and Random Sets, *Computer graphics and Image Processing* 12, 99-126, 1980.

[129] **J. Serra** *Image analysis and mathematical morphology,* Academic Press, London, 1982.

[130] **J. Serra** Descriptors of flatness and roughness, *J. of Micr.*, vol. 134, pp. 227-243, 1984.

[131] **J. Serra,** *Image analysis and mathematical morphology, part II: theoretical advances,* J. Serra ed., Academic Press, London, 1988.

[132] **J. Serra** Mathematical Morphology for Boolean lattices, chapter 2 in *Image Analysis and Mathematical Morphology*, vol. 2, J. Serra (ed.), London: Acad. Press, 1988

[133] **J. Serra** Les fonctions aléatoires booléennes, Internal report CMM-57 *Ecole des Mines, Paris*, (1985).

[134] **J. Serra,** Boolean random functions, *J. of Microscopy*, Vol. 156, N°1, 41-63, 1989.

[135] **J. Serra** Toggle mappings, in "*from Pixels to Features*", J.C. Simon ed., pp 61–72, North Holland, 1989.

[136] **J. Serra and L. Vincent** An Overview of Morphological filtering , *IEEE Trans. on Circuits, Systems and Signal Processing*, Vol. 11, N°1, pp.47-108,1992 .

[137] **J. Serra,** Lecture Notes on Morphological Operators int. report CMM, 150 p., School of Mines, Paris, June 2001[C06/01/MM].

[138] **J. Serra** Equicontinuous functions, a model for mathematical morphology. In *Non linear algebra and morphological image processing SPIE,* Vol. 1769, San Diego, July 1992, pp. 252-263.

[139] **J. Serra and P. Salembier** Connected operators and pyramids. In *Non linear algebra and morphological image processing SPIE,* Vol. 2030, San Diego, July 1993, pp. 65-76.

[140] **J. Serra** Cube, cube-octahedron or rhombododecahedron as bases for 3-D shape descriptions", *Advances in Visual Form Analysis, C. Arcelli and Al. (eds.)* World Scientific 1997, 502-519.

[141] **J. Serra** Connectivity on complete lattices *JMIV*, 1998, Vol. 9, pp. 231-251

[142] **J. Serra** Connectivity for sets and functions *fundamenta Informaticae,* 41 (2000) 147-186

[143] **J. Serra** Morphological descriptions using three-dimensional wavefronts (to be presented at *ISS'*2001,Bordeaux, France sept. 2001)

[144] **M. Schmitt** Estimation of the density in a stationary Boolean model. *J. of Applied Prob.,*1991, vol. 28

[145] **P. Soille** Spatial distributions from contour lines : an efficient methodology based on distance transformations, *Journal of Visual Communication and Image Representation* 2(2), (1991), 138-150.

[146] **P. Soille, J.F. Rivest and J. Serra** Dimensionality in image analysis and processing. *Proc. SPIE, Image Science and Technology*, San Jose, Feb. 1992, Vol.1658.

[147] **P. Soille** *Morphologische Bildverarbeitung,* Springer, 1999, 316 p.

[148] **H.R. Solomon**, Distribution of the Measure of a Random Two-Dimensional Set. *Ann. Math Stat.* 24, 650-656, 1953.

[149] **M. Staub** (personnal communication).

[150] **S.R. Sternberg** Morphology for grey-tone functions, *Computer Vision, Graphics and Image Processing* 35, pp 333–355, 1986.

[151] **D. Stoyan** On some Qualitative Properties of the Boolean Model of Stochastic Geometry, int report *freiberg Akademie*1978.

[152] **A. Tarski** Sur les classes closes par rapport à certaines opérations élémentaires, *Fund. Mat*16, pp.181-305 (1929)

[153] **E.E. Underwood** *Quantitative Stereology,* Addison Wesley 1970 .

[154] **C.Vachier** *Extraction de caractéristiques, segmentation d'images et morphologie mathématique.* PhD thesis, Ecole des mInes de Paris, 1995.

[155] **P.W. Verbeek, H.A. Vrooman and L.J. van Vliet** Low level image processing by max-min filters, *Signal Process.,* vol. 15, pp. 249-258, 1988.

[156] **L. Vincent,** ElMathematical morphology for graphs applied to image description and segmentation, *electronic Imaging West*, Pasedena CA (USA), pp 313–318, April 1989.

[157] **L. Vincent** Graphs and mathematical morphology, *Signal Processing, special issue on Math. Morph.,* vol. 16 (4), pp 365–388, April 1989.

[158] **P.D. Wendt, E.J. Coyle & N.C.Jr. Gallagher** Stack filters, *IEEE transactions on acoustics, speech and signal processing,* vol. ASSP-34 (4), pp. 898–911, August 1986.

[159] **E. R. Weibel** *Stereological Methods,* Vol 1 and 2, Ac. Press, London 1981.

[160] **O. Yli-Harja, J. Astola & Y. Neuvo** Analysis of the properties of median and weighted median filters using threshold logic and stack filter representation, submitted to ASSP-EDICS 4.4., 50 p., 1989.